FATIGUE AND FRACTURE BEHAVIOUR OF PVC AT ELEVATED TEMPERATURES

A dissertation submitted to the Faculty of Engineering and the Built Environment, University of Cape Town, in fulfilment of the requirements for the degree of Master of Science of Engineering

Prepared by: L. von Zwiklitz
Department of Mechanical Engineering
University of Cape Town

Date: February 2008

ABSTRACT

A series of failures in underground water-carrying uPVC piping in a luxury resort in Dubai gave rise to a research opportunity to determine the effect of temperature on fatigue life performance of uPVC piping. Two different modes of testing were used to determine this temperature effect, namely SN and Fracture Mechanics Paris testing. The temperatures tested were 20˚C and 45˚C. In addition to temperature tests, a potential ageing effect was also investigated by comparing pipes which had been in service in the resort, and previously unused piping.

The SN tests consisted of externally and symmetrically stressing, across the diameter, sections of pipe from the luxury Madinat Jumeirah resort in Dubai where the failures had occurred. The Paris equation generating FM tests used Compact Tension specimens and produced an equation relating the crack growth rate to the cyclic stress intensity amplitude. In addition, material properties were measured which could then be used for fatigue lifetime predictions.

In addition to the lifetime tests, fracture toughness tests were also completed. These were done with a view to determining the fracture toughness of the material, and also to ascertain if there was an orientation effect for crack growth. The potential ageing effect was also investigated. This was achieved by means of using differently orientated specimens. SENB specimens were used to determine circumferential fracture toughness and C-Shaped specimens for longitudinal cracks (the direction of on-site crack growth).

Fracture surfaces were inspected and calculations performed to indicate critical flaw sizes were broadly consistent with linear elastic fracture mechanics (LEFM). Using the material properties garnered from the Paris fatigue and fracture toughness tests, lifetime predictions were made and compared to the SN data for cycles to failure.

The research studies revealed that there was a distinct difference in fatigue performance as a result of a temperature increase from 20˚C to 45˚C, as characterised by both SN and Paris fatigue tests. There was also, but to a lesser degree, an ageing effect. The temperature performance factor for the SN curves was between 1.6 and 4.6, while for the Paris characterisation the temperature performance factor was between 3 and 3.5.

The Paris values for NEW i.e.: unused type material, at 20˚C and 45˚C were as follows:

$$\frac{da}{dN}_{20°C} = 2.7 * 10^{-8} \Delta K^{3.26}$$

$$\frac{da}{dN}_{45°C} = 8.55 * 10^{-8} \Delta K^{2.85}$$

Life predictions based on Paris data correlated with the actual SN data curves. Using the Paris equation and SN curves for 20˚C and 45˚C conditions, a relationship between the predicted cycle count to failure and the actual cycles to failure on the SN curves was established.

It is believed that this study may contribute to the better engineering use and understanding of PVC piping in hot environments.

DECLARATION

1. I know that plagiarism is wrong. Plagiarism is to use another's work and to pretend that it is one's own.

2. I have used the Vancouver convention for citation and referencing. Each significant contribution to, and quotation in, this thesis from the work, or works, of other people has been attributed, and has been cited and referenced.

3. This thesis is my own work.

4. I have not allowed, and will not allow, anyone to copy my work with the intention of passing it off as his or her own work.

SIGNED:

……

Leon von Zwiklitz

DATE: February 2008

ACKNOWLEDGEMENTS

My thanks and appreciation goes out to the following individuals who have assisted me throughout the duration of this project:

- Professor R.B Tait – Supervisor

  For providing time, patience and insight in assisting and explaining (numerous times) all facets of this project. Also the enthusiasm and encouragement served to motivate me further.

- Professor R Knutsen and staff of the UCT Materials Centre

  The material centre personnel were always supportive and helpful during the two years of this project. There was always someone to ask for advice on many different subjects.

- AFRICON and Ermis Marques for the supply of piping material

- Mr J Mayer – Principal Technical Officer, Mechanical Engineering, University of Cape Town

  For his assistance with the temperature controller and for insights into making the testing process safer.

- Mr Glen Newins, and all members of the Mechanical Engineering workshop, University of Cape Town

  For the assembly of testing apparatus, and the cutting of a vast number and array of samples, and always with a smile. The workshop staff were always on hand to re-cut specimens and for any problems, no matter how trivial.

- To my family and friends who kept the motivation high and ensured the end product was always in sight.

- Mr G Izaaks for drawings of specimens and design of equipment

TABLE OF CONTENTS

LIST OF FIGURES

LIST OF TABLES

CHAPTER 1. INTRODUCTION

Poly-Vinyl Chloride (PVC) and luxury coastal resorts are generally not mentioned in the same sentence. However, the opulent Madinat Jumeirah – meaning the "City of Jumeirah" – resort on the shores of Dubai, and unplasticised-PVC (referred to as uPVC) have come to have an association, albeit, not a completely positive one. The Madinat Jumeirah resort adjoins the more well known Burj Al Arab 7 star hotel, shown in Figure 1, and this Madinat resort has been experiencing PVC water pipe failures [1] since the mid construction period, in 2003. These pipes were transporting desalinated water underground throughout the Madinat Jumeirah resort. The Madinat Jumeirah resort is shown in Figure 1.1 to the right of the shore, with the famous sail-shaped 7-star hotel to the left of the resort.

FIGURE 1.1: Burj-Al Arab hotel, alongside the Madinat Jumeirah luxury resort [2]

1.1 MADINAT JUMEIRAH

According to Sterling Publishing Group (SPG), an international media company which provides internet reference portals, as well as business conferences and forums [3], construction on the Madinat Jumeirah resort began in 2002, and was completed in early 2004, costing an estimated

$340m. Covering 400 000 m^2 of land, there are two five-star hotels each offering 300 rooms, as well as courtyard villas offering clusters of 340 rooms and suites. In addition to the rooms and suites, there are a vast array of restaurant and dining facilities. Surrounding the hotels is 200 000 m^2 of landscaped garden. Shown in Figure 1.2 is a glimpse into what can only be described as sheer magnificence. Figure 1.3 shows an aerial view of the resorts location in relation to the coastline. It also gives an indication of the size of the resort, and just how much development there is along this Dubai coastline, which puts a strain on resources, especially given that it is essentially a desert region.

FIGURE 1.2: One view of the extravagant Madinat Jumeirah resort, with the Burj-Al Arab in the background [4]

FIGURE 1.3: Aerial view of Dubai beachfront showing location of Madinat Jumeirah [5]

1.1.1 FACILITY CAPABILITIES

According to SPG Media [3], Madinat Jumeirah houses the largest spa and fitness centre in the region, and in addition to several swimming pools, there are also traditional steam rooms and baths.

There are in total 120 shops, cafes and restaurants throughout the resort. There is a convention centre which caters towards conferences, banquets and weddings. A ballroom seating 1400 guests as well as smaller function halls are also available.

1.1.2 DESERT LIFESTYLE

As shown in Figure 1.3, the resort is actually rather small when compared with all the other developments in the region. The resort is located in an area adjacent to the sea, and has magnificent views and opulent living conditions; it is still, however, located in a desert. In addition to the searing high temperatures (in summer in the vicinity of 50˚C), there is a distinct lack of potable water. This problem of a lack of potable water for the region has been solved by the process of desalination of, locally abundant, sea water.

1.2 DESALINATION AND WATER TRANSPORT IN MADINAT JUMEIRAH

The Encyclopaedia of Desalination and Water Resources [6], notes that desalination – the conversion of saline water to fresh potable water – was developed over the last forty to fifty years of the 20th century. It is used in areas where there is a lack of freshwater supplies, and where there is a generous supply of saline water bodies – for examples, coastal areas, and in particular when it is cost effective, as it is an expensive process.

The process involves distilling the liquid, thereby separating the fresh and the salt water. The salt water is boiled, with the salt remaining while the fresh water vapour is boiled away. This water vapour is then cooled, condensing

the steam into water again, as shown in the Figure 1.4. However, the water is not cooled extensively, but to typically just above that of the local ambient temperature, leaving the plant at a temperature in the vicinity of 50˚ C [1].

The above process is similar to the natural hydrological cycle where water evaporates from water source surfaces, such as seas and lakes, from the suns energy, and then this water vapour condenses as clouds when it comes into contact with cooler air, re-condensing into rain. By using alternative sources of heating and cooling, the natural process can be performed more swiftly, albeit at some expense.

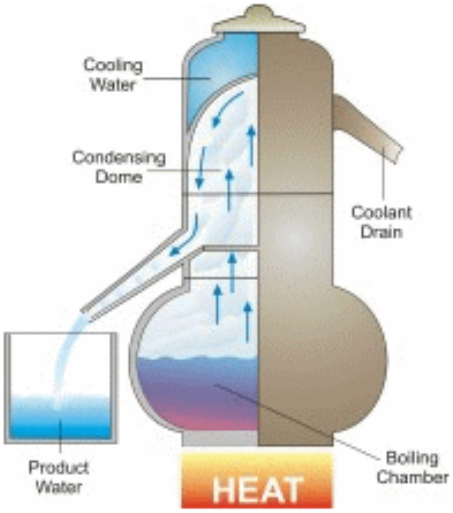

FIGURE 1.4: Schematic of desalination process [6]

Once the clean, desalinated water has passed through the desalination plant, it is pumped throughout the resort via underground uPVC piping, entering the piping system at the previously mentioned temperature of approximately 50˚ C. An example of the pipe used to transport the water is shown in Figure 1.5. This piping was buried ideally two to three metres deep underground, although during construction there may have been aberrations from this depth, sometimes to as low as one metre of overhead soil [1]. This lower level of soil coverage as well as occasional poor compaction meant that the pipes were vulnerable to high loads from overheard traffic during the construction process.

FIGURE 1.5: An example of the piping used to transport desalinated water around the resort

1.3 PIPE FAILURES

Between June 2003 and August 2005, 28 catastrophic failures of underground water-carrying uPVC pipes occurred at the resort, in predominantly high-traffic areas. Some of these failures could perhaps be attributed to initial damaging of the pipes during installation of fittings. However, the majority of the failures, in the form of longitudinal cracks or splitting from the inside outwards, occurred on the lower surface of the pipes in regions isolated from fittings [1]. An example of one of the failures is shown in Figure 1.6.

FIGURE 1.6: Example of pipe failure from the resort [7]

The pipe failures caused extensive damage to the road systems. In view of the sandy nature of the construction region, and the difficulty of compaction of the sand around the pipes, the escaping water steadily washed away sand, causing cavitations and ultimately collapse of the road. This necessitated

reconstruction of the road, as well as replacement of the piping. Damage to a road can be seen in Figures 1.7 and 1.8. This damage caused disruption to both traffic and water supply throughout the resort, loss of water and an embarrassment for the resort operators.

FIGURES 1.7 & 1.8: Damage caused to the road from pipe failure [7]

1.4 PRELIMINARY INVESTIGATION

Professor R.B Tait, together with the South African company, Cape Residual Stress (now Origen Engineering Solutions) was approached in August 2005 to investigate and determine the causes of the pipe failures. After having assessed the operating conditions and manner in which the piping was buried underground, the causes of failures were determined to be due to a combination of factors published in a preliminary report [1]:

- Overhead construction traffic – the overhead traffic, sometimes with loads of up to 18 tons on an axle, would cause compression cycles on the pipe when passing. This would over time result in failure from fatigue.
- Incorrect or incomplete pipe backfill compaction – This meant the pipe was exposed to higher than realised and anticipated loads, as the traffic load was not adequately distributed.

- Insufficient soil coverage during construction trafficking (to as low as 0.5 to 1m) – This would have caused the pipe to be exposed to higher loads than anticipated, as mentioned above.
- A high operating temperature above the conventional and usual design temperature of 20 – 25˚ C. In this case, both the desalinated water (temperatures of 50 – 55˚C) as well as the high ambient desert temperature (often in excess of 40˚ C) both contributed. These higher operating temperatures lead to, it was reported [1], a drop in fatigue life.

1.5 REPORT RECOMMENDATIONS

In the preliminary failure analysis report prepared by Professor Tait and Origen, it was mentioned that had the pipes been correctly supported and buried to the necessary depth, they may not have failed to the same extent of frequency and reduced lifetime. It also mentioned that it was a reasonable assumption that had the operating temperature been lower the pipes would also not have failed, or certainly not as often, or as soon in their expected operational lifetime.

However, the combination of the poor burial and compaction of the pipes (while still subjected to construction traffic loading), and the high operating temperatures together contributed to cause the failures. This lead to the recommendation for “fatigue tests to develop SN curves over a range of relevant stresses and temperature [1]” on representative samples of PVC, in anticipation that “future testing will endeavour to establish a full fatigue SN curve at various stress levels, as a function of temperature [1]”. This would be done with a view to contributing towards the better and more reliable usage of similar piping applications worldwide, but particularly in the Middle East where ambient temperatures are higher.

1.6 SCOPE OF RESEARCH

The previously mentioned failure analysis report [1] and recommendations provided the basis for the research in this Masters project, concerning the hot fatigue behaviour of uPVC. This was to be assessed initially by the generation of the SN curves at a range of temperatures, including 20˚ C and nominally 45˚ C. The SN tests also utilised both so-called NEW and OLD pipes, in order to determine if, and by how much, there was a decrease in fatigue life with age.

A fracture mechanics based approach was followed, where a fatigue crack growth rate (da/dN) versus cyclic stress intensity (ΔK) curve, or so-called Paris equation, was generated for the NEW type material, at both ambient and elevated temperatures. This could be then compared to the data acquired from an earlier project into the Paris equation of the OLD type, and used in particular in subsequent pipeline "fatigue life prediction" assessments.

The input parameters for the life prediction would include:

- Stress spectrum and history
- Paris parameters *C* and *m*
- Fracture toughness
- Initial damage or crack size

The above approach is discussed further in Chapters 2, 4 and 5.

The scope also included fracture toughness testing of the uPVC material, with a specific view to determining if there was a difference in fracture toughness with regards the orientation of the specimens.

1.7 LAYOUT OF THE THESIS

This thesis consists of six main Chapters. The first Chapter covers the introduction, giving a brief background of the research and the scope.

The second Chapter reviews the literature about polymers and PVC in particular, especially with regards to PVC fatigue, and other such related material. The elements of fatigue both from a conventional SN approach and a fracture mechanics approach are also presented, together with a detailed review, such as can be found, of PVC fatigue itself.

Chapter three provides a description of the experimental details and procedure for each of the different phases of testing, and the relevant analysis and calculations that were necessary for the computation of results.

Chapter four presents the results from each of the testing phases, and highlights the behaviour and trends, while the Discussion Chapter (Chapter 5) interprets all data and behaviour obtained and its implication on fatigue life and operational suitability, and correlates with previously published literature.

In Chapter six the conclusions and findings of the research are reviewed, as well as recommendations following on from the research and knowledge garnered from testing.

CHAPTER 2. LITERATURE REVIEW

2.1 INTRODUCTION TO POLYMERS

Polymers have been around since the 1500's, when Mayan children in Central America played with balls made from the local rubber trees. Since those early days, the development of polymers has spanned the centuries. From the synthesis of Bakelite in 1907 by Leo Baekeland, to the stage where modern polymers are more widely used as a material than steel in America, polymer choice is abundant and they have come into our lives with a positive influence [8 – 13].

Polymers have a wide range of applications. Polystyrene, invented in 1930, is used in packaging, cups, and thermally insulated containers, while Ekonol, developed by James Economy in 1970, is used in electronic devices and aircraft engines [8]. Examples of how polymers have found their way into our lives can be seen in Figure 2.1.

FIGURE 2.1: Examples of polymers in everyday life

While polymers may be more popular than other materials such as steel due to their economic advantages, or resistance to corrosion [12], as with any

material, polymers are vulnerable to cracking, and ultimately failure. In fact, polymers can be more susceptible to failure from a combination of sunlight, or chemical attack than conventional materials such as steel, or concrete.

Two types of polymers exist – natural and synthetic. Natural polymers have been around since the first days of the earth, while human-made polymers have a more extensive modern history, as discussed above.

Examples of Natural polymers are proteins (collagen and keratin), carbohydrates (cellulose and starch) and rubber. Synthetic polymers include for example: poly-ethylene, poly-propylene and poly-vinyl chloride (PVC). In today's modern era, the processed polymer industry has become larger than the aluminium, copper and steel industries combined [8].

2.1.1 ADVANTAGES OF POLYMERS

Polymers have advantages over materials such as steel in a number of departments [12, 14]:

- Favourable strength to weight ratio
- Good damping properties
- High wear resistance
- Economically more viable
- Minimal corrosion, therefore no requirement for cathodic protection

2.1.2 APPLICATIONS OF POLYMERS

The popularity of polymers resulted from their wide range of applications, in addition to advantages such as weight savings and ease of installation.

Polymer uses extend from the use of biomaterials for heart valve replacements and blood vessels, to windshields for fighter planes and automobile parts. Polymers are also used for clothing, floor coverings and garbage bags. They are also used for sports equipment such as golf clubs and protective helmets [8].

2.2 THERMOPLASTIC POLYMERS

Polymers are composed of a long chain of molecules, with a backbone of carbon atoms covalently bonded [15]. An example of the Carbon chain backbone with the circles representing the Carbon atoms is shown in Figure 2.2. The example depicts Polyethylene, which is composed of a Carbon atom, with two hydrogen atoms in a chain. Different combinations of atoms on the backbone produce different types of polymers, each with their own thermal, mechanical melt and corrosion-resistance properties [16].

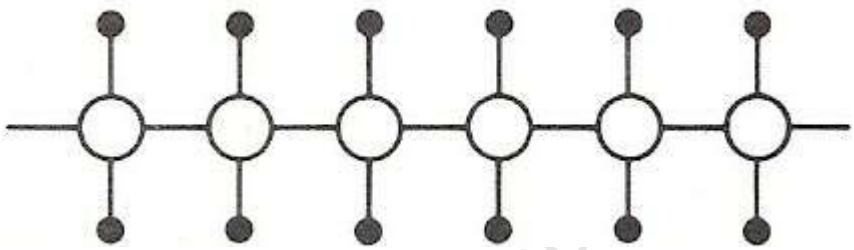

FIGURE 2.2: Carbon chain backbone, in this case Polyethylene [17]

Polymers are held together by two types of bonds:

- Strong Covalent Bonds – These bond the long molecules together to form the backbone of Carbon atoms
- Weak secondary bonds – These bond the "backbone" chain of Carbon atoms together

Thermoplastics are classed as linear polymers due to the absence of cross-linking of the polymer chains. On heating, the secondary bonds binding the molecules break, causing the polymer to melt and flow like a viscous liquid. This flow is possible due to the *absence* of the afore-mentioned melted cross-linking bonds. It is for this reason that linear-chain thermoplastics are the most commonly used polymers - as they can easily be formed. From being drawn into sheets, the molecules become aligned in the plane of the sheet, leading to an increase of modulus and strength.

Linear polymer molecules' are packed together in different configurations, with different molecular weights. Due to the packing configurations, and molecular weights, there is no sharp melting point for a thermoplastic. This causes the viscosity to fall over a range of temperatures; i.e.: over a decreasing gradient [15], which is elaborated on in the next Chapter.

Examples of thermoplastics [18]:

- PVC – Floor coverings, underground piping, rain coats
- Polycarbonate – safety helmets, lenses, light globes
- Polypropylene – bottles, luggage, packaging film

2.3 GLASS TRANSITION TEMPERATURE OF POLYMERS

The glass transition temperature (T_g), is the temperature at which the weak secondary Van der Waals, or Hydrogen bonds start to break down. These secondary bonds break down at a lower temperature than the primary bonds. Therefore the weaker bonds determine the polymers operating temperature. This ensures that the materials integrity is upheld [15].

An understanding of the glass transition temperature is best summarised by Ashby and Jones [15]:

> "Cumbersome side-groups, atacticity, branching and cross-linking all hinder crystallisation. In the melt, thermal energy causes the molecules to rearrange continuously. This wriggling of the molecules increases the volume of the polymer. The extra volume (over and above that needed by tightly packed, motionless molecules) is called the *free-volume*. It is the free-volume, aided by the thermal energy, that allows the molecules to move relative to each other, giving viscous flow. As the temperature is decreased, free-volume is lost. If the molecular shape or cross-linking prevent crystallisation, then the liquid structure is retained, and free-volume is not all lost immediately (Figure 2.3). As with the melt, flow can still occur, though naturally it is more difficult, so the viscosity increases. As the polymer is cooled further, more free

volume is lost. There comes a point at which the volume, though sufficient to contain the molecules, is too small to allow them move and rearrange. All the free volume is gone, and the curve of specific volume flattens out (Figure 2.3). This is the *glass transition temperature*, T_g. Below this temperature the polymer is a *glass*."

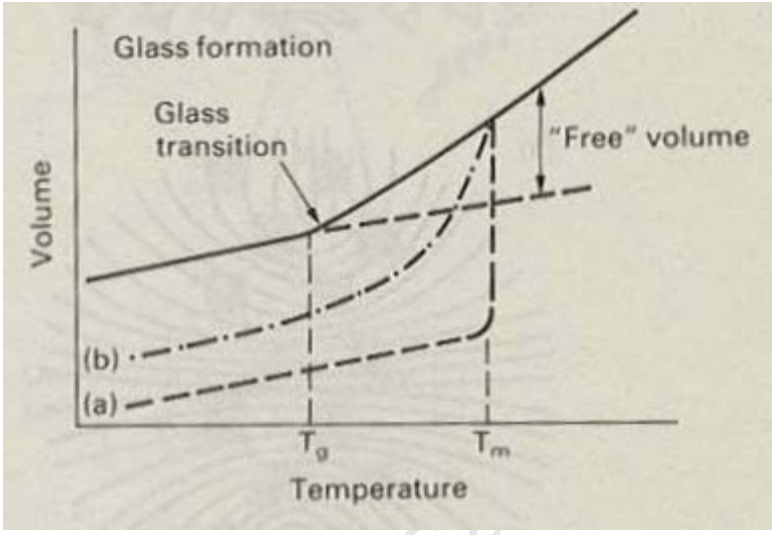

FIGURE 2.3: Graph showing the effect of temperature on free volume of polymers [15]

When the material is heated to the glass temperature, the secondary bonds sever, leaving the covalent bonds intact. This is turn causes the modulus to drop. When the temperature is below T_g, a polymer may have a modulus in the region of 3000 MPa; when the temperature rises above T_g, the modulus can drop to 3 MPa, or less. Secondary bonds also creep when loaded, causing a decrease in modulus. At temperatures above T_g, the secondary bonds sever completely. This causes linear polymers to become viscous liquids, and cross linked polymers to become rubbers. Conversely, at temperatures below approximately $0.75T_g$ polymers are considered as brittle [15].

The above paragraph suggests there is a sharp transition which occurs at T_g, when rather, the transition occurs over a temperature interval of some 10 Kelvin; i.e.: the performance of the material decreases as the temperature approaches T_g with a ruinous drop of three orders of measure [17], as shown in Figure 2.4. This ties in with the previously mentioned fact that there "is no

sharp melting point for a thermoplastic [15]". Figure 2.4 uses normalised temperature – that is, the ratio of temperature to the glass temperature.

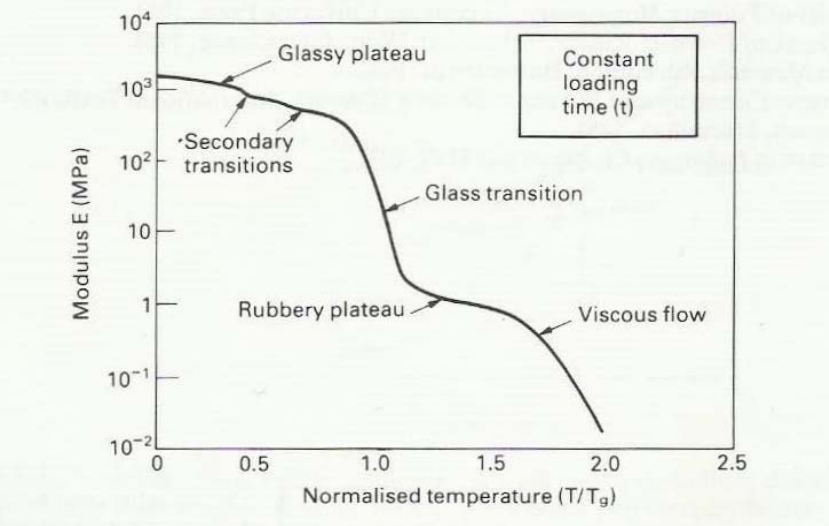

FIGURE 2.4: Graph showing effects of temperature on polymers [15]

In summary: A polymer's mechanical state, stiffness and strength properties are dependent on its molecular weight and operating temperature, that is, the operating temperature with respect to its glass temperature [15].

For uPVC, the glass transition temperature is in the vicinity of 80˚C [19, 20].

2.4 PVC

PVC stands for Poly-Vinyl Chloride, and is composed of carbon chains with chlorine atoms which are mainly atactic, that is, randomly arranged, as shown in Figure 2.5. Different variants of PVC are available, and it is a highly versatile material.

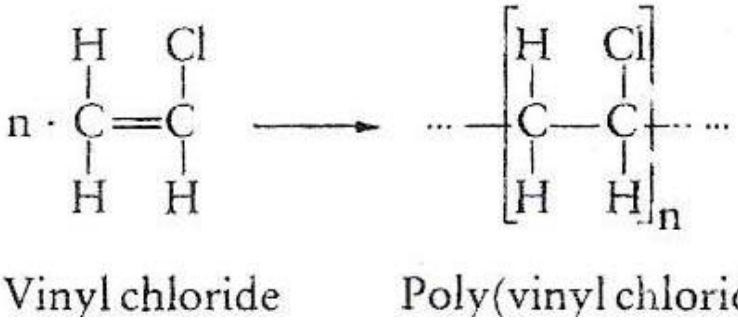

FIGURE 2.5: Illustration of the Carbon backbone for PVC [21]

2.4.1 HISTORY OF PVC

PVC was developed in the late 1920's in the United States [21]. In mining applications, steel pipes were the preferred water carrier, until the mid 1970's, when PVC piping was first introduced. A high level of reusability of PVC has been shown, with piping being reused after removal from mines [22].

In Australia, 70% of the PVC market is piping, while PVC is the choice in the domestic drain market 95% of the time [23].

2.4.2 uPVC

uPVC, or Un-plasticised PVC is PVC *sans* plasticiser. The plasticiser renders the stiff and brittle PVC into a soft and flexible material. It is the absence of this plasticiser which gives uPVC good chemical and weathering resistance, such as a resistance to ultraviolet light. In addition, uPVC is also self-extinguishing – an extremely important characteristic when used in flammable applications [17, 21, 24].

Although uPVC is tough and has high strength and creep resistance, it can experience FCG – Fatigue Crack Growth [25]. Table 2.1 shows some general properties of uPVC, as compared to other materials.

TABLE 2.1: General Properties at 25˚C for uPVC and other materials [24, 26]

	E	Yield Strength	Tensile Strength	Fracture toughness	Density
	[GPa]	[MPa]	[MPa]	[MPa$\sqrt{m}$]	[kg.m^{-3} * 10^{-3}]
uPVC	2.4 – 4.0		50 – 60	2.4	1.4 - 1.5
Steels	200 – 220	200 - 1800	350 - 2300	80 - 170	7.8 – 7.9
Al alloys	70	25 - 500	70 - 600	5 - 70	2.7 – 2.8

2.4.3 APPLICATIONS OF PVC

PVC is a widely used polymer. In the building industry, it is used for piping, gutters and blinds, while in the machine and equipment industry it is used for containers, pressure piping and ducting. PVC is also used in the electrical industry, in items such as cable and wire ducting and conduits, and in the packaging industry for bottles and beakers [21].

2.4.4 DISADVANTAGES OF PVC

While PVC is an extremely versatile and useful material, it is by no means a flawless material. The list below shows that there are limitations to PVC [12]:

- Can be damaged from striking impact of tools, or other mechanical means
- Chemicals, heat and sunlight can degrade and embrittle the Polymer
- Rough handling or abrasion can weaken PVC, and in some cases cause fracture.
- PVC is not a universal material. That is, there are limitations to its usability and some applications cannot utilise PVC as a material of choice.

2.5 FAILURE IN POLYMERS

Even though polymers have become increasingly more popular than metals, they are, as is any other material, prone to failure. In certain conditions, polymers will suffer from the fundamentals of fracture. Some of these fracture fundamentals include [27]:

- Toughness
- Fracture Mechanics
- Ductile to Brittle transition
- Fatigue
- Wear
- Stress-corrosion cracking

Material Failure may be regarded as the point at which the material is no longer able to perform the task required, due to the compromising of the materials integrity. Failure in pipes may be regarded as “the point at which leakage occurs”, that is, when the crack depth is equal to the wall thickness of the pipe [28]. Failure is a culmination of the progressive weakening of mechanical properties of the specimen, until failure occurs from mechanical fatigue [29].

There are three types of failure which can occur in a material [30]:

- Functional Failure – An item cannot perform its required function
- Irreversible damage without fracture – This can be further subdivided into necking, crazing, cracking etc
- Fracture – The material separates completely

Polymers can fail under various conditions. Thermoplastics generally fail through brittle failure, which will initiate from some of the following and other sources [30]:

- Defects
- Points of weakness in moulding
- Presence of chemical environment
- Fluctuating stress

Brittle failure is due to the pipe’s inability to absorb and distribute stresses through the matrix of a material. This has the effect of causing premature failure at stresses below the ductile or failure yield line [22].

2.6 CAUSES AND MODES OF FAILURE IN POLYMERS

Fracture can be defined as “the complete or partial separation of a critical member of the component under service loading that renders the component non-functional”. In polymers, there are two types of “irreversible deformation mechanisms” which can occur. The two mechanisms are [27]:

- Dilatational – crazes, voids and micro-cracks
- Non-dilatational – shear bands

2.6.1 CRAZING

A craze is “a slit-like micro-crack filled with highly orientated fibrillar materials” [27], as shown in Figure 2.6. They have a width of 1 to 2 μm, but can grow to several millimetres.

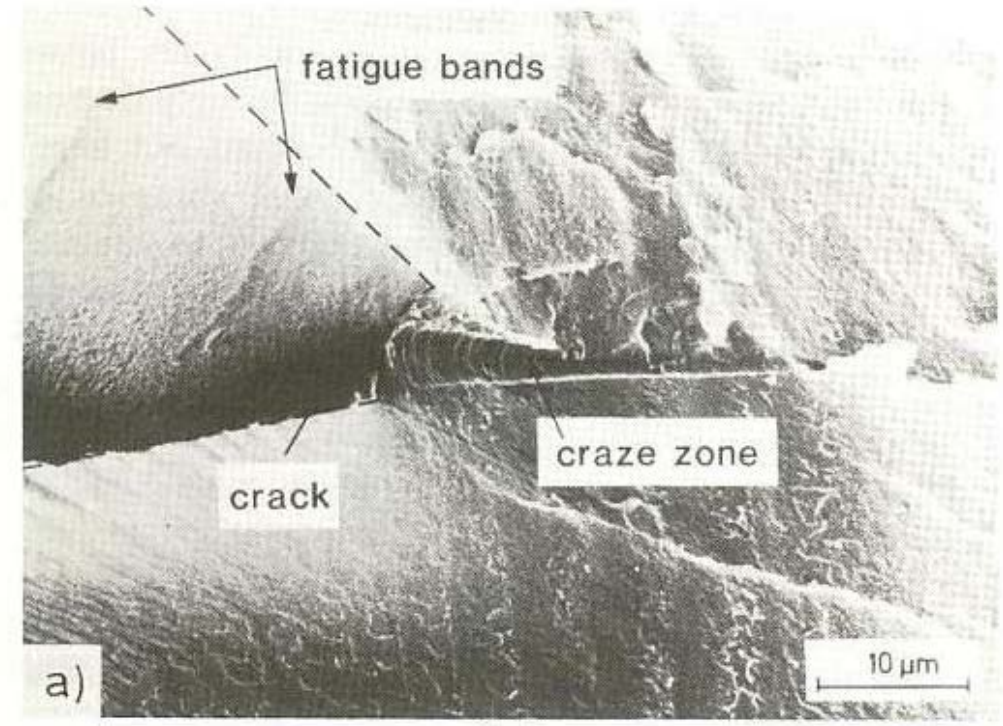

FIGURE 2.6: View into a crack opening and craze zone [31]

Crazing occurs in type I (normally brittle in tension) amorphous polymers such as Polystyrene (PS) and Poly Methyl Methacralate (PMMA). Amorphous refers to the non-crystalline state of a polymer that has a random molecular chain with no structural order [17].

Crazing is generally associated with brittleness although polymers with higher molecular weights have been shown to have greater resistance to fracture [27]. A high molecular weight means more entanglements per chain – therefore more stiff and brittle behaviour [17]. Crazing has also been known to occur under tensile-fatigue loading in semi-crystalline polymers, such as Polypropylene (PP), and in type II (normally ductile in tension) amorphous polymers, such as Polycarbonate (PC).

In brittle materials, such as PS, PMMA and uPVC, crazing tends to be the mechanism of failure [27].

2.6.2 FLAWS AND VOIDS

Pipes and fittings will have inherent manufacturing flaws when produced, and installations can also cause significant damage to either the pipe or fittings. PVC is an example of this. It is a brittle material which can easily be damaged, either during transportation, installation or use [12].

Strength can vary through a length of pipe, and this can be due to a variation in molecular structure during manufacture. Voids also contribute to weakening, and are often more prevalent in fittings than pipe lengths – this is due to the more complex structure of the fittings than the pipes. Generally, pipes are assumed to meet manufacturing safety standards, and are therefore not further inspected by the pipe operator [12].

Pipes manufactured in the UK in the 1960/70's were found to be failing. An investigation into these failures revealed the failures were due to extrusion processing problems and operational conditions. After the causes of the failures were understood, uPVC pipe production methods were improved by understanding the importance of the production process and the formulation of the uPVC [22].

If a brittle material has small defects or notches in the material, it can lead to unpredictable crack growth, ultimately leading to failure.

2.6.3 STRESS WHITENING

Yielding in polymers, as mentioned above, occurs by crazing. Within the voids of the crazes, so-called "stress whitening" arises. Crazes are associated with irreversible deformation and fracture of polymers, and lead to stress whitening [27]. Stress whitening is indicative of high stress failure, and therefore occurs in high stress zones, with plastic deformation also occurring [25].

2.6.4 DEGRADATION BY HEAT OR LIGHT

Polymers can degrade from exposure to heat or light. This type of degradation involves molecular weight reduction by several means. Following degradation, surface embrittlement causes micro-cracking, leading to crack initiation, and ultimately crack propagation.

PVC is susceptible to degradation from heat or light [27], and is one of the most sensitive plastic weathering and ageing effects, either natural or artificial. These effects also contribute to a loss in mechanical properties such as resistance to fracture [16]. This susceptibility led to a recommendation by the Plastics Industry Pipe Association (PIPA) of New Zealand not to expose PVC piping to direct sunlight, as this can lead to embrittlement of the pipe material. It is for this reason that pipes should not be stored for periods of longer than twelve months without sufficient cover in the form or Hessian sacks or other means of UV protection [32].

Material toughness reduction from photo degradation is generally only evident when a stress is concentrated on the exposed material, as this is the area where the energy required for crack initiation is less than for the unexposed material. Weathering damage is more acute in dry, desert regions, than in a tropical climate, given equivalent solar energy and temperature conditions. While the decrease in mechanical properties is possibly more serious for PVC, colour changes and surface ‘chalking’ are some of the other by-products of photo degradation [16].

2.6.5 ENVIRONMENTAL STRESS CRACKING

Environmental stress cracking (ESC) often poses unanticipated problems in service by causing embrittlement in plastic materials. This failure mechanism becomes apparent in specimens in contact with an aqueous environment (either a liquid or vapour form) together with an external or residual stress. The combination between the stress and aggressive medium can cause

premature failure. These failures often occur in conditions where failure to the material is unlikely if the stress or environment were removed [16].

Therefore, as a means of preventing ESC in service, at least one of the three factors causing cracking (stress – environment – material) needs to be removed to ameliorate the problem. For example, if operating conditions are a high stress and an aggressive environment, a suitable material needs to be selected that can survive the operating conditions.

2.7 DESIGNING FOR FATIGUE

A mechanism of failure frequently encountered is fatigue. Fatigue is defined as “the initiation and progressive growth of a crack, with each stress cycle, until failure occurs” [33], or “the failure resulting from the crack growth initiated by naturally occurring flaws in the matrix under repeated loads accompanied by relatively small deformations”. Every material may be regarded as having a finite fatigue life. Fatigue life may be regarded as “the number of cycles to break a specimen into two pieces at a particular stress for stress-controlled or at a particular strain for strain-controlled tests” [29].

There are two categories of fatigue:

- Static fatigue or creep rupture – Failure occurs after a period of steady load
- Dynamic fatigue – Failure occurs from a fluctuating stress

There are two methods for design taking fatigue into account. These are the traditional Stress-Cycles (SN) approach, and the Fracture Mechanics (FM) approach. While the SN approach is somewhat straightforward, the FM approach involves other factors such as stress intensity K and fracture toughness of the material.

2.7.1 SN DESIGN APPROACH

The SN approach involves reading graphs showing S (stress) versus N (number of cycles) off a graph. The relationship between stress and number of cycles is an inverse one; i.e.: as the stress increases, the number of cycles until failure decreases. A typical life cycle graph is shown in Figure 2.7.

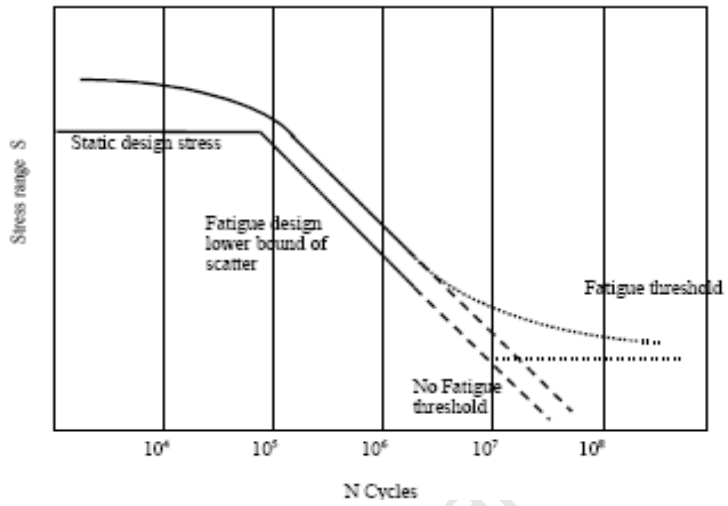

FIGURE 2.7: Typical SN life cycle graph [33]

The fatigue limit, or fatigue threshold shown in Figure 2.7, is the stress below which fatigue, and therefore failure, does not occur. The cycle count of 10^7 is an arbitrary choice to use as a means of comparison between materials [34]. The SN curve is read by relating a stress on the curve to a corresponding number of cycles, or relating a cycle count to the corresponding stress value on the curve. While the SN method is a quick means for calculating fatigue life for a material, it is often only applicable for the particular design condition for which the material was tested [35].

A fair amount of scatter is experienced in SN graphs, as shown in Figure 2.8. Fatigue life is affected by the crack initiation site, which can be at somewhat of an arbitrary point, and which subsequently affects the numbers of cycles to failure [29]. Other factors can also contribute to the scatter phenomenon [33]:

- Test method
- Specimen geometry
- Quality of specimen / test material

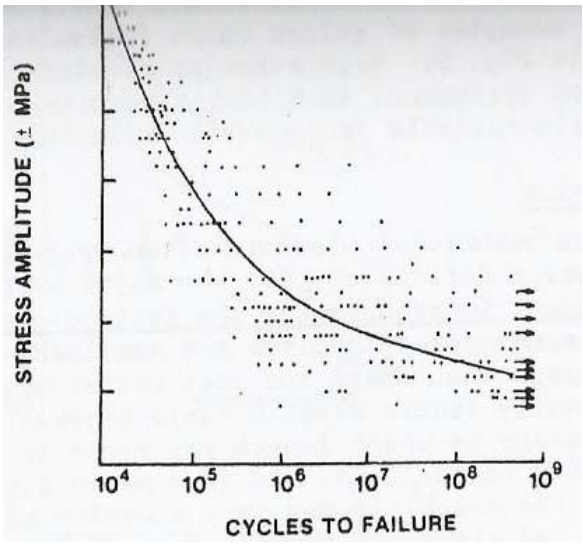

FIGURE 2.8: SN Test curve showing experimental scatter [35]

2.7.2 FRACTURE TOUGHNESS AND ITS ROLE IN DESIGN

Toughness may be defined as the property which provides a measure of "the resistance of the material to the extension of cracks" [11]. Every material has a specific fracture toughness, or resistance to crack growth. This is dependent on factors such as the mode of loading, chemical environment, material microstructure, test temperature and state of stress [36]. The different modes of loading and their designated nomenclature are as follows:

- I – Crack opening
- II – Sliding (in plane)
- III – Tearing (out of plane)

The fracture toughness aspect of this thesis focuses on the mode I, crack opening case. That is, when fracture toughness in reported, it is with the designation K_{IC}, where 'I' is the mode of crack propagation, and 'C' is the critical toughness value.

Fracture toughness plays a role in assisting lifetime predictions, which is further explained in Sections 2.7.3 and 2.7.4.

2.7.3 FM PARIS APPROACH

Another, and more accurate means of predicting failure and lifetime, is by utilising the methods of Fracture Mechanics (FM). FM provides a "quantitative relationship between stress, flaw size and toughness [37]". These three factors are inter-related to each other by use of the so-called "Triangle of integrity", which links the three variables together, as shown in Figure 2.9.

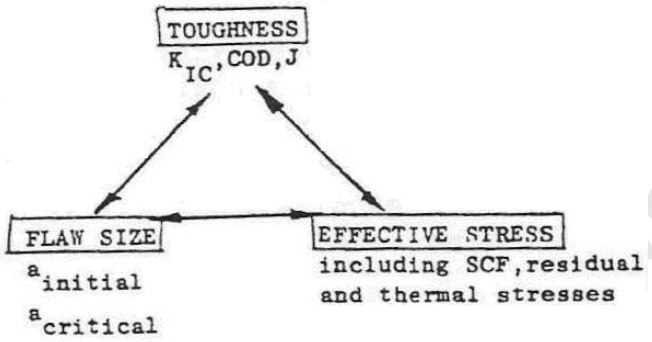

FIGURE 2.9: Triangle of integrity for FM [37]

Linear Elastic Fracture Mechanics (LEFM) shows the relationship by the three variables in the equation:

$$K = \sigma Y \sqrt{\pi a} \qquad \text{[Equation 2.1]}$$

Where:

- K = stress intensity factor. When K approaches and exceeds K_{IC}, the material fracture toughness, fracture occurs.
- σ = total effective stresses – including stress concentration factors, residual stresses and thermally induced stresses
- Y = geometrical correction factor
- a = flaw size

LEFM is relevant for situations where the material exhibits small crack tip plastic zones. In the situations where there is greater ductility and the crack tip plastic zone is not small compared to the crack or sample dimension, Elastic Plastic Fracture Mechanics (EPFM) is used.

Toughness characterisation in EPFM is CTOD, or COD – Crack (Tip) Opening Displacement, often depicted by δ. This is "the measure of the separation of the two faces of a fatigue crack under load due to blunting at the tip of the crack, just before additional tearing or rupture occurs [37]". This CTOD value can then be applied to a similar triangle of integrity relating stress and flaw size, as for LEFM, to yield a "fitness for purpose" analysis. This is most easily achieved, using codified standards – for example, PD6493 [38].

2.7.4 PARIS EQUATION AND LIFETIME PREDICTION

As mentioned in Section 2.7.3, the Fracture Mechanics design method allows for a prediction on lifetime, based on material characteristics, and taking into account flaw sizes and the stress to which the material is exposed. The lifetime prediction is made possible by using the Paris equation, postulated by Paris, Gomez and Anderson in 1961 as reported by Suresh [36]. This is done by characterising the material fatigue behaviour from a log-log graph of da/dN vs. ΔK, as shown in Figure 2.10.

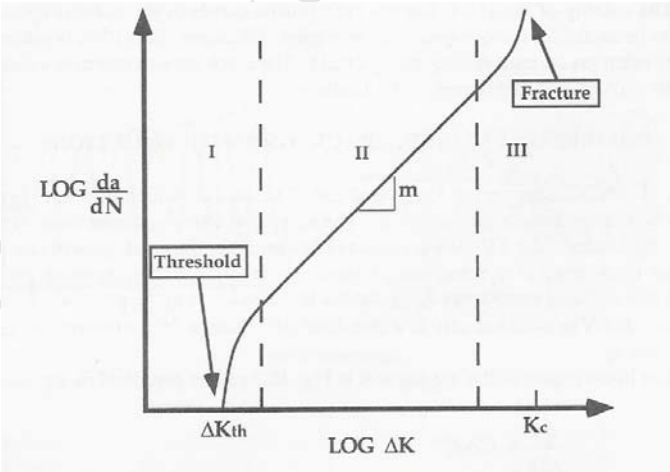

FIGURE 2.10: Graph of da/dN vs. ΔK [39]

The graph is characterised by three regions [40]:

- I – Near threshold regime below which crack growth will not occur.
- II – Crack growth regime
- III – Crack growth rapidly approaches fast fracture.

The second regime is the important one with regards to predicting lifetimes, as it contains data for constant and steady crack growth propagation. Paris *et al* [36] proposed that crack growth be characterised by the equation:

$$\frac{da}{dN} = C\Delta K^m \qquad \text{[Equation 2.2]}$$

This equation relates the crack growth rate (da/dN) with the material characteristics and resistance to crack growth in terms of the cyclic stress intensity amplitude, ΔK. By substituting Equation 2.1 into Equation 2.2 for the ΔK variable, and integrating each side of the equation, between initial and critical flaw limits, a means of predicting lifetime is provided:

$$N_f = \int_{a_i}^{a_{critical}} \frac{da}{C(Y\Delta\sigma\pi)^m a^{m/2}} \qquad \text{[Equation 2.3]}$$

Where:

- N_f = number of cycles until failure
- a_i = initial flaw size
- $a_{critical}$ = critical flaw size at failure

A graph of da/dN for a range of materials, including PVC is shown in Figure 2.11. This plot shows the range of ΔK for PVC, in relation to other materials. The K_{IC} value, for PVC is, according to Vernon John in his book "Introduction to Engineering materials [24], in the region of 2.4 MPa√m.

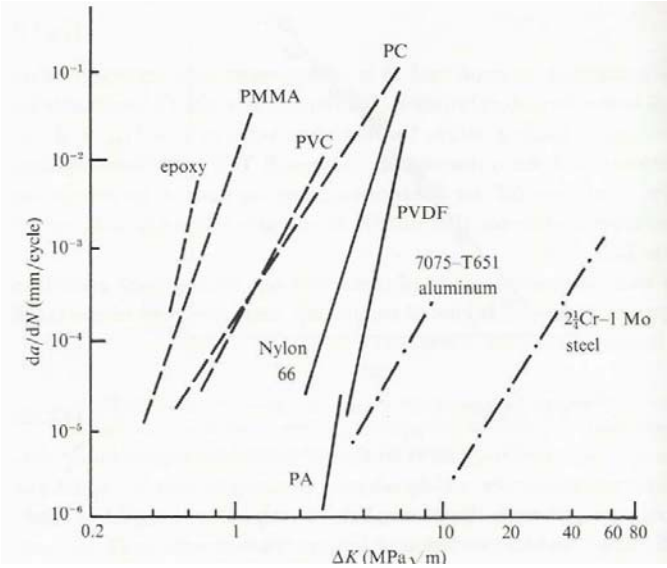

FIGURE 2.11: ΔK range of PVC compared to other materials [36]

2.8 PREVIOUS STUDIES RELATING TO PVC FATIGUE

Literature data was difficult to obtain relating specifically to PVC fatigue and it appears that there is a lack of data available. This lack of data is especially apparent with regard to the temperature effect on PVC fatigue. A few of the results to be found are presented in this Section, along with graphs showing trends from literature.

2.8.1 SN PREVIOUS STUDIES

EARLY RESEARCH

In 1972, Robert Hucks [41] ran fatigue tests on 2 and 4 inch pipes, cycling at a test frequency of approximately 0.4 Hz. A base pressure of 0.34 MPa and a range of peak stresses were used, at what was assumed to be room temperature. The reproduction of Hucks' data is shown in Figure 2.12.

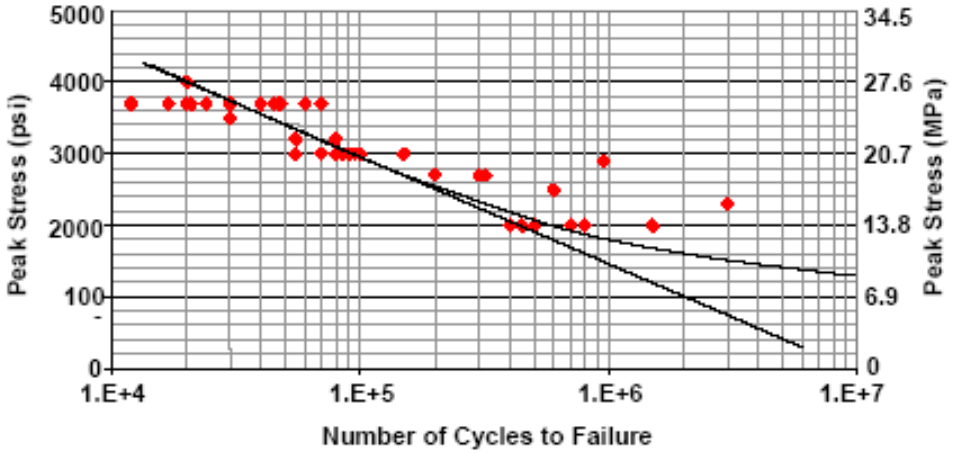

FIGURE 2.12: Reproduction of Hucks' data [42]

In 1975, Herbert W. Vinson [43] conducted tests on 152 mm PVC pipes, cycling from a hoop stress of between 2.76 MPa and 3.45 MPa up to a peak hoop stress of 44 MPa. Again, the assumption is made that this testing was conducted at room temperature (~20˚C), as there is no mention to the contrary. His data is shown in Figure 2.13. He also derived an equation for a straight line fit to his data (on a log-log scale):

$$N = (5.05 * 10^{21})(\sigma_{peak})^{-4.906} \qquad \text{[Equation 2.4]}$$

Where σ_{peak} is measured in psi for this equation.

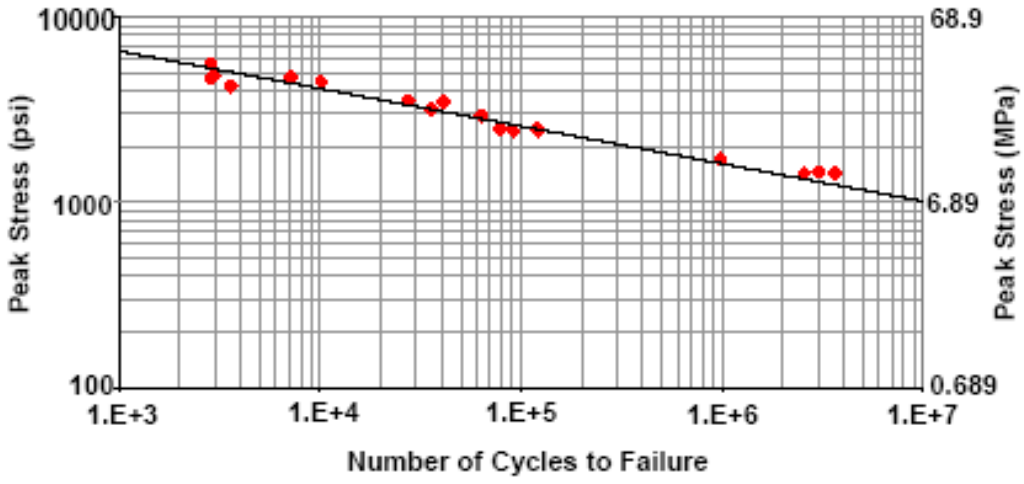

FIGURE 2.13: Reproduction of Vinson's SN fatigue data [42]

Vinson's equation was the standard method for predicting fatigue life in PVC piping and was used in design for many years. However, his method was found to be inconsistent with the typical fatigue failure prediction methods used for other materials.

Some of these studies by Hucks [41], Vinson [43] and others have been reviewed by Jeffrey, Moser and Folkman [42], which includes allied PVC studies by Bowman [44], Moser [45] and Marshall *et al* [46].

MARSHALL, BROGDEN AND SHEPHERD

In 1998, Marshall, Brogden and Shepherd [46] ran tests on different types of PVC pipes in the UK, studying the effects of "surge and fatigue". They tested pipes under cyclic hydraulic conditions at room temperature (~20˚C). Their data is reproduced in Figure 2.14.

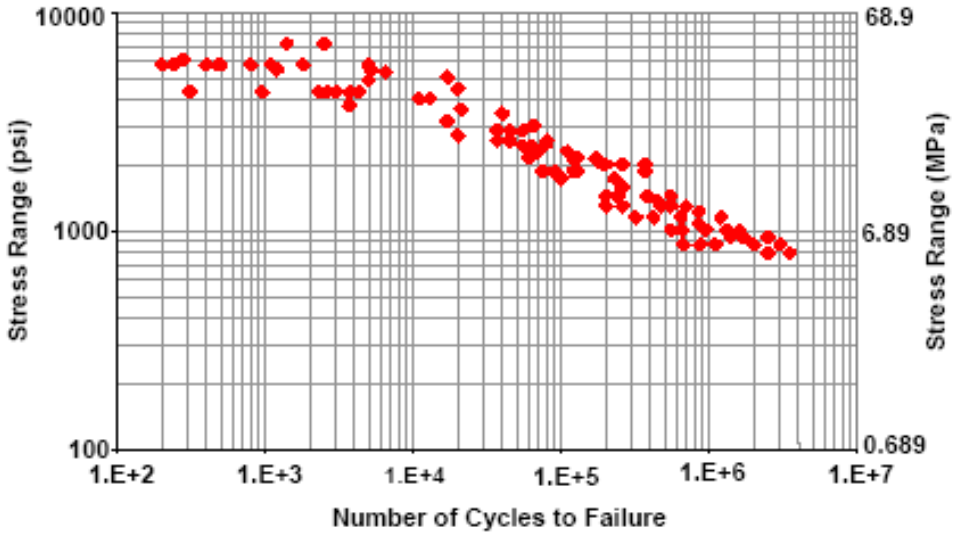

FIGURE 2.14: Reproduction of Marshall *et al* data [42]

JOSEPH AND LEEVERS

Joseph and Leevers [25] conducted SN fatigue tests to failure on 100 samples of pipes in a testing medium of 20˚C±0.5˚C and frequency of 1 Hz with an approximately trapezoidal waveform. The specimens used were sections of 445 mm length, and nominally 60 mm diameter. Tests were run in

a hydraulic cyclic pressuring rig, which allowed internal pressurization of the pipes.

Failure in this case was taken as any leakage, and it was noted that failure always resulted from an axial crack. Within the sample batch of 100, there were pipes manufactured by four different UK manufacturers. The tests formed part of an investigation into the failure of plastic pipes, with the results to be used in the design and installation of pipes. The SN curve generated by Joseph and Leevers is shown in Figure 2.15.

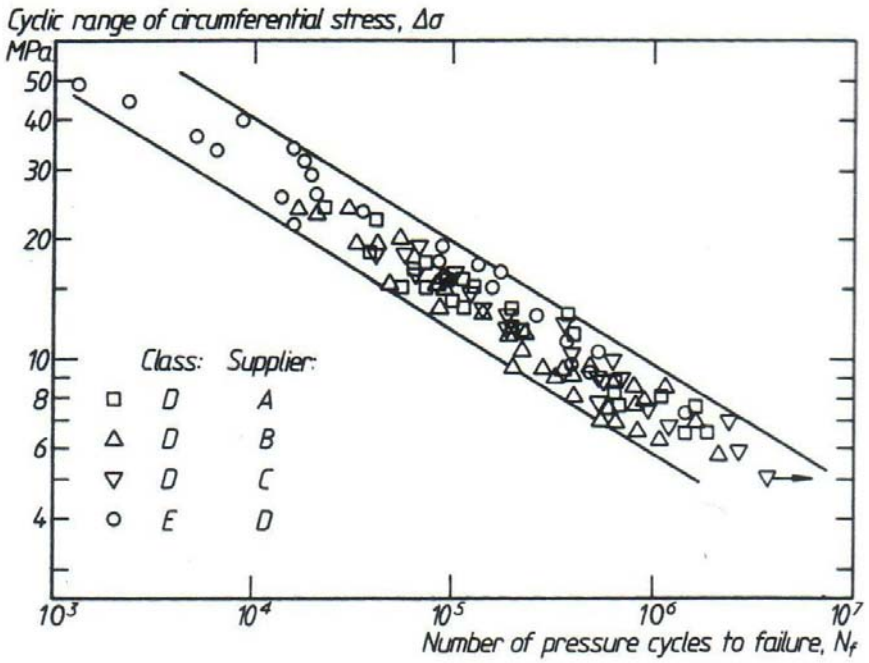

FIGURE 2.15: SN Graph for failure of uPVC at 20˚C from Joseph and Leevers [25]

As can be seen, the results can be grouped into a corridor, with the results generally of a linear fashion. As the tests were carried out at ambient temperatures (20˚C) they can be assumed to represent typical fatigue behaviour of uPVC at ambient temperatures.

Failure modes in the tests varied with stress levels. At levels of 33 MPa and above, failure occurred after a few thousand cycles with “extensive stress whitening and plastic deformation”. For levels below 33 MPa, crack growth progressed from an initiation point to the outer surface, where leakage then

occurred, resulting in failure. At stresses of between 15 MPa and 23 MPa, they reported multiple crack initiation sites.

COLLECTIVE DATA FROM PREVIOUS STUDIES

Combining the data from Vinson [43], Hucks [41], Marshall *at al* [46] and Joseph and Leevers [25], and plotting them on the same set of axis, Figure 2.16 is produced. For Marshall *et al*, a hand-drawn trend line encompassing lower and upper limits was used for reporting the data, in a similar fashion as that for Joseph and Leevers. However, these limits were only consistent up to approximately 25 MPa, as can be seen in Figure 2.14 [42].

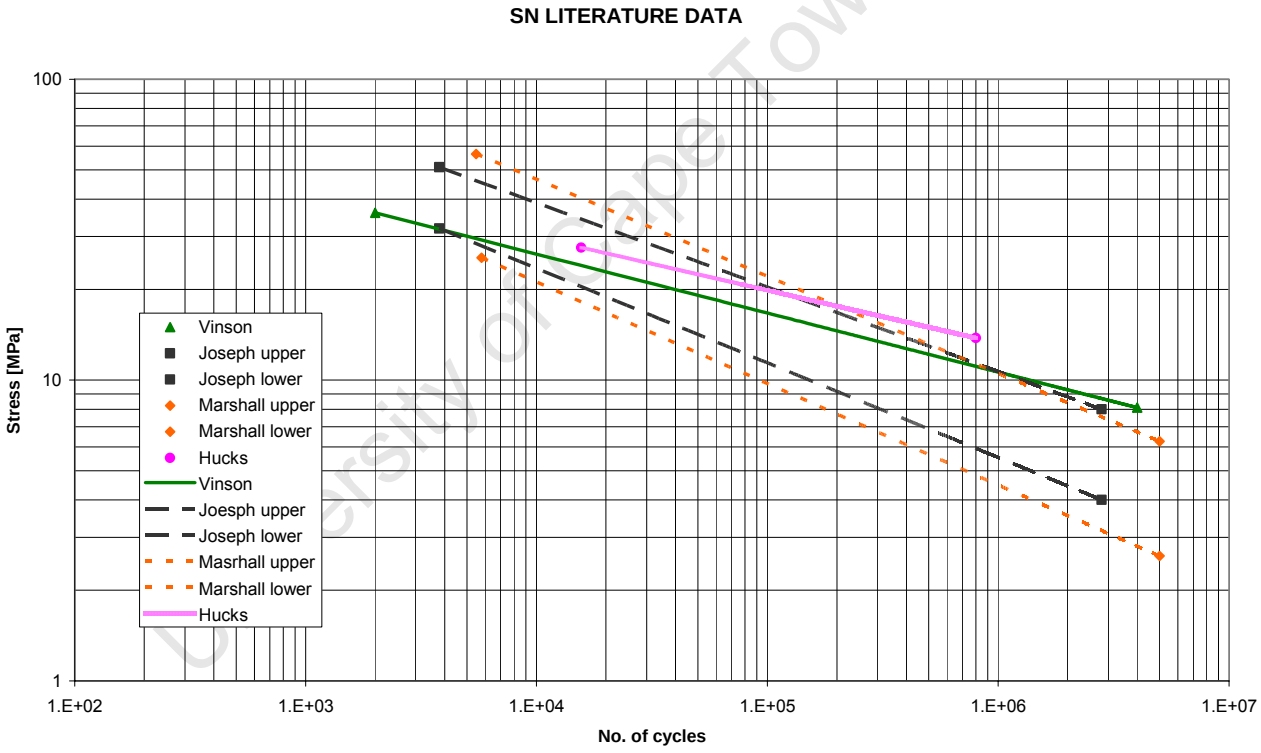

FIGURE 2.16: Composite SN graph of previous studies [42, 25]

The plots for Vinson, Hucks, Marshall *et al* and Joseph and Leevers all conform to the same general trend. Figure 2.16 also represents results of tests 20˚C. There were however, very few studies of PVC fatigue at temperature, and these are mentioned below.

WHITTLE AND TEO

Whittle and Teo [47] conducted a series of fatigue tests by rotational bending on PVC-M and PVC-U pipes. PVC-M is Modified-PVC, which was introduced in pressure piping in Australia in the late 1990's. One aspect of this study was to determine the difference in resistance to crack growth in these two PVC materials at temperatures of 20˚C, 30˚C and 40˚C.

The two batches of specimens were produced from extruded pipes, which were heated to 120˚C and then flattened and cooled to room temperature. These sheets were then turned to rods of 10 mm diameter, and 130 mm in length. A sharp circumferential notch was cut 90 mm from one end, reducing the diameter at the notch point to 7.5 mm. The rods were mounted in a rotating bending machine with a variable speed motor, and were then subjected to a bending moment. For the 20˚C tests, an electric fan was used to keep the temperature constant, while for the 30˚C and 40˚C tests, the bending equipment was placed in an air-circulating oven. Tests were conducted at a frequency of 3 Hz.

Even though it was found that the two materials (PVC-U and PVC-M) exhibited near identical cyclic fatigue behaviour, it was found that there was a temperature effect on the material. As shown in Figure 2.17, tests conducted at 20˚C, 30˚C and 40˚C showed a decrease in performance in both the PVC-U and PVC-M. An increase in crack growth rate was also observed for increasing temperatures. The temperature effect was more noticeable from the 20˚C to 30˚C range than that for the 30˚C to 40˚C.

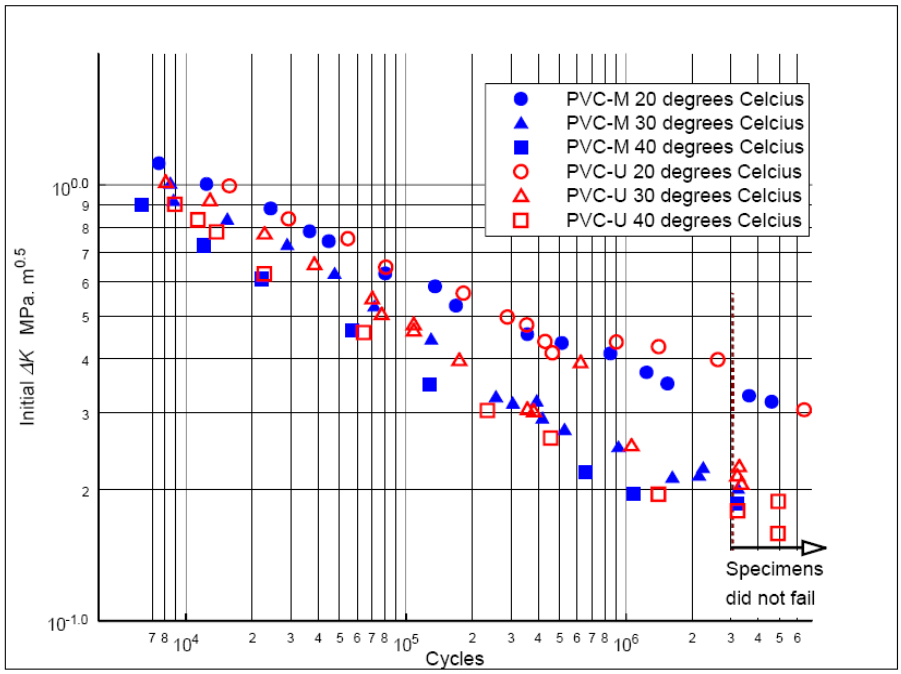

FIGURE 2.17: SN curve showing decrease in performance over temperature ranges [47]

The parameters chosen for the representation of data in Figure 2.17 with ΔK vs. Cycles, as opposed to Stress vs. Cycles is both unusual and non-conventional. It is for this reason that the data was not included with Vinson, and Joseph and Leevers in Figure 2.16.

TAIT AND PRESS

R.B Tait and J Press [1, 48] conducted preliminary tests in early March, 2006 (as a limited part of a failure analysis) to determine if there was a temperature effect on fatigue, in response to the underground water-carrying PVC pipe failures in the Madinat Jumeirah resort, mentioned in Chapter 1. Testing from samples of underground pipe samples, was undertaken at temperatures of 20˚C, and also at what was approximately 45 – 48 ˚C. Test specimens comprised sections of pipe 110 mm long, similar to those shown in Figures 3.1 and 3.2, and discussed in the next Chapter. These pipes were fatigued under compression until failure.

They reported that fatigue cracking was found to always occur in the submerged half of the pipe during 45˚C tests, and that fatigue life was

reduced at the higher (45˚C) temperature. The results of this very limited testing, and how they compare to Vinson [43] at 20˚C is shown in Figure 2.18.

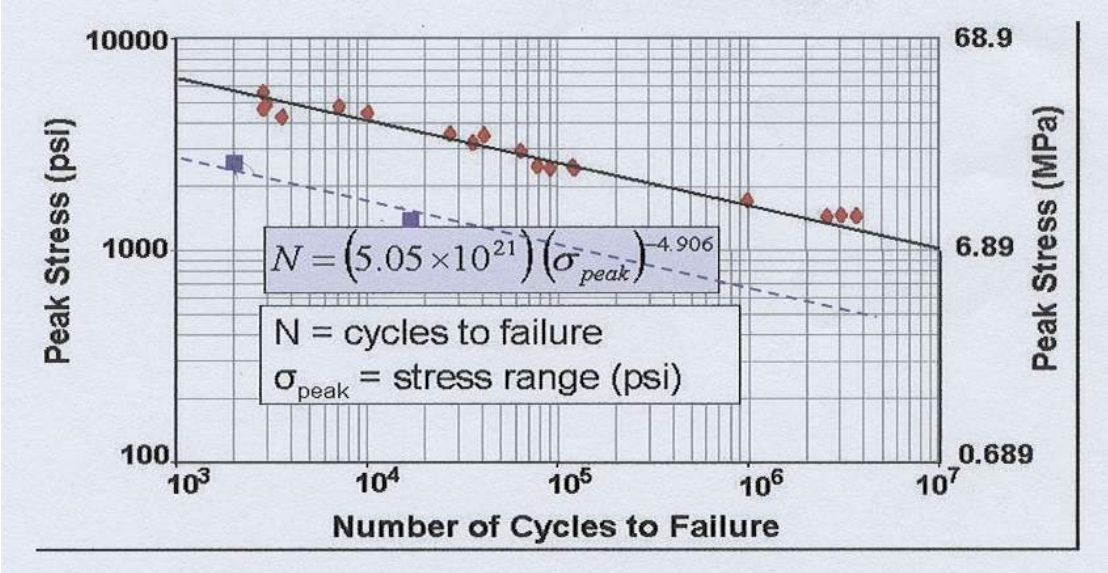

FIGURE 2.18: Temperature effect on fatigue life of uPVC pipes from limited tests at 48˚C by Tait and Press [1] compared to Vinson (20˚C) [43]

2.8.2 PARIS RELATED PREVIOUS STUDIES

MADDOX AND MANTEGHI

Maddox and Manteghi [28] conducted fatigue tests on 22 bend SENB specimens, manufactured from flattened 10 mm thick pressure pipe. Of the 22 specimens tested, six were tested in air, while 16 were tested in three different water environments; distilled water (pH = 7) and chlorinated water (pH = 5.5 and 8.5). The air temperature was measured at between 19 – 23 ˚C, and the water temperature was maintained between 18.5 – 21 ˚C. Tests were conducted with a span of 160 mm, and a frequency of 5 Hz. R-ratios of between 0.1 – 0.5 were used, and for calculation purposes, a fracture toughness of 2.5 MPa√m was used. It should be noted that SENB, and not Compact Tension specimens were used for these tests.

Specimens were made from flattened 10 mm thick class 20 uPVC piping. This was accomplished by heating the cut pipes in an over at 115˚C for 15 min, and then flattened between metal plates. This was similar to the test specimen method employed by Whittle and Teo [47].

Results from this study showed:

- There was nominally no difference in crack growth between the air and the three different water environments
- The R-ratio did not affect crack growth rate in the ranges 0.1 – 0.9.
- The highest crack growth data was obtained in air and the corresponding values for m and C were 2.80 and 1.26 * 10^{-7} respectively.

A da/dN vs. ΔK curve showing the test values and values from literature is shown in Figure 2.19. The other references included in Figure 2.19 were used for comparative purposes using different R-values in the study by Maddox and Manteghi [28, 50, 51].

A study by Kim *et al* [49], studied the fatigue crack growth in uPVC in water at a test frequency of 5 Hz and R-values of 0.03 to 0.5, similar to the test procedure by Maddox and Manteghi [28]. The Kim *et al* tests covered stress intensities of between 0.5 – 4 MPa$\sqrt{m}$. Maddox and Manteghi compared these results to their own, and found that there was “good agreement” between the two sets of data. The graph of Maddox and Manteghi with fatigue crack propagation results compared to that of Kim *et al* for fatigue *in water* is shown in Figure 2.20.

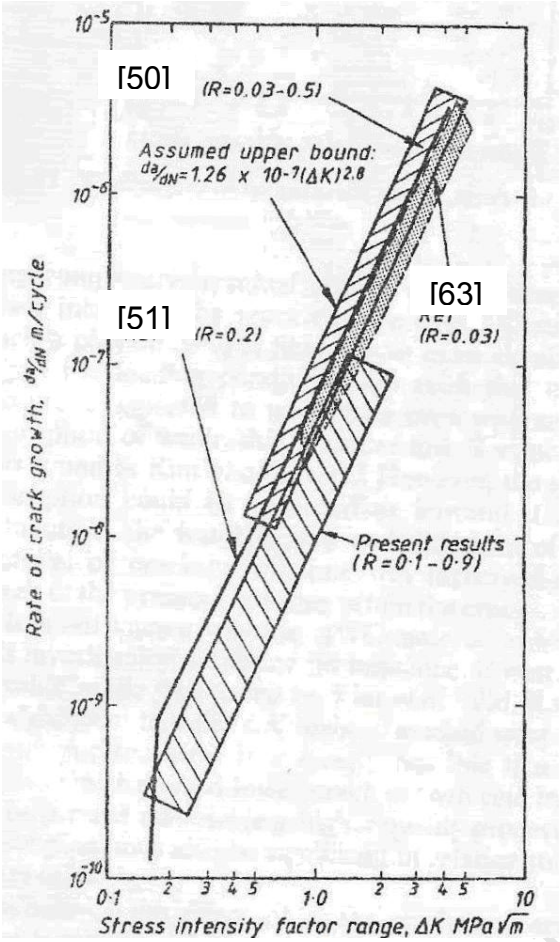

FIGURE 2.19: Maddox and Manteghi test results in air compared to literature [28]

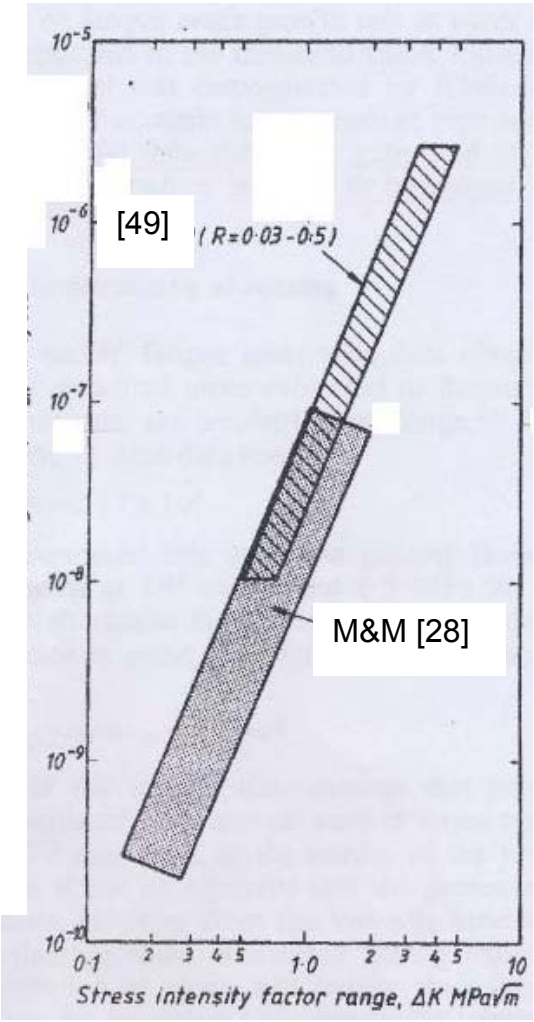

FIGURE 2.20: Maddox and Manteghi fatigue results with Kim *et al* [28] *in water*

JOSEPH AND LEEVERS

Joseph and Leevers [25] found that Paris parameter values for C and m were $10^{-7\pm0.25}$ and 2.75 respectively for tests at 20˚C. These tests were performed on flat, rectangular plates, with the crack growing parallel to the leading edge.

2.8.3 FRACTURE TOUGHNESS VALUES IN LITERATURE

As mentioned above, Maddox and Manteghi [28] used a fracture toughness of 2.5 MPa√m. Kim *et al* [50] reported a K_{max} that was as high as 5 – 6 MPa√m,

although for short term fracture toughness tests, a toughness value of 2 MPa√m is believed to be more applicable [51].

2.9 SUMMARY

Chapter 2 has looked briefly at polymers in general and PVC in particular, their role in everyday life and the advantages they bring to the world at large, in both the engineering and non-engineering sense. Glass transition temperature, and the effect of operating at temperatures near or at the T_g were also shown. It was noted that the T_g for uPVC is approximately 80˚C.

Failure in polymers and the modes of failure were presented. Modes of failure included, to name a few, crazing, stress whitening and environmental stress cracking. Fatigue was a mode of failure applicable for polymers, and fatigue was expanded on to show the methodology for designing for fatigue. Those methods were the traditional SN, and more definitive approach of FM. A means of predicting fatigue lifetime using FM and fracture toughness was also presented.

Finally, research pertaining specifically to PVC fatigue obtained from literature was presented. For 20˚C tests, the experimental procedures and conditions (where available) and published data of Hucks [41], Vinson [43], Marshall *et al* [46] and Joseph and Leevers [25], who had performed SN tests on PVC piping, were presented. Their data was also collectively combined on one set of axis, with all the data apart from Hucks conforming to a trend. The data of Whittle and Teo [47], and Tait and Press [48] who had performed SN tests on PVC at temperature, and had found that there was a temperature effect which caused a decrease in fatigue life over the range of temperatures, were also presented.

The Paris fatigue data of Maddox and Manteghi, as well and Joseph and Leevers for PVC at 20˚C were presented, as well as various values for fracture toughness, K. Both Maddox and Manteghi [28] and Joseph and Leevers [25] reported m and C values in the region of 2.75 – 2.80 and 10^{-7}

respectively. Fracture toughness values reportedly varied from 2 MPa√m [51] to as high as 6 MPa√m [50], although for calculation purposes, Maddox and Manteghi [28] used a fracture toughness value of 2.5 MPa√m.

The issue of any contribution to cracking by “static fatigue” mechanisms (of the da/dt vs. K – SCC – type) has not been considered as no references to this have been found, but this topic is worth of further study.

As the literature data was relatively meagre for the 20˚C fatigue data (both SN and FM), and especially so for 45˚C, there was clearly a need to extend the understanding of fatigue of PVC at 20˚C and 45˚C. In addition, fracture toughness values for uPVC were required to facilitate producing a means of lifetime prediction given certain scenarios which could be experienced in real-life circumstances.

CHAPTER 3. EXPERIMENTAL DETAILS

This Chapter contains the details regarding testing objectives, experimental materials, test procedures and analysis of the test data. The setup of each group of testing is discussed, as well as the loads that were used for each group of testing. Finally, the process for calculating the necessary final values is presented.

3.1 INTRODUCTION AND OBJECTIVES

As shown in Chapter 2, there is a dearth of research which has been carried out on the subject of uPVC fatigue at elevated temperatures. This therefore presented an opportunity for experimentation on this subject with a view to contributing to the understanding of fatigue of PVC at higher temperature.

In addition, from a practical engineering perspective, a means of predicting fatigue lifetime was required, and this assessment requires reliable backup data in the form of Fracture Toughness values, to determine critical flaw size in the life prediction integration process.

Where possible, some experimental data for this material was available but it was decided to complement this with further experimental work to accommodate the material types and crack orientation.

3.1.1 INTRODUCTION

Fatigue life characterisation, which then facilitates fatigue life prediction, can be accomplished by two methods – a traditional SN (Stress vs. Number of cycles) graph, and a Fracture Mechanics approach which involves the derivation of the

Paris equation used for lifetime prediction. These methods were discussed in Section 2.7.

3.1.2 CONVENTIONAL FATIGUE – SN CHARACTERISATION

Tests were conducted to generate data to populate an S-N curve type characterisation showing the inverse relationship between the stress level (S), and the number of cycles until failure (N) on a log-log scale. The intention was to generate a curve similar to that shown in Figure 2.7, Section 2.7.1. The SN curve is a traditional design approach, and an approach which can readily supply fatigue answers to a given load or lifetime scenario. For example, if a design engineer wishes to know how long a specimen will last at a specific stress level, he/she can trace the number of cycles value corresponding to the given stress level. This is an easy but approximate means of life prediction, but is not entirely accurate due to the large amount of scatter prevalent in SN curves (Section 2.7.1).

In the SN curve characterisation, the normal approach is to record the number of cycles to complete rupture of the sample. In this present case involving crack development in pipes, it was possible to record the number of cycles to first appearance of a crack, and in this experimental programme this was recorded as well. This was not always possible, however, especially at high stress levels, where catastrophic failure followed shortly after crack development.

3.1.3 FATIGUE FROM A FRACTURE MECHANICS PERSPECTIVE

The Paris equation generated from fatigue testing is a more accurate means of determining a specimen's lifetime, utilising material characteristics, as discussed in Section 2.7.4.

The so-called “Paris equation” to be generated was:

$$\frac{da}{dN} = C\Delta K^{m} \qquad \text{[Equation 3.1]}$$

Where

- da/dN is the rate of crack growth per number of cycles [m/cycle]
- C and m are constants (influenced by material microstructure, environment, test temperature and load ratio, R [36])
- ΔK is the stress intensity [MPa$\sqrt{}$m]

3.1.4 FATIGUE AS A FUNCTION OF TEMPERATURE

Tests were conducted at 20˚C and 45˚C to determine the effects of temperature on the uPVC material. 20˚C was used as it was a design recommended temperature, and 45˚C was used as the effective operating temperature [1]. As reported in Section 2.3, it is believed there is a temperature effect on polymers which causes a decrease in performance as the operating temperature approaches that of the glass transition temperature of the polymer. It was necessary to quantify if indeed there was a discernible decrease in fatigue performance as a function of temperature.

3.1.5 LIFE PREDICTION AND FRACTURE TOUGHNESS

As shown in Section 2.7.4, fatigue life prediction utilises the Paris equation, levels of cyclic stress and stress spectrum as well as initial and critical flaw sizes. For this latter criterion, a value for $K_{IC,}$ (the fracture toughness value) is required. This therefore necessitated fracture toughness testing of samples from the uPVC supply, particularly, as a function of material type and orientation.

Once these values were obtained, they could be used in lifetime prediction calculations to provide a means of predicting the fatigue performance of the material under typical operational loads. This formed part of the Fracture

Mechanics approach to the problem of life prediction and took into account the initial and final flaw size, as explained in Section 2.7.3.

3.2 MATERIALS TESTED

All specimens were manufactured from the same surplus of uPVC piping manufactured for the resort in Dubai. These were delivered to the university in bulk, wrapped in muslin sacks and were stored prior to specimen production.

3.2.1 MANUFACTURE OF MATERIAL

The pipes were produced by extrusion. This involves a stream of molten polymer being forced by a screw through a die into a desired shape, in this case pipes [17]. A potentially slightly damaging effect of the extrusion process is the internal welds which arise from the recombining of the melt after splitting through the die. These internal welds result in a potential weakness of the finished product at the weld join [16], although, in the present study there was no significant evidence of prior cracking along such weld lines. Issues of fabrication, such as additives to aid gelation, were not considered since the project focused on fatigue of manufactured pipes.

3.2.2 "OLD" AND "NEW"

There were two different types of pipe for specimens – so called "OLD" and "NEW" material. The OLD type denotes that it had been in service underground in the resort, and was excavated from different locations throughout the Madinat Jumeirah site. The NEW type was, as the name denoted – new, unused pipes as supplied by the manufacturers to the same and original specification as that of the OLD type.

Testing was done on these two different types to determine if there was an ageing effect on the fatigue performance of the material, and how much of an effect there was. This could then be used to determine if the OLD pipes were required to be replaced. This would be regarded as a safety measure, and the pipes would be replaced, regardless of whether they had failed in service.

A photograph of the two material types, OLD and NEW is shown in Figure 3.1. The inner part of the pipe was sometimes encrusted with sand and other residue, perhaps as a result of having transported water.

FIGURE 3.1: Samples used for S-N curve testing: OLD (left) and NEW (right)

3.3 TEST SPECIMENS

Where applicable the specimens were manufactured according to the ASTM standards [52, 53]. All specimens were produced from the same supply of pipes depending on the requirement, i.e.: OLD or NEW specimen type. Manufacturing drawings for all the different specimens can be found in Appendix A.

3.3.1 PIPE SECTION FOR SN TESTING

The pipes were cut into sections of 110 mm in length, with no change to either the internal or external diameter. The external diameter was nominally 220 mm with a nominal wall thickness of 13 mm. Figure 3.2 shows the pipe and its dimensions in mm.

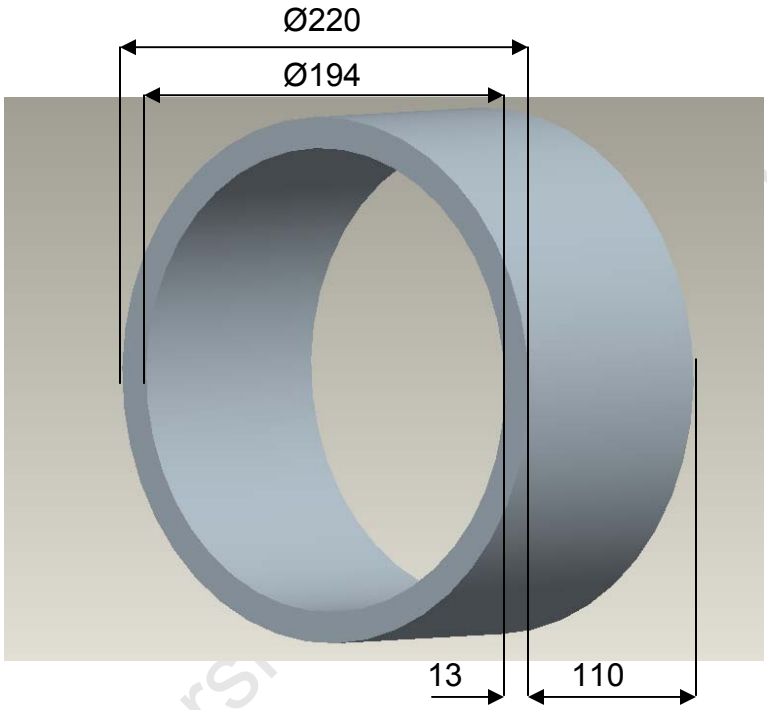

FIGURE 3.2: Pipe used for 20˚C and 45˚C SN testing

3.3.2 COMPACT TENSION SPECIMENS

The Compact Tension (CT) specimens were machined according to ASTM E647 [53]. For orientation purposes, it is important to align the fatigue crack, and hence specimen in the appropriate direction, in this case with the crack longitudinal. When describing the orientation of a sample with respect to the pipe, the first letter describes the specimen direction, and the second indicates the crack direction [52]. Figure 3.3 shows the CT specimen, with nominal dimensions. Dimensions for the CT specimens are shown in Appendix A. In the present case, CT specimens were machined in the CL orientation (i.e.: specimen loading in the

circumferential direction, and the crack propagation in the longitudinal direction). Figure 3.6 shows the CT specimen with respect to the pipe orientation.

The width dimension W, that is, the distance to from the bottom of the specimen to the centre of the holes for CT specimens, was a standard length of 50 mm. In the codes [52], the ratio of W:B (where B = specimen thickness) is stated to be nominally two. However, the specimen thickness was limited by the curvature of the pipe wall, and that the pipe wall only had a nominal thickness of 13 mm. Therefore, to maximise the thickness but allow for curvature, a value of seven mm was used for the CT specimens.

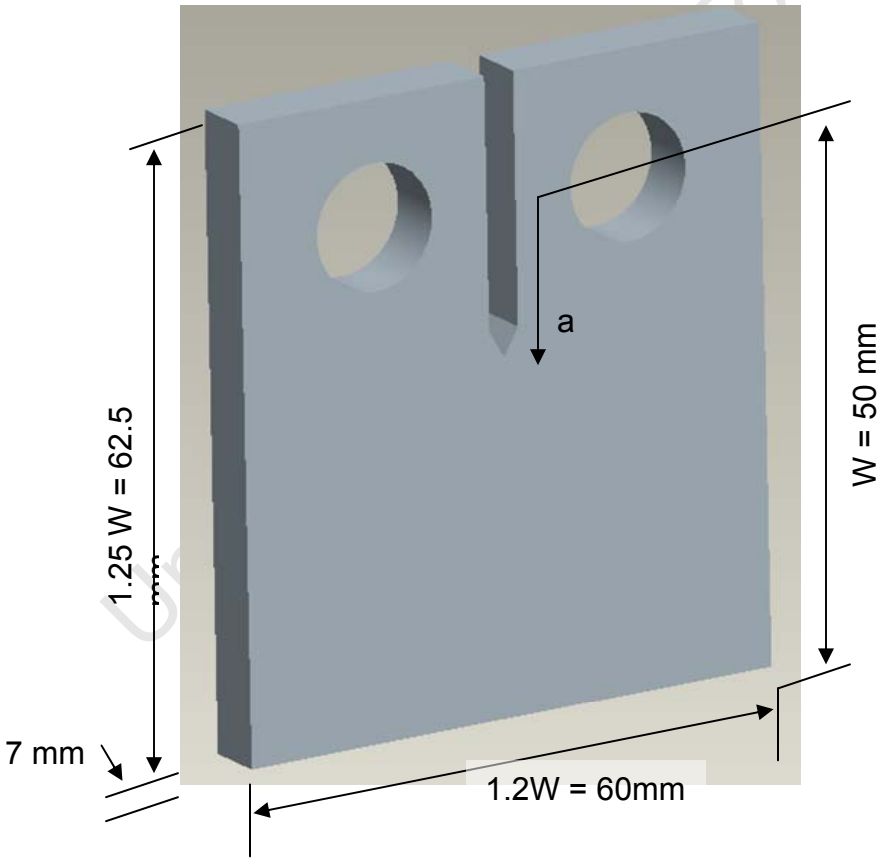

FIGURE 3.3: Compact Tension specimen [54]

3.3.3 SENB AND C-SHAPE SPECIMENS

Two different specimens were tested for fracture toughness testing, namely, Single-Edge Notched Bend (SENB) and C-Shape, both in accordance with its toughness code [52, 53]. The two different specimens were used to determine if there was an orientation effect with regards to fracture toughness. That is, if there was a change in fracture toughness according to the specimen and crack direction. The SENB specimen is shown in Figure 3.4, and the C-Shaped specimen in Figure 3.5. The SENB specimens were in the L-C direction (Longitudinal-Circumferential), and C-shaped specimens in the C-R orientation (Circumferential-Radial). Dimension requirements for the SENB and C-shape specimen can be found in Appendix A.

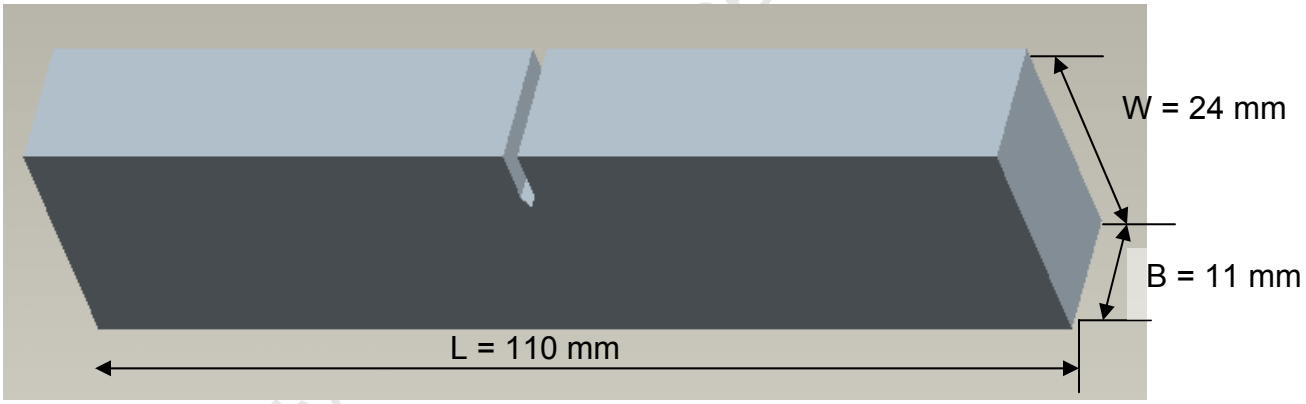

FIGURE 3.4: SENB specimen [54]

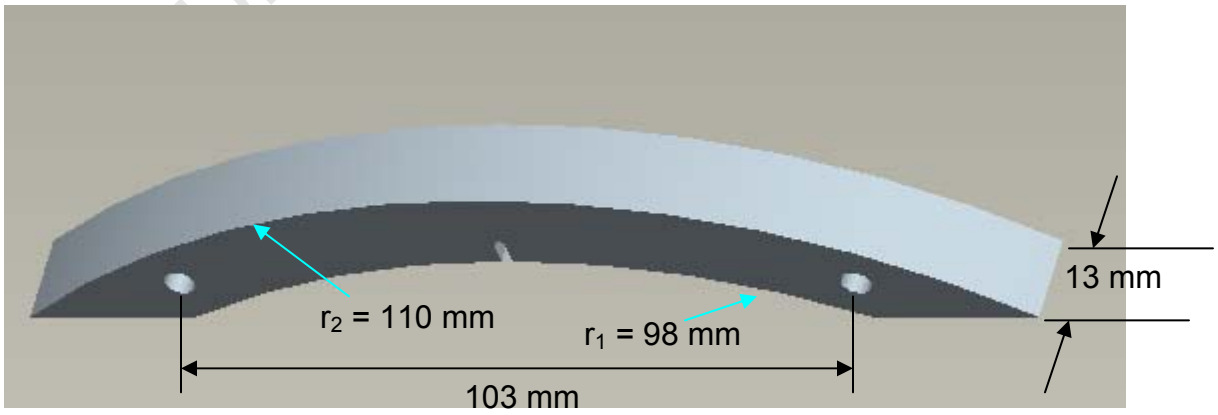

FIGURE 3.5: C-shaped specimen [54]

SENB specimens are one of the standard methods for determining the Fracture Toughness. However, the geometry of the specimen meant that were SENB specimens to be used, the crack direction would not have been in the same direction as that in the in-service cracking situation, where the cracks grew in a longitudinal direction. C-shaped specimens were therefore used as the orientation of the specimen allowed for crack growth in the same longitudinal direction as that in service. C-shaped specimens could also be used since they accommodate a range of values for r_1/r_2, (where r_1 = inner radius, and r_2 = outer radius), as shown in Figure 3.5, and as long as the cylinder is hollow [52], which the pipes were. Figure 3.6 shows the fracture toughness specimens, and the CT specimen and their orientations with respect to the extrusion direction.

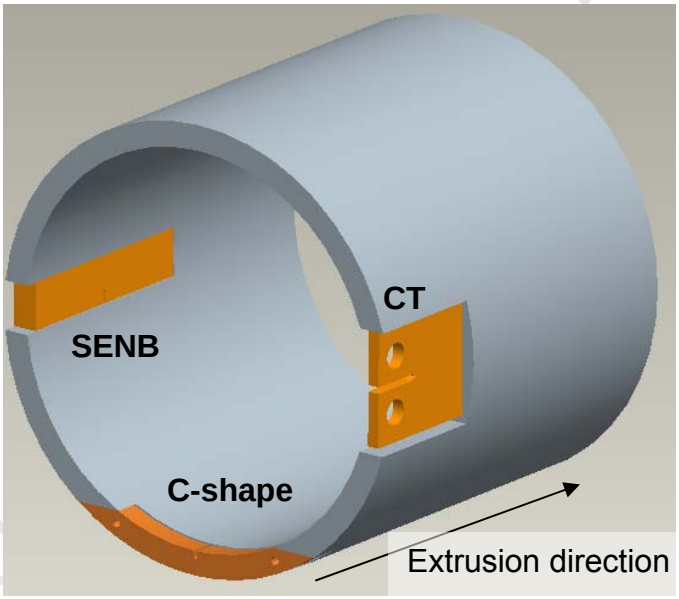

FIGURE 3.6: Fracture toughness and CT specimen orientation with regards extrusion [54]

3.4 TESTING EQUIPMENT

All testing was performed in the Centre for Materials Engineering at the University of Cape Town. All fixtures and parts were manufactured on-site in the mechanical engineering workshop.

3.4.1 ESH TESTING MACHINES

The two machines used for testing were both ESH electro-servo hydraulic Fatigue machines. A 50 kN machine was used for the SN and Fracture toughness testing, as well as the 20˚C testing for Paris data generation. For the 45˚C Paris testing, a 100 kN machine was used as a special rig for high temperature (45˚C) testing was designed for an undergraduate thesis [54]. The two machines are shown in Figures 3.7 and 3.8.

FIGURES 3.7 & 3.8: 50 kN ESH machine (left), and 100 kN ESH machine (right)

3.4.2 SN TESTING

These tests had common equipment for both the 20˚C and 45˚C tests. For the 45˚C tests, additional equipment was used. The testing setup for a 20˚C test is shown in Figure 3.9. This involved placing a section of pipe in a bath, and placing a piece of steel on top of the pipe to distribute a force over the whole top section of the pipe. This setup allowed observation of both the top and bottom sections of the pipe during testing.

FIGURE 3.9: Testing setup for SN testing

3.4.2.1 COMMON EQUIPMENT

A bath, constructed from stainless steel, was designed and fabricated for the SN tests, shown in Figure 3.10. It was screwed onto the actuator of the 50 kN ESH machine, and secured in place with locknuts. While it was not essential for 20˚C testing, it was easier to keep the bath permanently installed, and it also provided a base for the pipe specimens. The bath was later modified to include a sheath for an immersion heater and a holder for a float switch for 45˚C testing (see below). All the manufacturing drawings for the bath can be found in Appendix B.

FIGURE 3.10: Stainless steel bath for SN testing

A flat steel plate was placed on top of the specimens to provide a distributed compressive force over the top of the pipe. This acted as a complementary force distribution to the bath. A flexible optic light source was used to detect cracks in the pipes during testing.

3.4.2.2 45˚C TESTING EQUIPMENT

As mentioned above, for 45˚C testing, additional and specialised equipment was required.

3.4.2.2.1 IMMERSION HEATER

A 350 Watt immersion heater was used to heat the water to the necessary 45˚C. The heater handle was modified by enclosing it in PVC, so that it would fit into a specially designed sheath attached to the bath. This was undertaken as a safety measure, and ensured that the heater was stable and secure, thereby minimising the risk of fire and subsequent damage to surrounding equipment. A further modification to the heater was the changing of the two-pin plug to a three-pin plug to fit the plug hole of the thermo-controller. The immersion heater in its protective PVC covering is shown in Figure 3.11.

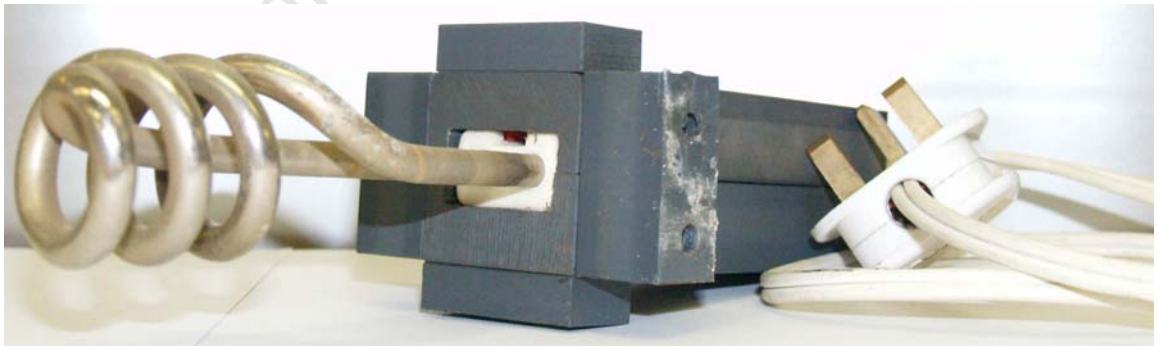

FIGURE 3.11: Immersion heater

3.4.2.2.2 THERMO-COUPLE AND THERMO-CONTROLLER

A thermocouple was used to monitor the temperature and facilitate temperature feedback from the bath, and was plugged into the thermo-controller. The thermo-controller operated on a feedback system to maintain the temperature at 45˚C. The thermo-controller was able to accurately maintain the temperature 45˚C, with a deviation of approximately 1˚C. The thermo-controller was able to maintain the temperature by regulating the flow of power to the immersion heater. If the water temperature dropped below 45˚C, power would be supplied to the heater to raise the temperature to 45˚C, and if the temperature rose above 45˚C, power was cut to the immersion heater. In this way, the temperature could fluctuate about 45˚C with ever decreasing amplitude until the temperature could be regarded as constantly 45˚C. The thermo-couple and thermo-controller is shown in Figure 3.12. The block attached to the thermo-couple wire shown in the photo was merely to keep the thermo-couple wire submerged.

A short explanation on how to program the thermo-controller can be found in Appendix C.

FIGURE 3.12: Thermo-couple and thermo-controller

3.4.2.2.3 DIGITAL THERMOMETER

A digital thermometer was used to check temperature values against that of the thermo-controller. A thermo-couple rested in the bath, and the thermometer attached by magnet to the ESH column support.

3.4.2.2.4 FLOAT SWITCH

As an additional safety measure, a float switch was added to the setup. This addition was added to ensure safety even with dropping water levels due to evaporation, and consequent exposure of heater coils and subsequent overheating occurring during extended hours of testing. The float switch had the effect of cutting power to the heater completely if the water level dropped below a certain level in the bath. Shown attached to its holder in Figure 3.13, the float switch in its current position would not allow power to the immersion heater as the switch is too low, as there in no water to raise it.

The level at which power would be cut, was set approximately at the height of the top heater coils, to prevent exposure of the coils which would then attempt to heat the surrounding air to the required temperature of 45˚C. The bath used for SN testing, Figure 3.10, shows the float switch attachment in relation to the sheath for the heater.

FIGURE 3.13: Float switch installed in the bath

3.4.2.2.5 AQUARIUM PUMP

A small 20 Watt aquarium pump, delivering 1000 litres/hour was fitted into the bath for hot tests to stir the water and thereby regulate a constant temperature around the bath, and not allow the water in the immediate vicinity of the heater to rise to a higher temperature. Sampling of the water temperature in the bath with the digital thermometer indicated that the bath temperature was everywhere within 1˚C of the specified 45˚C.

3.4.3 FRACTURE MECHANICS FATIGUE – PARIS TESTS

For the fracture mechanics fatigue crack growth rate testing, so-called Paris tests, Compact Tension specimens were used as they have a relatively long and stable crack length regime (compared to SENB and C-shaped specimens). CT specimens were fatigued on both the 50 and 100 kN ESH fatigue machines, depending on the test condition. Setups differed between the two different machines.

3.4.3.1 20˚C TESTING

The 50 kN ESH Fatigue machine was utilised to develop the Paris equation for the 20˚C testing. A standard clevis-pin arrangement was used, as well as a light source and travelling microscope. Spacers manufactured from High Density Polyethylene were used to keep the specimen in a consistent manner and to prevent it from “floating” or “walking” along the holding pin. The spacers were manufactured to replace existing individual steel washers which were difficult to work with.

A binocular Olympus optical microscope with up to 4X magnification, a base, and a graticule in the right lens was used to track the crack length. The specimen surface was illuminated by a flexible optic light source, and by angling the light

obliquely close to the surface, it was possible to better focus the view. The setup is shown in Figure 3.14.

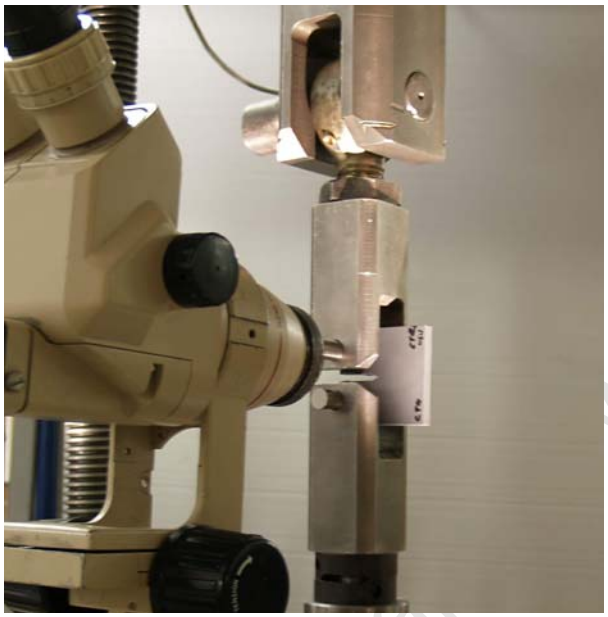

FIGURE 3.14: setup of 20˚C CT testing

3.4.3.2 45˚C TESTING

The 45˚C testing was carried out on the 100 kN ESH fatigue machine. This was because a stainless steel bath, similar to that used for the SN testing was required for the heated water.

The setup for the 45˚C fatigue testing was developed for an undergraduate project by Mr G Izaaks [54]. It involved a structure of four compression columns, protectively coated in an anti-corrosive paint attached to the top crosshead. At the bottom of the four-pole arrangement a clevis was attached, with the other clevis attaching to the actuator. This clevis arrangement was therefore similar to the testing setup on the 50 kN machine but avoided having a waterproof seal at the lower clevis. The four column structure, attached to the crosshead of the 100 kN ESH machine, with clevis in place is shown in Figure 3.15.

FIGURE 3.15: Four-column structure with clevis arrangement

A water bath with a window was required. This was because the specimen was required to be submerged to at least above the notch, and therefore the bath wall height needed to be such that water could fill to that level. Therefore a section of the bath was clear plastic, to facilitate observation of the test and to track crack growth. The bath is shown in Figure 3.16.

FIGURE 3.16: Stainless steel bath with window used for 45˚C CT testing

The bath was similar in design to that used for the SN testing in that it had a slot for an immersion heater. This was the same heater that was used for the prior

SN testing. Other equipment used in the same manner as before were the thermo-couple, thermo-controller, aquarium pump and digital thermometer. The thermo-controller was modified as the float switch was not used. This was because the tests were not run over an extended period of time, and there was no danger therefore of the water level dropping below that of the heater coils, which could potentially lead to a fire. The float switch interlock was omitted for these tests, with an overriding attachment installed for power to be supplied to the heater. The digital thermometer was again used to verify the temperature.

Temperature control proved to be more difficult during the Paris fatigue testing than during the SN testing. This was due to the larger surface area of the so called “Paris bath”. This meant that heating the water and maintaining a constant temperature was not as straightforward as before. However, through adding heated water, and manipulating the thermo-controller to heat more quickly, it was possible to maintain the temperature at 45˚C, with a deviation of < 2˚C at the specimen itself due to careful water circulation. A setup for the 45˚C testing is shown in Figure 3.17, with a close-up of the testing shown in Figure 3.18.

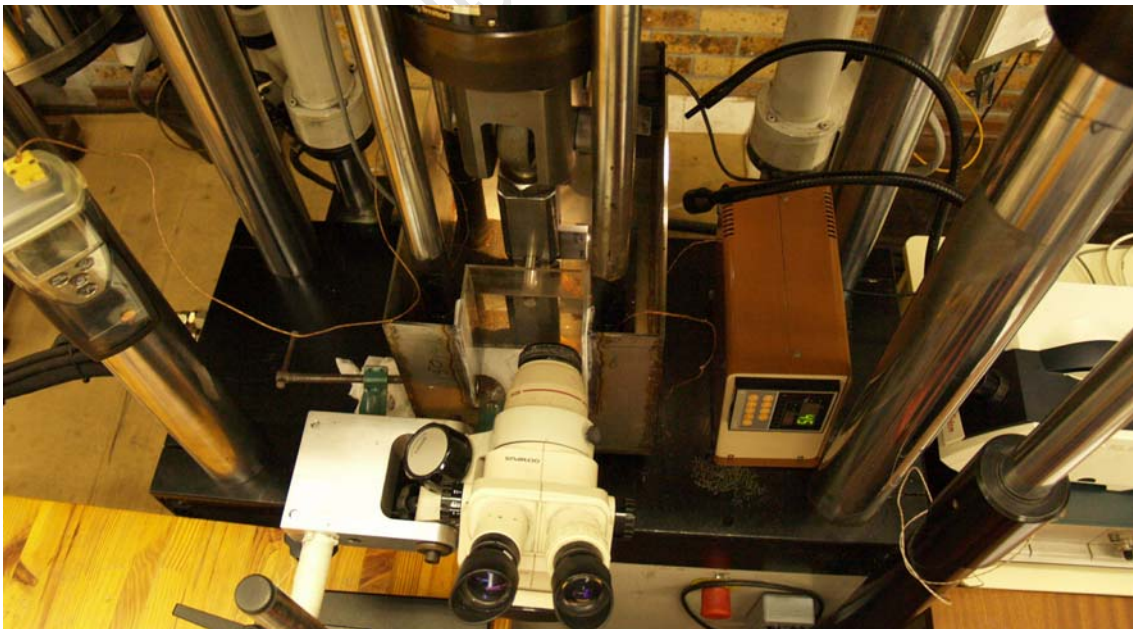

FIGURE 3.17: Test setup for 45˚C CT testing

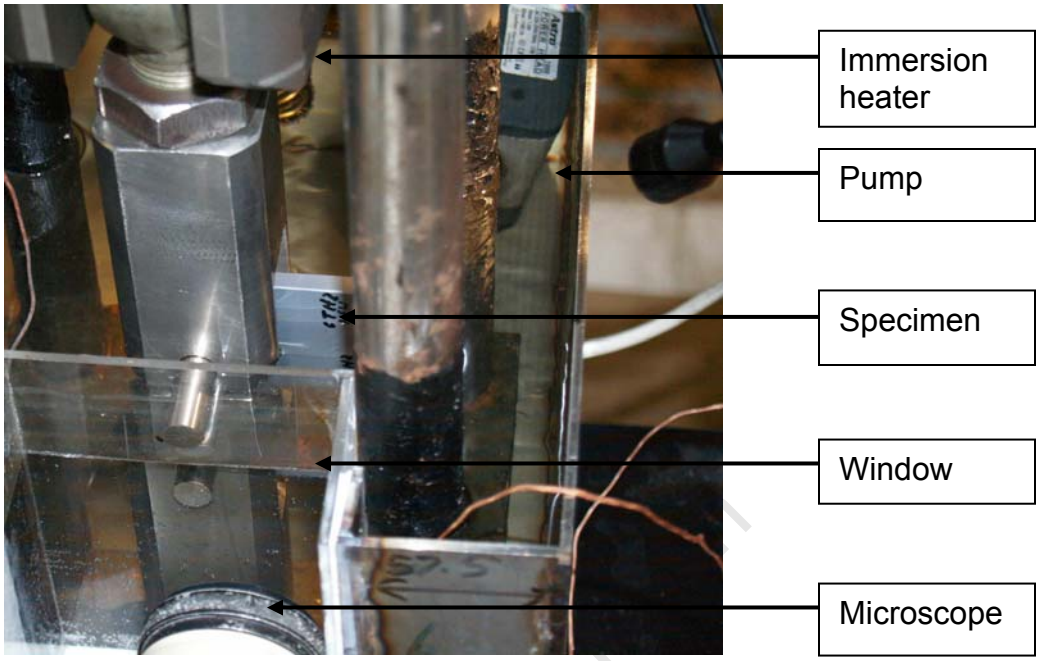

FIGURE 3.18: Close-up of Setup of 45˚C CT testing

3.4.4 FRACTURE TOUGHNESS TESTING AND RAMPING EQUIPMENT

The 50 kN fatigue machine was used for the fracture toughness testing, with standard grips and fixtures. The testing setup was similar for both the SENB and the C-shape testing, with respect to fatigue pre-cracking in bending. The only difference being the span – the distance between the two supporting rollers which is expanded on in Section 3.5.3.

Under monotonic loading (i.e.: ramping) the SENB specimens were loaded in bending (compression) whereas the C-shape specimens were loaded in tension using custom built clevis attachments.

The same Olympus microscope used for the Paris fatigue testing was again used to track the crack growth along the specimen. The fixture used for the fracture toughness testing for both the SENB and C-shaped specimens is shown in Figure 3.19.

FIGURE 3.19: Fixtures used for toughness testing

A clip gauge, attached by means of knife edges to specimens, was used in conjunction with a strain-gauge amplifier for monitoring load deflection behaviour during ramping tests after the initial pre-crack had been grown. The output of the clip gauge was graphed on a plotter – producing a graph of Load vs. Crack opening displacement. The three systems used for ramping are shown in Figure 3.20.

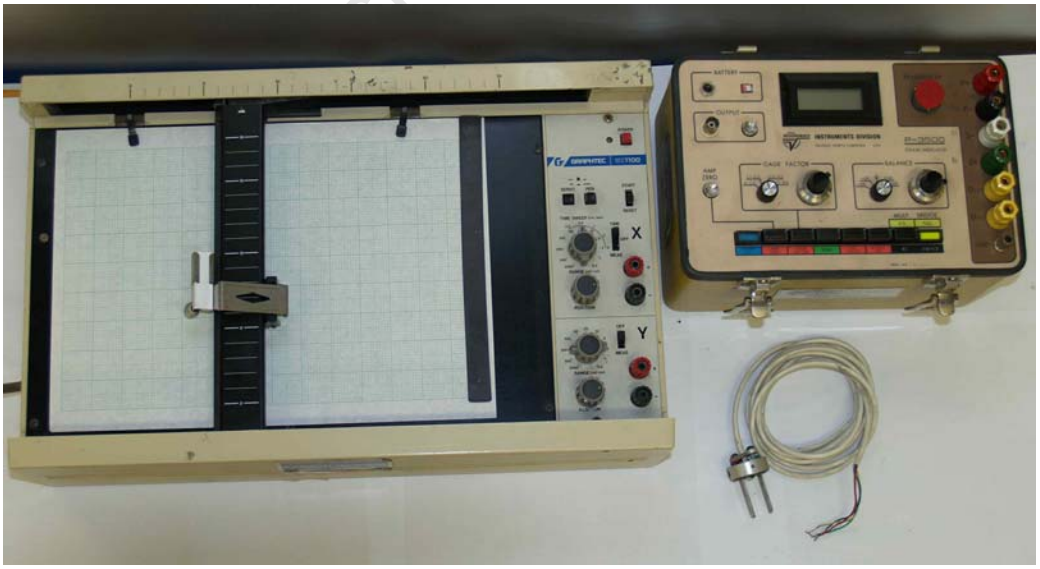

FIGURE 3.20: Ramping equipment

3.5 TESTING PROCEDURE

Where applicable, the testing process was according to that detailed in the codes [52, 53, 55].

3.5.1 SN FATIGUE PROCEDURE

This testing was selected to simulate the actual conditions believed to be experienced by the pipes in service under the roads of the Madinat Jumeirah resort. A range of loads were tested, to simulate extreme loading conditions.

3.5.1.1 SUMMARY OF TESTING PARAMETERS

The stress levels tested were: 10, 15, 20, 25, 30, 35 and 40 MPa. It was felt that these levels best illustrated the fatigue behaviour of the uPVC, by covering a broad range of stress levels. Actual stress levels experienced by underground pipes due to overhead construction traffic loading in Dubai and internal pressure cycling were calculated to be 6 MPa [1]. This is only slightly higher than a suggested fatigue threshold of 5 MPa by Vinidex, an Australian thermoplastics pipe manufacturer [33]. However, there was insufficient time to run these SN tests at this low stress level as they would potentially have taken months till failure. A limit of 400 000 cycles was taken as so-called “run-out” test, i.e.: tests run for 400 000 cycles for which there was no cracking, and no failure, were reported as “run-out” tests. In this category this was only relevant for some of the 10 MPa tests.

Frequency was maintained at 1.5 Hz, although for the high stress tests (35 and 40 MPa) the frequency was lowered to 1 Hz as it was not possible to attain the necessary load at the higher frequency because of the compliance and fatigue machine response. It was believed that any frequency effect on lifetime was negligible at this range even though frequency can have a distinct effect on

fatigue in polymers [14]. A fringe benefit was that this lower frequency also slowed the test slightly and gave more time for observation of the pipes, in the shorter fatigue lifetimes at high stress levels.

As mentioned above, tests were conducted at two different temperatures, and these temperatures were either 20˚ (ambient) or 45˚C. A summary of the testing parameters is shown in Table 3.1.

TABLE 3.1: Summary of testing parameters for S-N curves

Frequency [Hz]	Stress Range [MPa]	Temperature range [˚C]
1 - 1.5	10 - 40 (increments of 5)	Ambient (20) and 45

3.5.1.2 DERIVATION OF LOADS FOR SN TESTS

The original loads were derived from an equation for maximum wall stress, from a discussion on vertical loading by Benham et al and Dally et al [1, 56, 57]. The equations used were:

$\sigma = 0.9\frac{PR}{wt^2}$ - Benham et al [56] [Equation 3.2]

$\sigma = 1.09\frac{PR}{wt^2}$ - Dally et al [57] [Equation 3.3]

Where:

- σ = Stress [MPa]
- P = Load [kN]
- R = Mean radius [mm]
- w = Length of pipe [mm]
- t = thickness of pipe [mm]

Using an assumed load of 1.75 kN (derived from 17.5 kN/m run), a mean diameter of 207 mm, a length of 100 mm and a thickness of 13 mm, the

corresponding stress was calculated to be 10.3 MPa. The corresponding loads were then calculated for each stress level, and are shown in Table 3.2 [1].

TABLE 3.2: Load values for each stress level

Stress [MPa]	10	15	20	25	30	35	40
$F_{max\ [kN]}$	1.72	2.58	3.44	4.30	5.16	6.01	6.87
$F_{min\ [kN]}$	0.34	0.52	0.68	0.86	1.03	1.20	1.37

The fatigue load ratio R (the ratio of F_{min}/F_{max}) was selected to be 0.2 always. A ratio of R = 0.1 is generally used for steels, however, for polymeric materials there is an option of using R-ratio from 0.1 to 0.9 according to research carried out by Maddox and Manteghi [28]. An R-ratio of 0.2 was therefore chosen as R = 0.1 was felt to be too low and difficult to work with.

3.5.1.3 SETTING UP FOR TESTS AND START-UP

The bath, with a screw fixture attached, was fixed onto the bottom mounted actuator. Once it was aligned, it was secured in place with lock-nuts. The lock-nuts were used to maintain position and to prevent the bath threads from becoming fatigued themselves and also to facilitate easy release.

The pipe was placed symmetrically in the bath, and the steel plate placed on top of the pipe. The bath was then raised, until the pipe experienced a compressive force, thereby securing the top plate against the top of the pipe.

The ESH machine in use had two modes of control – Stroke and Load control. All pre-loading and adjustment was made in Stroke control, which converted to a load on the pipe, as once appropriate loads were established the system was switched to Load control, so the fatigue test itself was conducted under Load control conditions.

The pre-load was placed on the pipe – half of the sum of the maximum and minimum loads for the particular stress level. For example, 25 MPa tests, with

force limits between 4.30 kN and 0.86 kN, the pre-load mean would be 2.58 kN. Once the pre-load in Stroke control was set, the load control potentiometer was zeroed to ensure “bumpless” load transfer, i.e.: this load control potentiometer was zeroed so that when modes were switched from Stroke to Load, the load on the pipe would remain essentially constant at the pre-load.

The counter was also zeroed, and the test started building the amplitude up from zero. Once the test had begun, the amplitude was steadily increased until the pipe was experiencing the full cyclic fatigue load. Where necessary, the mean level was also adjusted, to ensure that the loads were peaking as close to the desired levels as possible, as displayed by the ESH Amplitude Control Unit.

3.5.1.4 MANAGING TESTS

Once the levels had stabilised, the pipe was observed continually/intermittently to determine when the first crack, and ultimately failure occurred. This was sometimes a difficult process as turbulent and splashing water sometimes obscured the lower sections of the pipe during hot temperature tests. It was found though, that the process of observing for cracks was made easier by shining a light source at an angle on the inner surface of the pipe. Close observance of high stress level tests was dangerous, especially of the OLD type, with catastrophic failures sometimes experienced. The sudden failure made close observation hazardous, given that there was often no initial crack, but rather explosive and rapid catastrophic failure. This was obviously a dangerous situation when one considers that to observe the pipe meant peering in as close as possible. Protective goggles were therefore required and used.

Failure of the pipe, and hence the end of the test was taken as the point at which either:

- The pipe could not carry the full load

- The crack had run the full length of the pipe, or had run to an edge. This would in effect be termed as “leakage”, a parameter for failure according to [28] and referred to in Section 2.5. An example of this edge crack is shown in Figure 3.21.
- Pipe had disintegrated by catastrophic failure

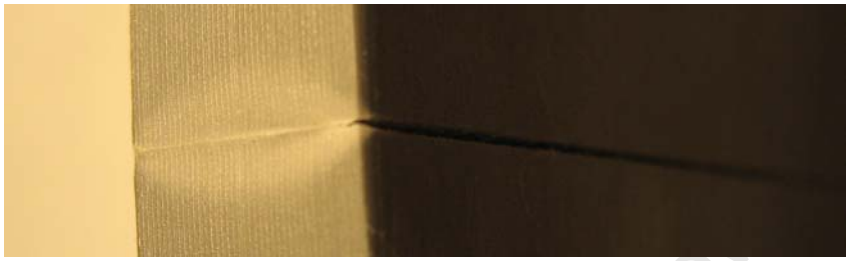

FIGURE 3.21 Example of crack which had run to the edge of a surface

3.5.1.5 45˚C TESTS

The bath was half filled with pre-heated water for hot tests. By only immersing the lower half of the pipe, the cracking section was theoretically confined to the lower half as only the lower half would be at the higher 45˚C temperature and ultimately crack. While this is not truly representative of the real-life scenario, the hot water would still affect the lower half of the pipe and cause cracking. In these higher temperature (45˚C) tests the failure or cracking always occurred in the lower half (wet) section of the pipe, except at tests of exceptionally high stress levels.

The thermo-controller was programmed so that the heater would heat the water to the vicinity of 45˚C, and would maintain the temperature with a deviation of not more than 1 degree throughout the test. However, during the heating process, it was not possible for the heater to stop at precisely 45˚C, and so therefore there was a period of oscillation between temperatures above and below 45˚C. Thereafter the temperature stabilised, and remained essentially constant throughout tests. The entire heating process initially lasted for two hours,

although the process was refined in later tests as pre-heated water was placed in the bath, allowing the time between room temperature and 45˚C to be shorter.

During tests that necessitated topping up of the water level, water was taken from the hot tap and mixed with cold water to produce a mixture which was in the vicinity of true 45˚C. This was measured against a digital thermometer. This water was then added to the remaining heated water, and the consequent loss of heat in the test bath was negligible, at such times of topping up.

3.5.2 FRACTURE MECHANICS FATIGUE – PARIS TESTING

Different machines were used for the 20˚C and 45˚C tests. However, the basic procedure was the same for both tests, and both sets of tests were conducted at a frequency of 5 Hz. Specimens were identical for both tests. The specimens used were Compact Tension specimens of the NEW type with gradation lines inscribed for ease of following the crack growth. The NEW results were compared with OLD results, which were tested during an undergraduate thesis in October 2007 [54].

3.5.2.1 DERIVATION OF LOADS FOR PARIS TESTING

Strictly, loads are calculated based on the equation $K = Y\sigma(\pi a)^{1/2}$, but in practice loads were determined from the following equation, based of the fracture toughness codes BS7448 [55] and ASTM E399 [52]:

$$\Delta K = \frac{Y \Delta P}{B W^{1/2}} \qquad \text{[Equation 3.4]}$$

Where

- K = stress intensity [MPa√m]

- Y, or f(a/W) = geometrical factor, dependent on the relative crack length, or a/W from Haigh and Richards [58]
- ΔP = change in load [N] ($F_{max} – F_{min}$)
- B = thickness [mm] (constant)
- W = width to centre of holes [mm] (constant)
-

(The values B and W can be seen in Appendix A – Dimensions of CT specimens)

The load values, P_{max}, P_{min} and hence ΔP could be chosen according to the desired K value. Assuming the specimen had a crack length of 17 mm, with W = 50 mm, a/W would be 0.34, and the corresponding f(a/W) would be 6.35 [58]. By using this f(a/W) value, and a thickness, B of 7 mm and an assumed value of ΔK = 2.5 MPa√m [28] the resulting ΔP value would be 616 N.

An R-ratio of 0.2 was used throughout, thus to find P_{max} and P_{min}, it followed that:

$$\Delta P = P_{\max} - P_{\min} \qquad \text{[Equation 3.5]}$$

Where the Ratio R is defined as:

$$R = \frac{P_{\min}}{P_{\max}} \qquad \text{[Equation 3.6]}$$

It therefore follows that:

$$P_{\min} = RP_{\max} \qquad \text{[Equation 3.7]}$$

And so therefore:

$$\Delta P = P_{\max} - RP_{\max} \qquad \text{[Equation 3.8]}$$

In the case of R = 0.2

$$P_{\max} = \frac{\Delta P}{0.8} \qquad \text{[Equation 3.9]}$$

Substituting in the value for ΔP, which for simplistic reasons will be taken as 600 N , and utilising Equation 3.7, the value for P_{max} is 750 N. Substituting that value into Equation 3.5, and using R = 0.2, the value for P_{min} is 150 N. The tables used for f(a/W) for Paris fatigue testing can be found in Appendix D.

3.5.2.2 20˚C PROCEDURE

The clevis and pin arrangement was assembled and arranged in a manner such that should the actuator inadvertently jump to full stroke in compression, the fixtures would not crash into each other and cause damage. The specimens were mounted and secured in place with the locking pins, as shown earlier in Figure 3.14.

The microscope was focused for observation of the crack growth, and the cycle counter reset to zero. As with the SN tests, the pre-load was an average of the maximum and minimum loads, and was set while in Stroke control. Once the pre-load was set, the machine was switched across to Load control. The test began and the amplitude was increased until full load was realised.

Observations were made at regular intervals to monitor the crack growth. Generally readings of the crack length were taken every 1000 cycles, although towards the end of the testing, readings were taken every 200 cycles, such was the rapid crack growth. A light source was directed onto the crack, to improve observation of the crack.

Throughout the test, the amplitude was constantly monitored, and when necessary adjusted to maintain the loads that were set at the beginning of the test. It was important for the loads to be maintained, as this would result in consistent fatigue results in the form of the Paris formulation. This would produce a crack vs. number of cycles graph that was ideally similar in trend to that shown

in Figure 3.22. The increasing crack rate growth was also an indication of a constant load on the specimen throughout the test.

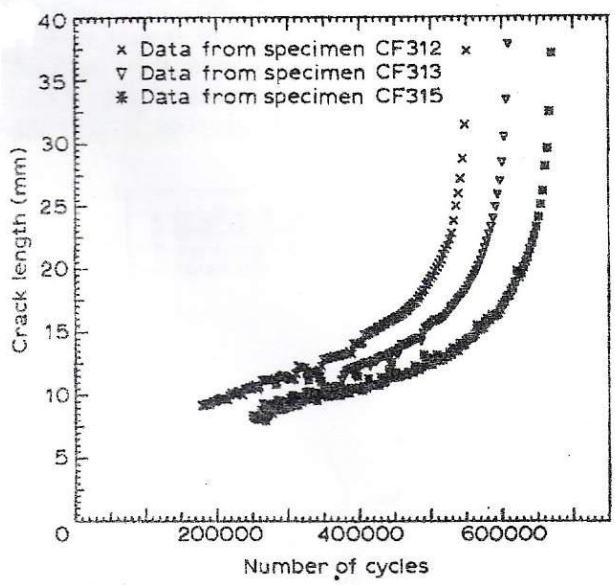

FIGURE 3.22: Ideal plot of crack growth vs. number of cycles [28]

As the crack length progressed, it was necessary to shift the microscope periodically to keep the graticule focused on the crack tip. A note of the reference measurement was made before the microscope was moved – this enabled the absolute crack measurement to be accurately measured.

Tests were repeated at different ΔK values to show repeatability and to generate a comprehensive behavioural curve for the NEW uPVC at 20˚C. The test was deemed to be complete when the specimen had either fractured or the load could not be raised sufficiently to maintain a constant load. A close-up setup of the 20˚C testing is shown in Figure 3.23, illustrating the use of the micro-scope and light source to track the crack, which is also shown.

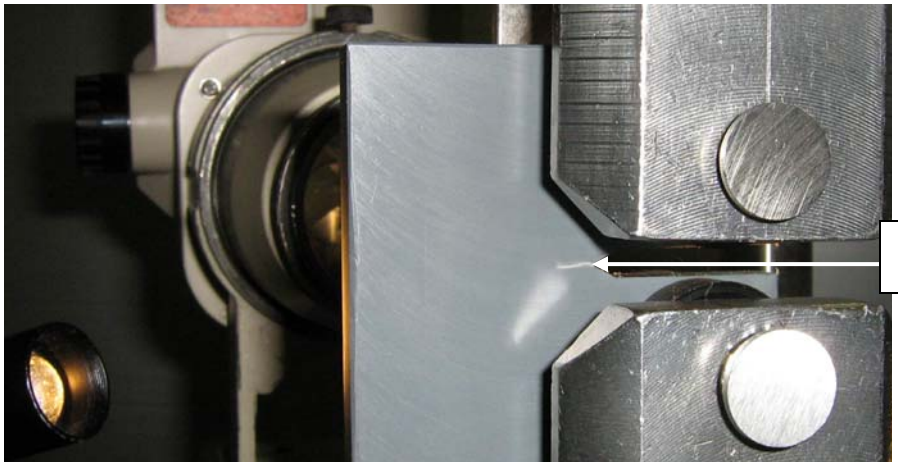

FIGURE 3.23: 20˚C CT specimen testing

3.5.2.3 45˚C PROCEDURE

45˚C testing was performed on the 100 kN ESH machine, in a manner similar to the 20˚C testing; however, the specimen was immersed underwater to cover the crack, with the water at a nominal temperature of 45 C. As mentioned in Section 3.4.3.2, this experimental method followed that of Mr G Izaaks in his undergraduate thesis [54], and which involved performing Paris fatigue tests on OLD specimens.

Procedure followed that for the 20˚C testing. However, the 100 kN was electronically controlled, so it was possible to have tighter control over the loads, using a gain of 8.0. The gain was required to be increased for tighter control over loads. An example of a submerged specimen with a crack is shown in Figure 3.24.

Crack length was again monitored optically with the travelling microscope and graticule system to yield plots of crack length versus number of cycles, again, ideally similar to Figure 3.22. This data was used to plot the crack growth in the Paris equation formulation of da/dN vs. ΔK, both on log-log scales (Section 2.7.4).

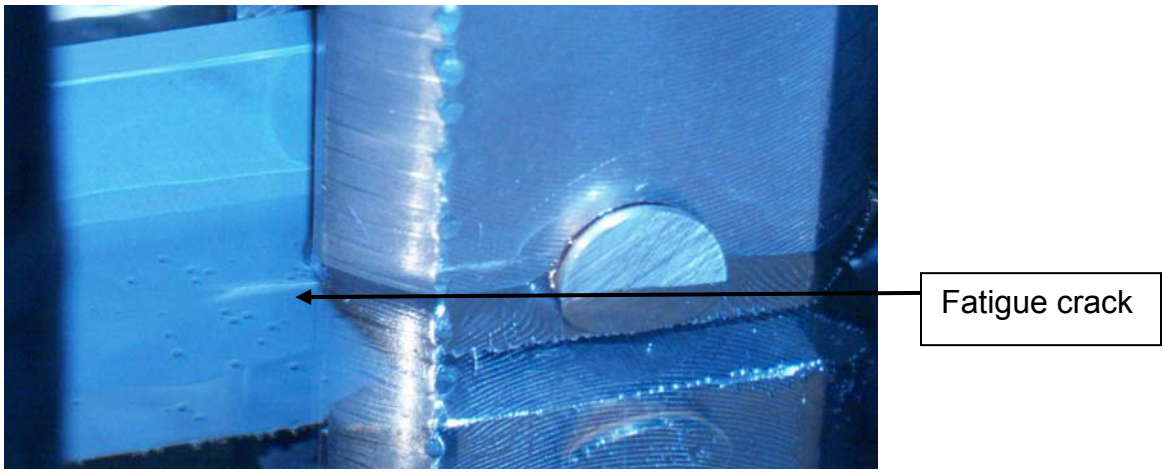

FIGURE 3.24: Submerged 45˚C CT specimen with crack

3.5.3 FRACTURE TOUGHNESS TESTING PROCEDURE

3.5.3.1 FATIGUE PRE-CRACK GROWTH

Testing procedure for the SENB and C-shaped specimens were initially similar at the fatigue pre-cracking stage, with the only difference being the span – that is the distance between the supporting rollers, and the length of the pre-crack. As mentioned in Section 3.4.4, the span for the SENB was 100 mm [52]. The SENB specimen undergoing pre-crack fatigue growth is shown in Figure 3.25. Both tests were run at a frequency of 5 Hz.

FIGURE 3.25: Close-up of SENB specimen undergoing fatigue pre-cracking

The C-shaped specimens were to be ultimately ramp tested in tension, but it was sufficient to grow the fatigue pre-crack in bending as it is more convenient, and in this case on a span of 115 mm [52]. The pre-crack growth of the C-shaped specimen is shown in Figure 3.26.

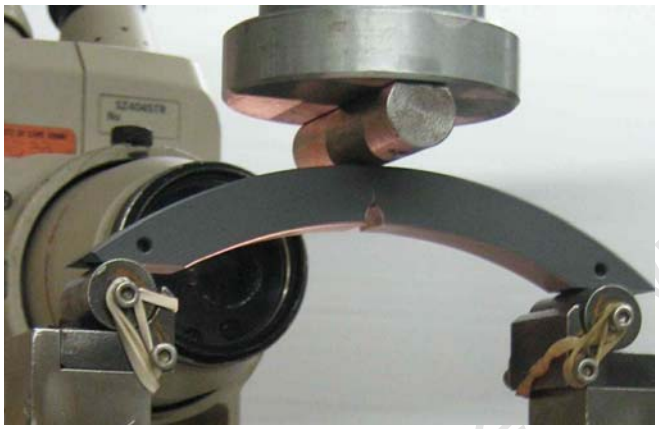

FIGURE 3.26: Close-up of C-shaped specimen experiencing bending fatigue pre-cracking

Sample dimensions were measured prior to testing. This was done to determine the required pre-crack length, and to have the necessary measurements for the calculation of the fracture toughness after ramping, and subsequent fracture. The fatigue pre-crack ratio of a/W (crack length over width) is ideally between 0.45 and 0.55 of the specimen width, with the crack length measured in accordance with the codes [52]. A blade was used to cut along the root of the notch to sharpen the crack and to facilitate crack growth.

The samples were then placed on the 3-point bending rig shown in Figure 3.19, and pre-loaded to the appropriate load. Once the microscope was correctly set up, the fatigue pre-cracking could commence in Load control with the amplitude gradually increased to full load. Further data about the loads is available in Section 3.5.3.2.

Readings were taken every 1000 cycles to determine the rate of growth of the crack, with cracks generally only starting to propagate after 7000 cycles (at these

stress levels). Once the crack had started to grow, loads were decreased so that the crack growth would be ideally in the 1 – 2 * 10^{-4} mm/cycle range. By keeping the crack growth at a low rate, a stable, straight crack would grow. Once the crack had grown to the pre-determined length, the specimen was unloaded, and put aside ready for ramp tests.

3.5.3.2 DERIVATION OF LOADS FOR PRE-CRACKING

In order to gain an insight into a potential crack-initiating load, the following equation from ASTM E399 [52] was used:

$$P_{yield} = \frac{B(W-a)^2 \sigma_y}{6W} \qquad \text{[Equation 3.10]}$$

Where:

- P_{yield} = Load at yield [N]
- B = Specimen thickness [mm]
- W = Specimen depth [mm]
- a = crack length [mm]
- σ_y = Yield Stress

P_{yield} is multiplied by a factor of 0.6 [52] to get P_{max}, which is subsequently multiplied by R to get P_{min}.

Using values of B = 11 mm, W = 24 mm (See Appendix A for drawings), a crack length of nominally 6.5 mm and yield stress of 50 MPa [42], P_{yield} is 1170 N, $P_{max\ –\ SENB}$ is therefore 700 N. Using a R-ratio of 0.2, $P_{min\ –\ SENB}$ would therefore be 140 N.

The above process would be used for C-Shaped specimens, using B = 15 mm, W = 13 mm and a crack length of 4.5 mm. The value of 50 MPa [42] is again used. Thus P_{yield} is calculated to be 700 N, $P_{max\ –\ C\text{-}shape}$ is 420 N and $P_{min\ –\ C\text{-}shape}$ is 85 N.

The above loads, shown in Table 3.3, would be an indicator of the loads which would initially be used, depending on the crack growth rate (ideally 1 – 2 * 10^{-4} mm/1000 cycles). The loads could then be adjusted to achieve a stable crack growth rate.

TABLE 3.3: Typical loads used for SENB and C-shape testing

Specimen	F_{max}	F_{min}
SENB	700	140
C-Shape	420	85

3.5.3.3 CLIP GAUGE

Once all the specimens had been pre-cracked, knife edges were attached in anticipation of the ramp testing. These knife edges were a distance of between 9 and 11 mm apart for the clip gauge to slip into. The clip gauge was then connected to a strain-gauge amplifier, which was in turn plugged into a plotter. The output of the load function from the ESH machine was also plugged into the plotter, thereby allowing for a graph of Load vs. crack opening displacement to be plotted.

3.5.3.4 RAMPING – SENB AND C-SHAPED SPECIMENS

Ramping, the application of a monotonic load at room temperature, was applied at a rate of 0.03 mm/s, consistent with the codes [52]. The graphs of the ramping process can be found in Appendix E. These graphs were subsequently used in the calculation of fracture toughness values, expanded upon in Section 3.6.3.

SENB RAMPING

Ramping of the SENB specimens was performed on the same apparatus as that done for the pre-cracking. The ramping process for the SENB specimen can be seen in Figure 3.27.

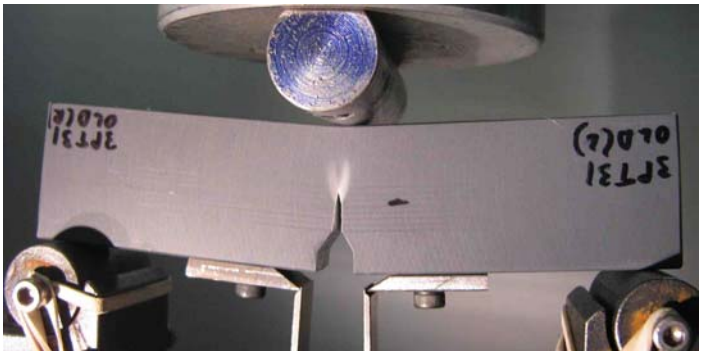

FIGURE 3.27: Ramping setup of SENB specimens

C-SHAPE RAMPING

The C-shape specimens were ramped in apparatus similar to that of the CT testing. However, additional fixtures were added to accommodate the smaller holes of the samples. Bushes were manufactured to seat the holding pin, the drawings of which can be found in Appendix F.

Whereas the SENB ramping was under bending (i.e.: compression of the load cell), the ramping of the C-shape specimens was under tension, shown in Figure 3.28.

FIGURE 3.28: Ramping setup of C-shape specimens

3.5.4 TEST PROGRAM

A summary of the testing procedure is set out in Table 3.4, detailing the number of tests performed for each stage of testing.

TABLE 3.4: Summary of test program

Test Program										
Test stage:	SN Tests				Paris Fatigue		Fracture Toughness			
Temperature:	20˚C		45˚C		20˚C	45˚C	20˚C			
Specimen type:	NEW	OLD	NEW	OLD	NEW	NEW	SENB		C-Shaped	
							NEW	OLD	NEW	OLD
Number of tests:	At least 2 tests per stress				Trend		12 tests each,			
	level				established					

3.6 DATA PROCESSING

Where appropriate, values were calculated according to the procedure documented in the relevant codes – ASTM E399 [52] and BS7448 [55].

3.6.1 SN CURVE GENERATION

Values of the first crack and final failure for 20˚C and 45˚C were plotted on a log-log scale with the stress level on the y-axis, and the value of either failure or first crack on the x-axis, in a manner similar to that shown in Figure 2.7.

Trend lines were superimposed on the graphs to show the relationships between 20˚C and 45˚C, as well as between OLD and NEW type to show the results of ageing in the pipes. Results for 20˚C for both OLD and NEW, as well as results from 45˚C for OLD and NEW were plotted together as a single group respectively to show a definite behavioural trend between 20˚C and 45˚C.

3.6.2 PARIS FATIGUE AND 9-POINT AVERAGE

The crack length vs. number of cycles data (ideally similar to Figure 3.22) is used to plot da/dN vs. Δ/K graphs on a log-log scale. In most cases this turns out to provide a linear relationship between da/dN and ΔK for the crack growth region II,

as shown in Figure 2.10. This linear relationship can be characterised by the Paris equation:

$$\frac{da}{dN} = C\Delta K^m \qquad \text{[Equation 3.11]}$$

When taking the log of each side, this reduces to:

$$\log\frac{da}{dN} = m\log\Delta K + \log C \qquad \text{[Equation 3.12]}$$

Where m is similar to the m' in:

$$y = m'x + C^* \qquad \text{[Equation 3.13]}$$

One can solve for m and C using intelligently selected widely separated data point pairs (ΔK_1 , $(da/dN)_1$),(ΔK_2 , $(da/dN)_2$). m can then be solved by:

$$m = \frac{\log\frac{cycles_2}{cycles_1}}{\log\frac{\Delta K_2}{\Delta K_1}} = \frac{\log[cycle]_2 - \log[cycle]_1}{\log[\Delta K]_2 - \log[\Delta K]_2} \qquad \text{[Equation 3.14]}$$

C can be determined by substituting back the relevant m value together with one (or both) of the data point pairs into equation 3.5. Worked examples are shown in Section 4.5.

The ΔK values were then plotted against the rate of crack growth, producing a plot similar to Figure 2.10. The rate of crack growth was calculated using a 9-point average to smooth the data and offer better trend information, the equation of which is [52]:

$$\left(\frac{da}{dN}\right)_{a=a_5} = \frac{a_9 - a_1}{N_9 - N_1} \qquad \text{[Equation 3.15]}$$

Once plotted, the values for m and C could be calculated, as discussed in Section 3.4.4.

3.6.3 DETERMINING FRACTURE TOUGHNESS

The method for determining the fracture toughness was followed from the codes [52, 55] and involved measurements from the Load vs. Displacement curve which was plotted during the ramping process. All of the traces for the different specimens can be found in Appendix E.

3.6.3.1 MEASUREMENT OF CRACK LENGTH

Once the specimens were ramped, they were broken apart to reveal the fracture surfaces, as shown in Figure 3.29. These surfaces were then photographed and measured to determine the crack lengths. The final crack length to be used for fracture toughness was averaged out according to:

$$a = \frac{(\frac{a_{LHS} + a_{RHS}}{2}) + a_{\frac{1}{4}} + a_{\frac{1}{2}} + a_{\frac{3}{4}}}{4} \qquad \text{[Equation 3.16]}$$

The different crack length measurements and illustration of the fracture surface is shown in Figure 3.29 for the SENB specimen. The methodology for crack measurement was the same for the C-shaped as for SENB specimens.

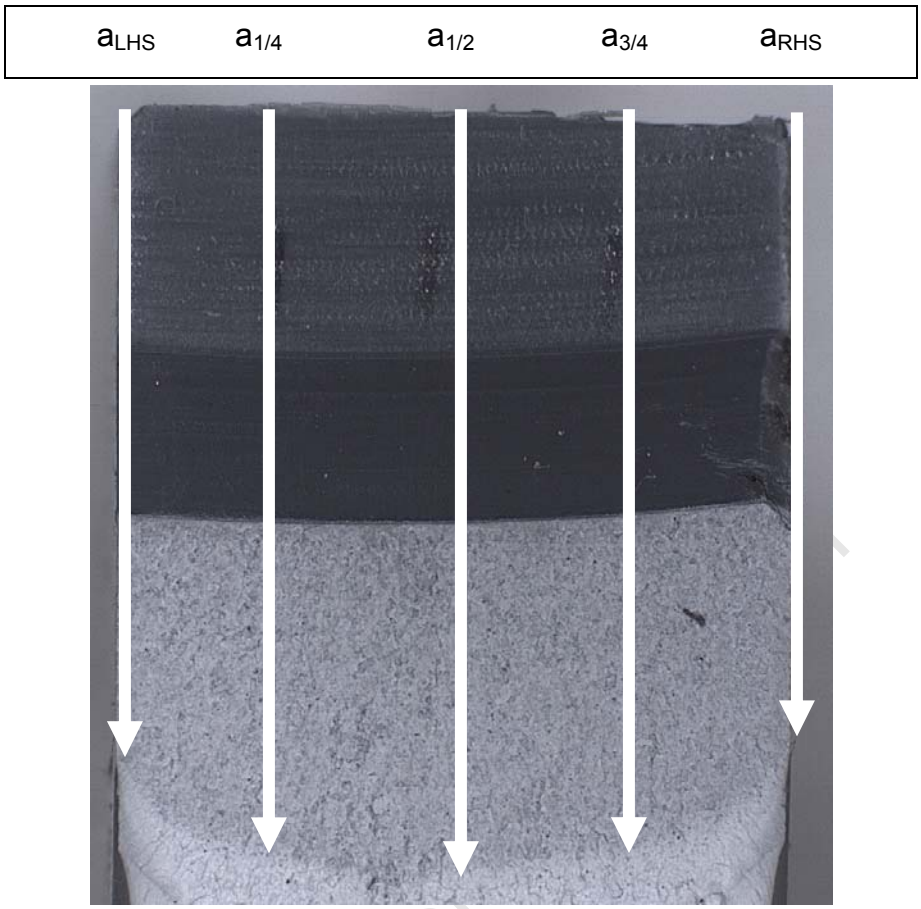

FIGURE 3.29: Fracture surface and crack measurements for SENB specimens

3.6.3.2 EVALUATION OF LOAD-DEFLECTION GRAPH

A trace of a typical Load-Deflection curve for a SENB ramping test is shown in Figure 3.30.

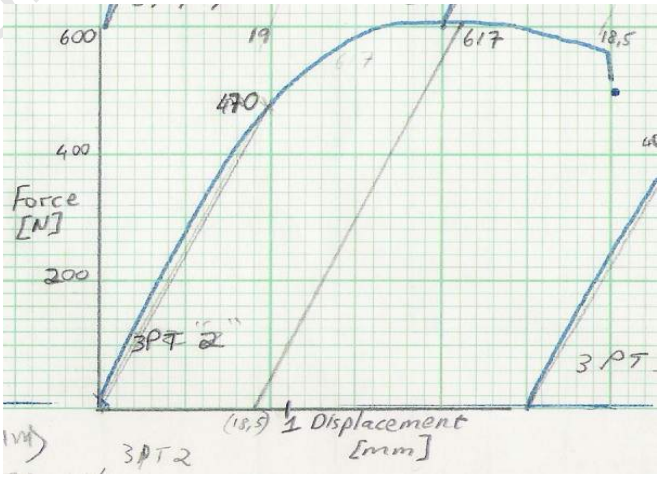

FIGURE 3.30: Example of load-deflection curve from SENB ramping test

A line was drawn through the origin at a 5% offset to the slope. The point at which this tangent line intersected with the graph was F_Q, while F_m was the maximum load on the graph, and verified by the digital readout on the 50 kN fatigue machine. Figure 3.31 shows an exaggerated Force-Deflection curve with the offset line.

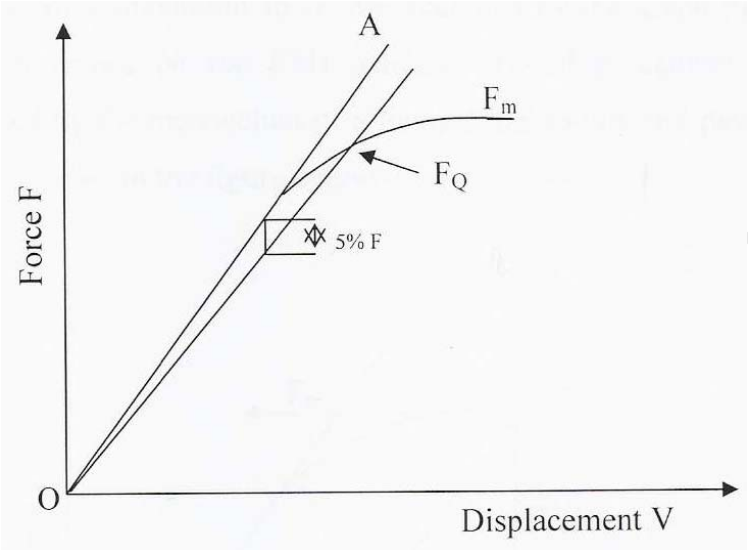

FIGURE 3.31: Exaggerated Force-Deflection curve

The final readings required of the Load-Deflection trace was V_P, the notch opening displacement. This was measured by drawing a line down from F_m parallel to the elastic region of the trace, as shown in Figure 3.32.

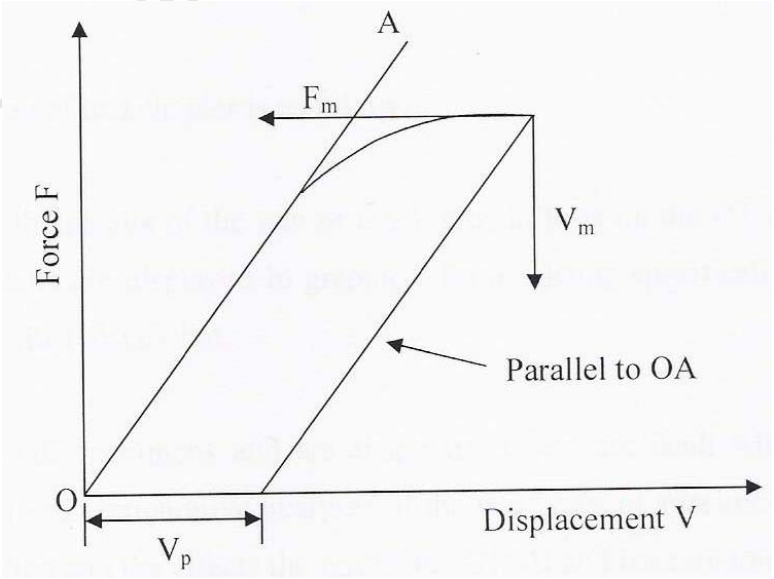

FIGURE 3.32: Method for determining V_P

3.6.3.3 MEASUREMENT OF SPECIMENS

Specimen dimensions were required for the calculation of the fracture toughness and Crack-Tip Opening Displacement. Common dimensions were, with their dimensions for calculation [52]:

- a – crack length [cm]
- B – specimen thickness [cm]
- W – Specimen depth/width [cm]
- z – height of knife-edges used for ramp tests

Additional measurements made for the C-shaped specimens were [52]:

- X – loading hole offset [cm]
- r_1/r_2 – ratio of inner to outer radii

Figure 3.33 shows the additional dimensions required for the C-shaped specimen.

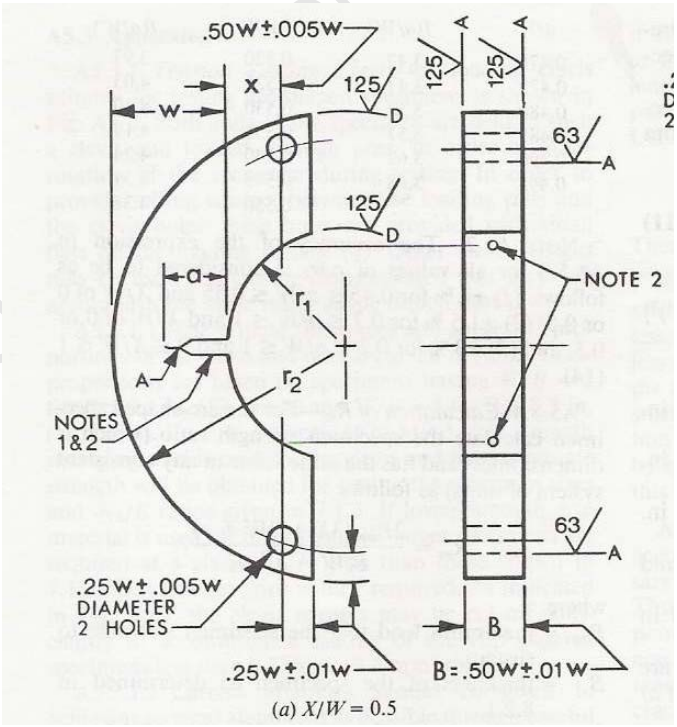

FIGURE 3.33: C-Shape specimen dimensions [52]

3.6.3.4 CALCULATING K

The following equations were used to calculate K, the fracture toughness. Worked examples of the following equations can be found in Section 4.5.

SENB SPECIMENS

$$K_q = (\frac{P_q S}{BW^{3/2}}) * f(\frac{a}{W})$$ [Equation 3.17]

Where $f(\frac{a}{W})$ was read from a table, shown in Appendix D.

S = span, 100 mm.

C-SHAPED SPECIMENS

Some calculations from the dimensions were required to be used in the final equation:

$$r_2 = \frac{L^2}{8(W+x)} + \frac{(W+x)}{2}$$ [Equation 3.18]

$$r_1 / r_2 = 1 - \frac{W}{r_2}$$ [Equation 3.19]

These were then substituted into Equation 3.20 to solve for K:

$$K_q = (\frac{P_q}{BW^{1/2}})[3\frac{X}{W} + 1.9 + 1.1\frac{a}{W}] * [1 + 0.25(1 - \frac{a}{W})^2 (1 - \frac{r_1}{r_2})] * f(\frac{a}{W})$$ [Equation 3.20]

Where $f(\frac{a}{W})$ was calculated as follows:

$$f(\frac{a}{W}) = [\frac{(\frac{a}{W})^{1/2}}{(1-\frac{a}{W})^{3/2}}] * [3.74 - 6.30\frac{a}{W} + 6.32(\frac{a}{W})^2 - 2.43(\frac{a}{W})^3]$$ [Equation 3.21]

3.6.3.5 CTOD – CRACK TIP OPENING DISPLACEMENT

The methodology for calculating the CTOD was similar for the SENB and C-shaped specimens. It comprises elastic and plastic components, with the first term the elastic component. A worked example can be found in Section 4.5.

$$\delta = [\frac{FS}{BW^{1/2}} * f(\frac{a_0}{W})]^2 \frac{(1-\nu^2)}{2\sigma_{YS}E} + \frac{0.4(W-a_0)V_p}{0.4W + 0.6a_0 + z} \quad \text{[Equation 3.22]}$$

3.7 SUMMARY

The experimental details and test processes have been presented in this Chapter together with the necessary equations and processes to analyse the data. All the different specimens were explained, as well as the dimensions used. The different fixtures that were used including new ones that were designed have been presented.

A section on the experimental procedure for each of the three different sets of tests was presented, with a derivation of the loads which were used for each test stage. Worked examples of these derived equations are presented in the Results section, Chapter 4.

Finally a step-by-step process for analysing the test results was shown, with steps involving measuring of dimensions, reading Load-Deflection traces and using these values in calculations to determine the necessary values such as the "C" and "m" constants for the Paris fatigue equation, or the K_{IC} values for fracture toughness.

CHAPTER 4. RESULTS

This Chapter examines the results of the testing which was explained in Chapter 3. Each of the phases of testing contributed towards an understanding of the materials behaviour. The results in this Chapter show the curves for both SN and Paris fatigue testing. The fracture toughness values for the SENB and C-shaped specimens are also presented.

4.1 S-N FATIGUE TESTING

Results for the S-N testing varied from no crack initiation and growth, and therefore no failure, to rapid catastrophic fast fracture. Testing was carried out at stress levels ranging from 10 to 40 MPa, in increments of five MPa. Each test was repeated for each stress level to show repeatability. In cases where there was unsatisfactory repeatability, further tests were done.

The testing attempted to determine the effect of temperature on the fatigue life, and the log-log SN plots show the comparisons between 20˚C and 45˚C results. In addition to determining the temperature effect, it was investigated whether there was an ageing effect on the pipes, and these are also presented. While there was scatter from the tests, with some tests not falling consistently into the trend, the trend line indicates the overall behaviour.

The cycle count for the appearance of the first crack cycle was also recorded; however it was not always possible to “catch” the first crack as it was difficult to monitor constantly the relevant area of the specimens during testing, particularly underwater. In the instances where the first crack and failure cycle count are close or the same, this indicated that the first crack was indeed the failure point. This was especially prevalent in the old type at the higher stress levels of 35 and 40 MPa, and was the case in both ambient and temperature samples.

4.1.1 20˚C vs. 45˚C IN SN TESTS

The effect of temperature on the curve of SN behaviour is shown in Figure 4.1. This gives an indication of the effect that the two testing temperatures of 20˚C and 45˚C had on the fatigue behaviour of PVC pipe material. Figure 4.1 includes all OLD and NEW type materials for both 20˚C and 45˚C. All datum points for each stress level for failure and first crack can be found in Appendix G.

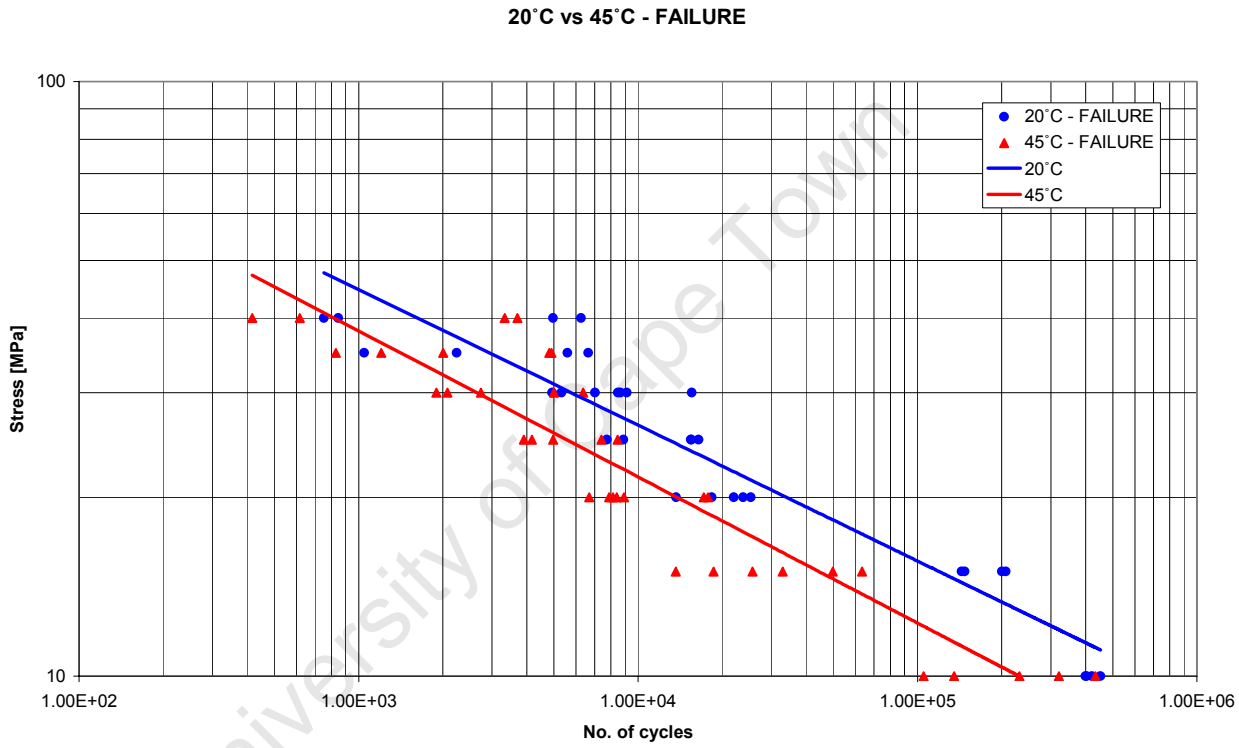

FIGURE 4.1: SN curve of failure for 20˚C vs. 45˚C

The general trend from Figure 4.1 shows a decrease in lifetime performance from the 20˚C to the 45˚C testing regime. The temperature effect was consistent from the lower to middle stress levels (10 – 25 MPa), but the effect was not as marked in the higher stress levels (30 – 40 MPa). This may be due to the shortness of the tests, with insufficient time for the temperature to have the full effect as that experienced in the longer tests.

At the lower and medium stress levels cracking occurred on the submerged half of the pipe for the 45˚C tests. However, for the high stress level tests

only, this was not always the case with some failures at the top as well as the base. Again, this could be attributed to the overriding effect of the high level of stress, and the lower cycle count until failure at these stress levels.

The curve showing the relationship for the First Crack between 20˚C and 45˚C is shown in Figure 4.2. This shows a slightly more skewed curve than that shown in Figure 4.1. This is due to the absence of cracking at the low (10 MPa) stress levels, and the closeness of the First Crack to Failure at the high (40 MPa) stress levels. Often the First Crack and Failure occurred at the same cycle count at the high stresses.

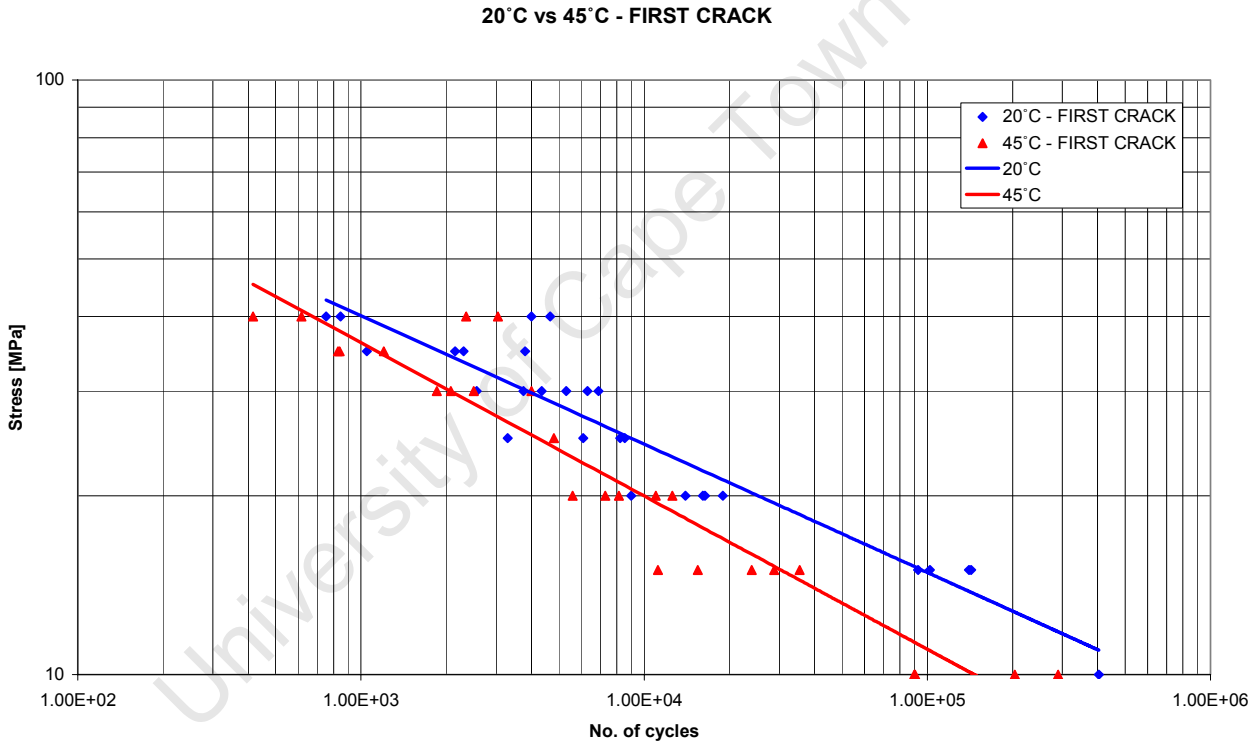

FIGURE 4.2: SN curve of first crack for 20˚C vs. 45˚C

4.1.2 EFFECTS OF AGEING IN SN TESTS

The effects of ageing were determined by comparing the SN fatigue life behaviour of both the NEW and OLD type at each temperature. The NEW and OLD comparison at 20˚C is shown in Figure 4.3, and the 45˚C comparison in Figure 4.4.

There was not a significant difference between the NEW and OLD type for the 20˚C tests, although there was a slight effect in the higher stress levels. For the 45˚C tests, there was a more noticeable effect at the lower stress levels, and again, a more pronounced effect at the higher stresses. There appeared to be an embrittling effect in the OLD type, which was noticed when the OLD type shattered whereas the NEW type would grow a fatigue crack at high (35 – 40 MPa) stresses.

The reason for this behaviour is unclear, but could perhaps be attributed to the older pipes being exposed to more environmental degradation (UV exposure before installation on site) compared to the NEW samples. Such UV exposure can lead to embrittlement, as mentioned from chain scission in Section 2.6.4. At lower stress levels (in fatigue) the effect was less marked, with the crack tip dominant, i.e.: the failure was driven more by fatigue crack tip effects rather than by environmental factors.

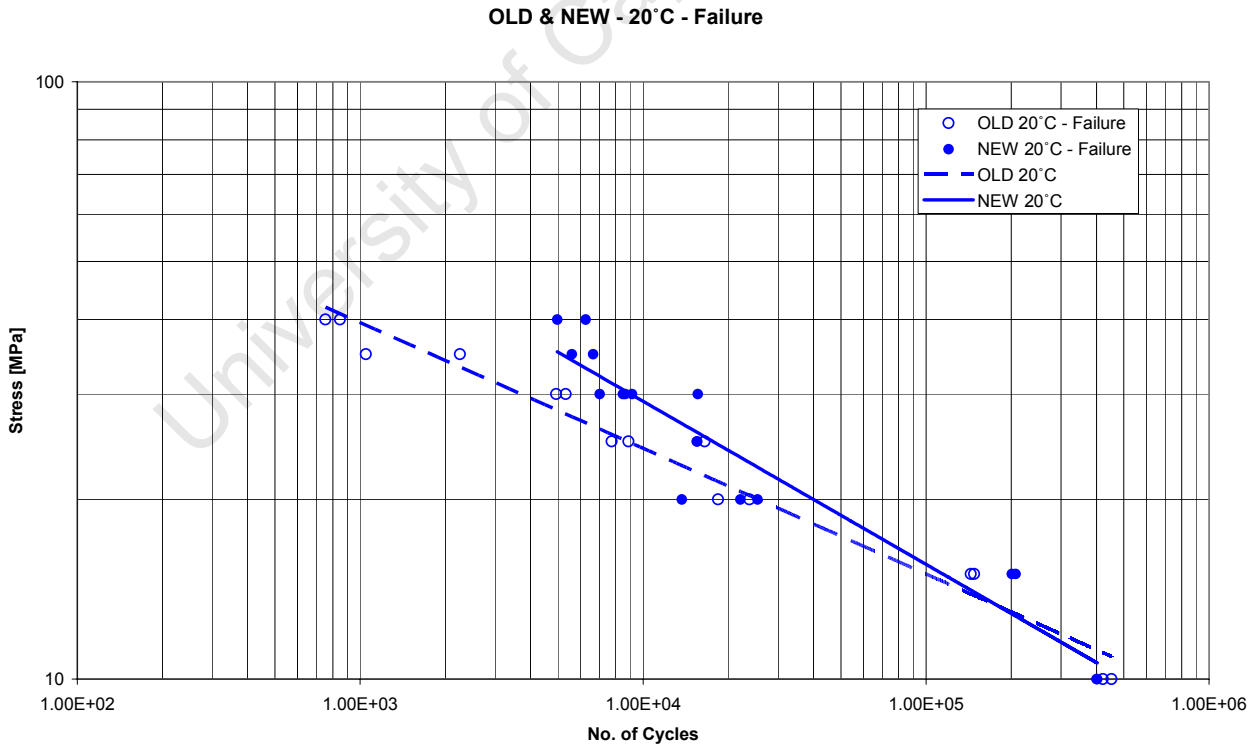

FIGURE 4.3: SN curve of OLD vs. NEW for 20˚C

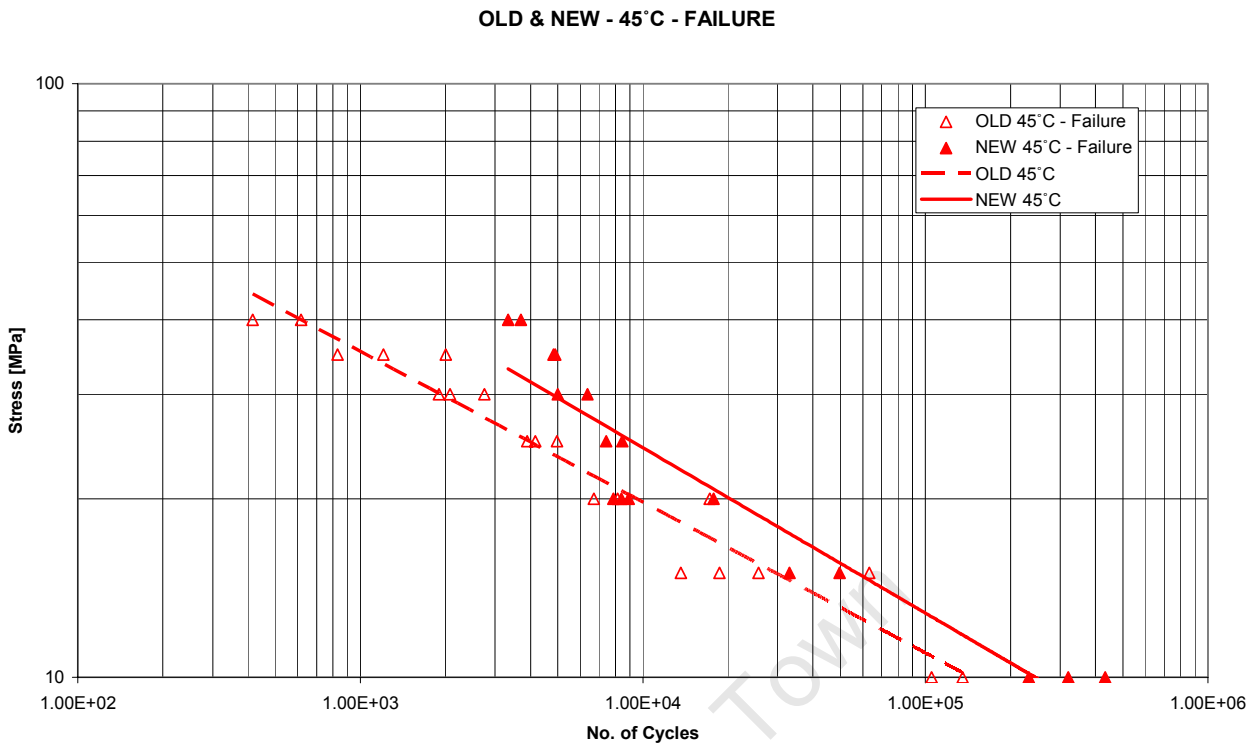

FIGURE 4.4: SN curve of OLD vs. NEW for 45˚C

4.1.3 TRENDS FROM SN TESTS

General trends were able to be identified from the S-N curves. Stable crack growth characterised the low to medium stress level tests (10 – 30 MPa) with cracks initially at crazes on the inside and propagating outwards, consistent with the fatigue crack growth in past test on uPVC fatigue [28], and with associated stress whitening along the edges and around the crack growth area. As the fatigue cracks reached critical flaw sizes as characterised by fracture mechanics (refer to Section 2.7.3) rapid catastrophic failure occurred. This was manifest by fast brittle cleavage and concoidal cracking and no stress whitening. This was the case for both on site fractures (Figure 4.5) and lab results (Figures 4.6 – 4.13).

For the 35 and 40 MPa tests, the OLD type failed predominantly by fast fracture. Failure at these levels was often catastrophic, and without significant warning. That is, there was no First Crack which could be identified. The force of failure in the 40 MPa tests was such that the pipe was largely destroyed.

The NEW type did not fail from fast fracture in any of the tests. However, crack growth was accelerated as the stress was increased.

The effect of increased temperature to 45˚C was to lower the number of cycles to failure for both the NEW and the OLD specimen types. However, in the very high stress tests for OLD, and sometimes for NEW, it is uncertain how much effect the temperature had on the material as failure emanated from the bottom and sometimes the top halves of the pipe. This was in contrast to what was expected to occur – that being that the lower half would deteriorate at the higher temperature and that failure would occur in this region. A possible reason for the failure of either top or bottom could be that the test was not long enough for the material to deteriorate due to temperature effects sufficiently for failure to occur in the submerged half of the pipe.

In order to be able to relate the SN results to the later fracture mechanics Paris equation correlation results, a similar set of constants, and prediction equation were considered necessary. By relating the Stress, Number of cycles and n (the gradient of the SN curve), it is possible to solve for a constant D, from the equation:

$$S = DN^n \qquad \text{[Equation 4.1]}$$

By making N the subject of the formula, it is possible to generate an equation which can predict the Number of cycles at a given stress, using constants in a manner analogous to the Paris equation (Equation 2.2 – Section 2.7.4):

$$N = AS^p \qquad \text{[Equation 4.2]}$$

Where the N is analogous to da/dN, S to ΔK, and p = 1/n. ‘A’ is solved by using the equation:

$$A = (\frac{1}{D})^{\frac{1}{n}} \qquad \text{[Equation 4.3]}$$

For example: Using the data for 45˚C, which had a gradient, n, of -0.245, and datum points of (100, 66.61), a value of D = 205.84 is obtained from Equation 4.1. This is then substituted into Equation 4.3, where 1/n would = -4.082, and realising a value of A = 2.77 * 10^9.

As a means of verification, Equation 4.2 should give the Number of cycles for 45˚C tests, at any given stress. Therefore, if a stress of 20 MPa were used, with the calculated constants, the corresponding N value would equal approximately 13540 cycles. A glance at Figure 4.1 would show this to be satisfactorily accurate.

The constants for the six material types are shown in Table 4.1. These values are discussed further in Section 4.4 and Chapter 5.

TABLE 4.1: Relative gradients and positions/intercepts of SN trend lines

Constant	20	45	NEW20	OLD20	NEW45	OLD45
n	-0.228	-0.245	-0.272	-0.210	-0.276	-0.251
D	215.86	205.84	359.84	168.60	311.29	199.67
p	-4.386	-4.082	-3.676	-4.762	-3.623	-3.984
A	17.3E+09	2.77E+09	2.50E+09	40.2E+09	1.08E+09	1.46E+09

4.1.4 FRACTOGRAPHIC COMPARISONS OF SPECIMENS

Upon inspection of the fracture surfaces from the pipe failures from the Jumeirah resort, the fracture surfaces clearly indicated a case of failure from fatigue (stress whitening). A fracture surface from a failed pipe recovered from the resort is shown in Figure 4.5.

Figure 4.5 highlights various features including: cracking from the inside outwards, clamshell markings, stress whitening as the crack grew to critical flaw size, and the (darker) brittle fracture (at the extreme ends of Figure 4.5). This particular crack was 235 mm long while the test specimens had a maximum crack length of 110 mm due to the length of the testing specimen.

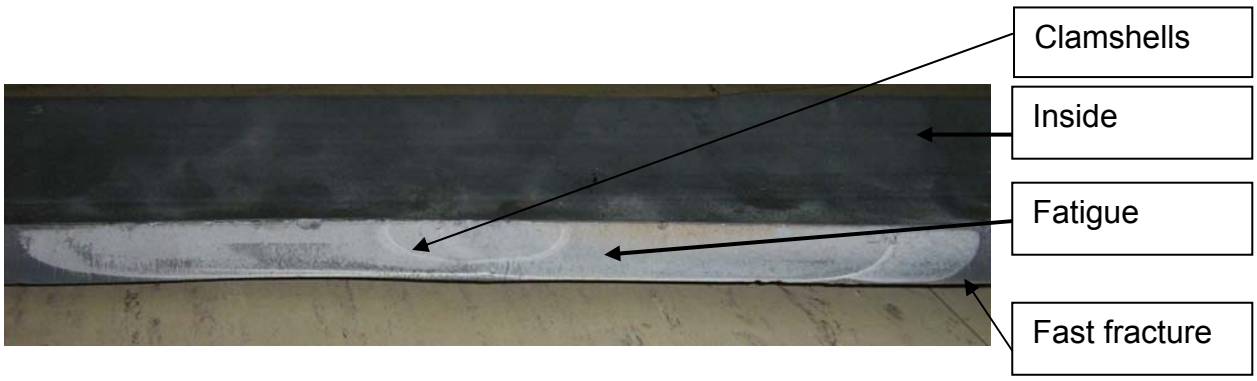

FIGURE 4.5: Fracture surface of a failed pipe from the Madinat Jumeirah resort

Fracture surfaces from SN fatigue testing in this project are shown in Figures 4.6 – 4.13 for fracture surfaces from tests ranging from 15 to 40 MPa. As can be seen in Figure 4.6, normal crack growth was experienced for the stress levels of 10 – 25 MPa for the 20˚C tests, and it was also observed that there was nominally no significant difference in the fracture surfaces in NEW and OLD specimens, although at the high stress level (25 MPa) the appearance of a critical flaw size begins to emerge.

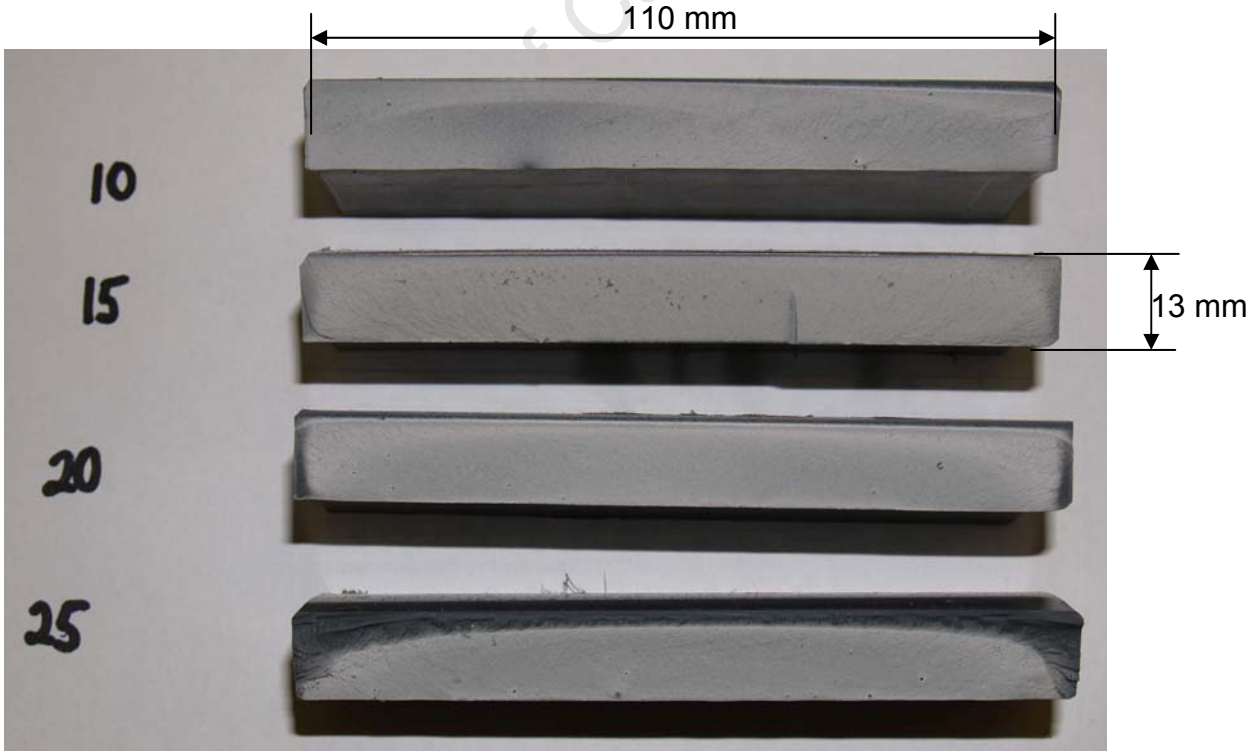

FIGURE 4.6: Fracture surfaces for 10 – 25 MPa and 20˚C

At the higher stress ranges (30 – 40 MPa) the critical crack length differed noticeably between the NEW and OLD materials. As shown in Figures 4.7

and 4.8, while the crack propagated through the NEW material (top) causing failure to be due essentially to fatigue, the OLD pipe (bottom) had a very short crack length before brittle failure became the failure mechanism.

FIGURE 4.7: Fracture surfaces of NEW (top) and OLD (bottom) at 30 MPa and 20˚C

FIGURE 4.8: Fracture surfaces of NEW (top) and OLD (bottom) at 40 MPa and 20˚C

These changing critical flaw sizes are broadly consistent with fracture mechanics behaviour based on measured fracture toughness values, as discussed further in Section 5.6.

An interesting phenomenon noticed about the fracture surfaces was the occasional presence of inclusions, from which the fatigue cracks originated. A close-up a fatigue fracture surface from a 10 MPa specimen is shown in Figure 4.6, showing inclusions, and the subsequent crack propagation is shown in Figure 4.9.

FIGURE 4.9: Inclusions of 10 MPa and 20˚C specimen

45˚C fracture surfaces followed a similar trend as that for the 20˚C specimens. The fracture surfaces for 10 – 25 MPa tests at 45˚C are shown in Figure 4.10. A noticeable difference between the 20˚C and the 45˚C fracture surfaces however, was that the 45˚C fracture surfaces appeared “whiter” suggesting that there is indeed some environmental degradation.

FIGURE 4.10: Fracture surfaces for 10 – 25 MPa and 45˚C

As with the 20˚C tests, the crack growth differed between NEW and OLD at the higher (30 – 40 MPa) stresses. The fracture surfaces from NEW (top) and OLD (bottom) 30 and 40 MPa specimens are shown in Figure 4.11 and 4.12.

FIGURE 4.11: Fracture surfaces of NEW (top) and OLD (bottom) at 30 MPa and 45˚C

FIGURE 4.12: Fracture surfaces of NEW (top) and OLD (bottom) at 40 MPa and 45˚C

As can be seen in Figure 4.12, the critical flaw size for this particular OLD type specimen was extremely small, an approximate size of 3 mm. A close-up of the crack showed an inclusion, surrounded by clamshells, indicative of a significant initiation point followed by failure by fatigue. The remainder of the fracture surface shows brittle failure. This is apparent in Figure 4.13.

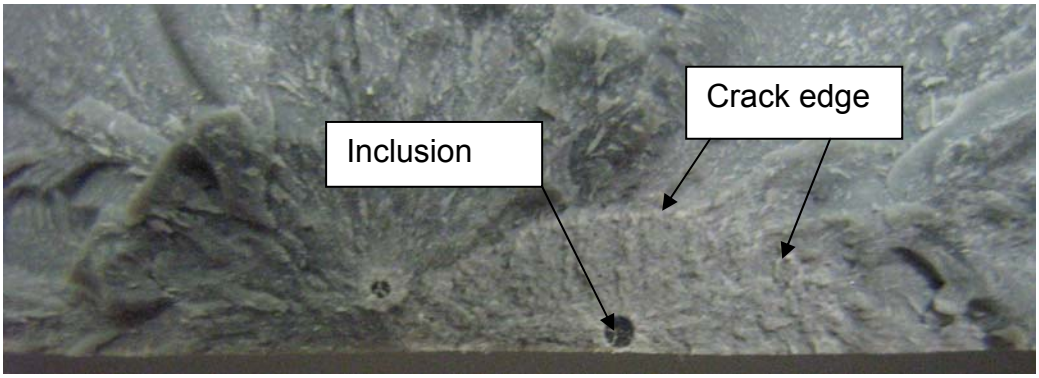

FIGURE 4.13: Inclusions and crack of 40 MPa and 45˚C specimen

4.2 PARIS FATIGUE RESULTS

Tests were conducted at 20˚C and at 45˚C to determine the crack propagation behaviour as characterised by the Paris equation (Equation 3.1, Section 3.1.3) using Compact-Tension (CT) specimens manufactured from NEW type material. These results were then compared with results from an undergraduate thesis, which was undertaken to provide data on Paris equation of the OLD type material, also nominally at both 20˚C and 45˚C.

4.2.1 20˚C VS. 45˚C IN PARIS TESTS

The results for all of the 20˚C and 45˚C, both NEW and OLD collectively are shown in Figure 4.14. While all of the data for the NEW (20˚C and 45˚C) type falls into an approximately linear corridor, the data from the OLD tests were more scattered, and it was decided that the OLD45˚C tests, while being represented in Figure 4.14, would not be included in the further calculation process as there was insufficient data to make an intelligent and thorough computation. The OLD 20˚C data would only be used as a means of determining ageing effects, and would not be grouped collectively with 20˚C data, when considering comparative temperature effects.

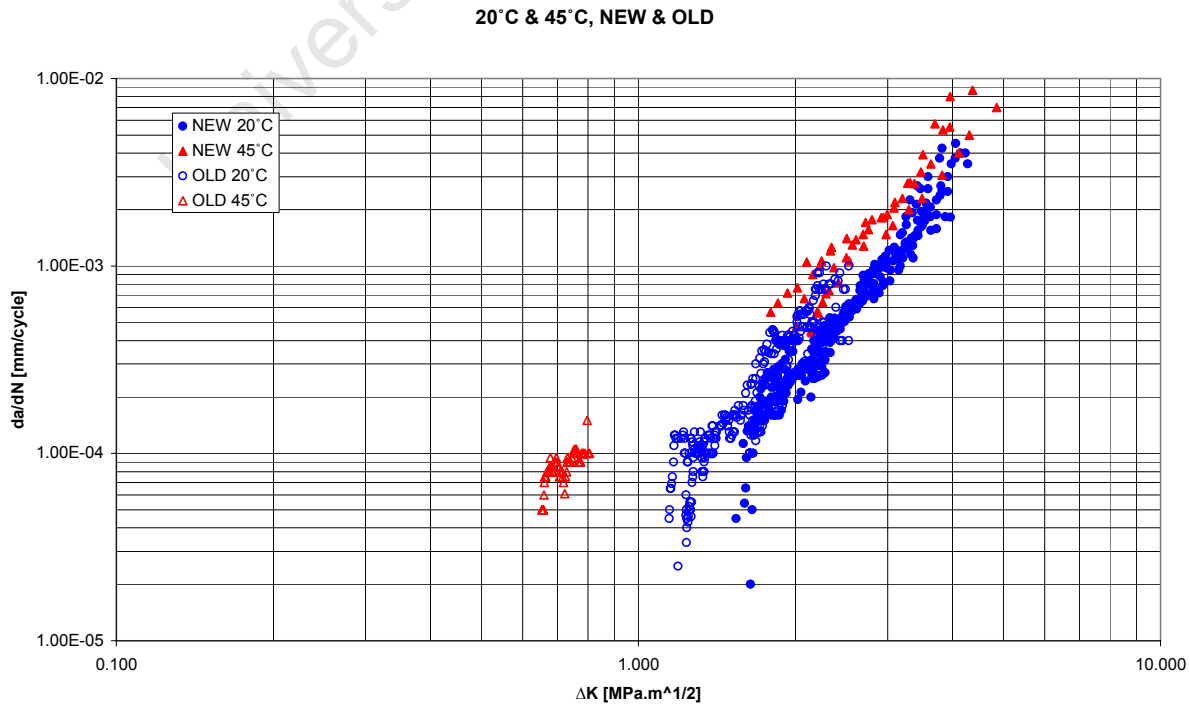

FIGURE 4.14: Paris curve for 20˚C and 45˚C, NEW and OLD

Using Equations 3.12 and 3.14, from Section 3.6.2, the constants in the Paris equation, m and C, were calculated. The Paris curves were truncated to only include the linear regions of the curve, the so-called “Phase II” explained in Section 2.7.3. The truncation cut off the data associated with fatigue thresholds (Phase I) and also those datum points at high growth rate (Phase III) beyond the rolling 9-point average system [52]. The truncated data and best fit lines for NEW20˚C and NEW45˚C are shown in Figure 4.15. Note that as mentioned above, the results for the OLD45˚C were excluded from calculation, and OLD20˚C data was used only for comparative ageing purposes, and therefore the data in Figure 4.8 is only of the NEW type material.

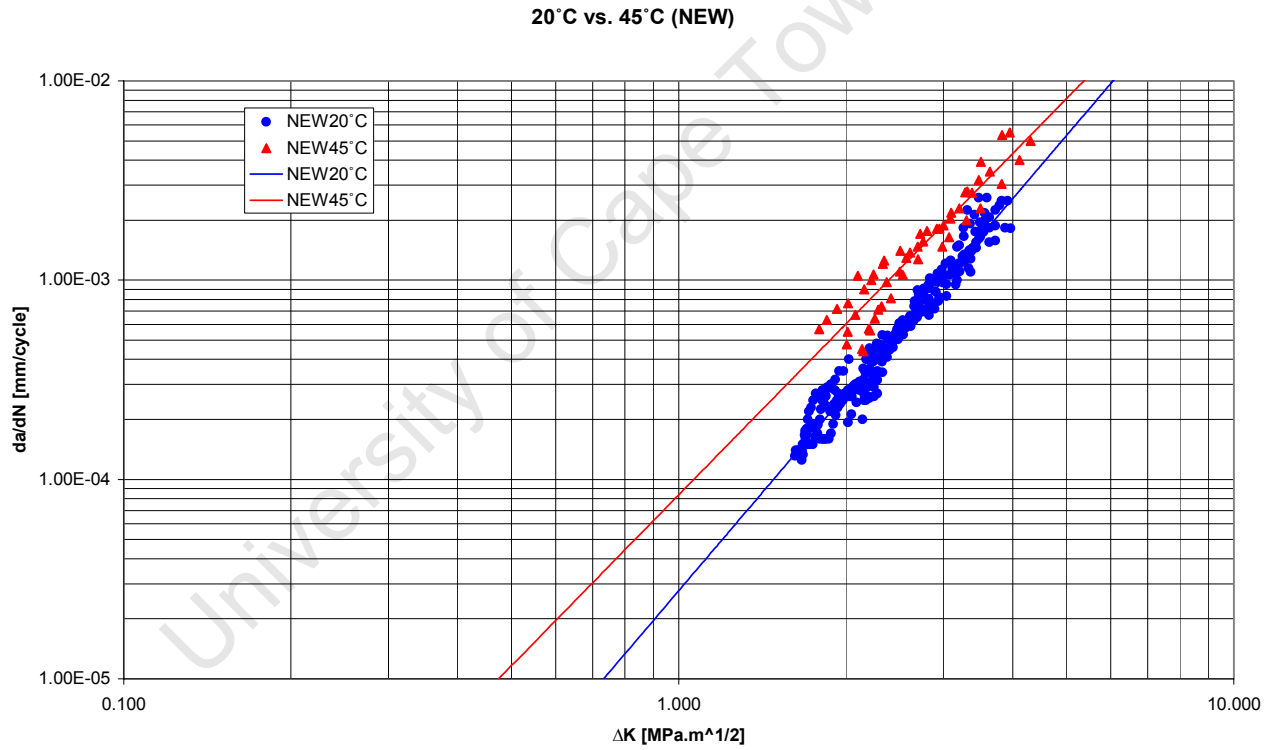

FIGURE 4.15: Paris curve for 20˚C vs. 45˚C

For example, to calculate the m and C values for the NEW 20˚C material, two sets of datum point pairs need to be selected from points from the curve, in this case $(6.13,\ 10^{-5})_1$ and $(0.737,\ 10^{-8})_2$. These are then substituted into Equation 3.14:

$$m = \frac{\log \frac{cycles_2}{cycles_1}}{\log \frac{\Delta K_2}{\Delta K_1}} = \frac{\log[cycle]_2 - \log[cycle]_1}{\log[\Delta K]_2 - \log[\Delta K]_2}$$ [Equation 3.14]

$$m = \frac{\log(10^{-5}) - \log(10^{-8})}{\log 6.13 - \log 0.737}$$

$$m = 3.26$$

m is then substituted into equation 3.12, along with one of the datum sets to determine C:

$$\log \frac{da}{dN} = m \log \Delta K + \log C$$ [Equation 3.12]

$$\log(10^{56}) = 3.26 \log(6..13) + \log C$$

$$C = 2.70 * 10^{-8} m / cycle$$

In addition to the best fit straight line through the data (so-called “line 2”), two other lines (1 and 3) were put through the datum points which could also be considered as acceptably representative trend lines for the behaviour. These different lines are shown in Figure 4.16.

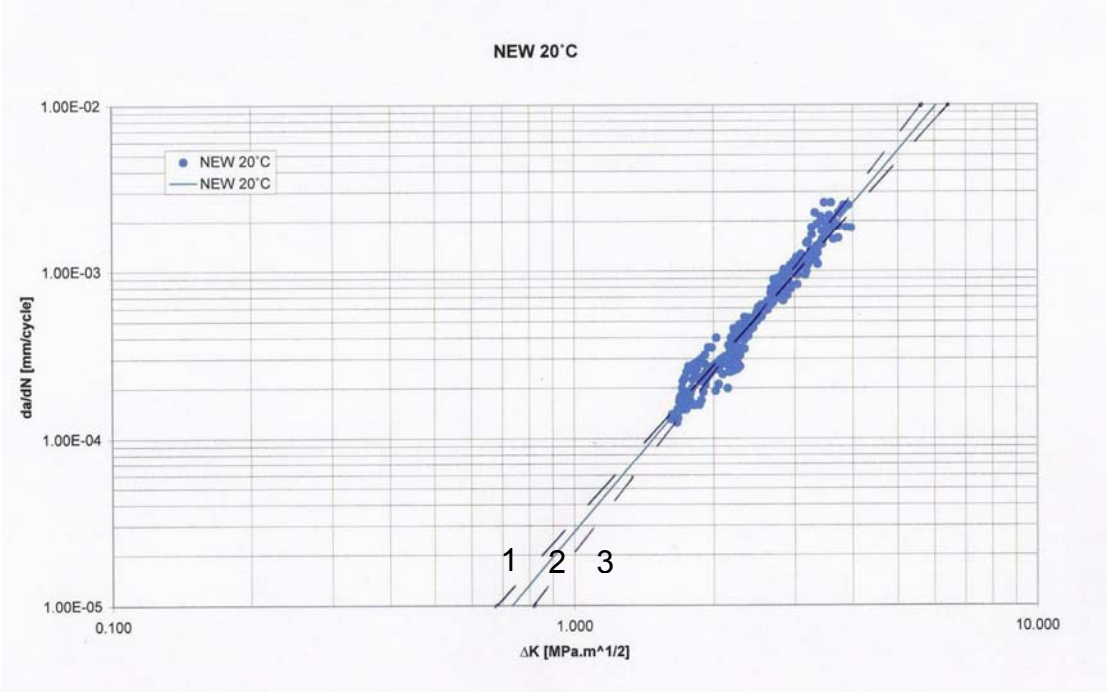

FIGURE 4.16: Trend lines 1, 2 and 3 for NEW20˚C

The m and C values for each line are also determined in a similar manner and shown in Table 4.2 as an indication of the potential error in m and C values.

TABLE 4.2: m and C values for NEW 20˚C and NEW 45˚C

Trend line	1	2	3
M - NEW20˚C	3.08	3.26	3.57
C – NEW20˚C	3.31E-08	2.71E-08	2.07E-08
m – NEW45˚C	2.46	2.85	3.10
C – NEW45˚C	13.4E-08	8.55E-08	6.81E-08

4.2.2 AGEING EFFECT IN PARIS TESTS

As was done for the prior SN fatigue tests, the NEW and OLD at 20˚C were analysed to determine if there was an ageing effect in the material. The Paris curves for NEW and OLD material at 20˚C are shown in Figure 4.17, but unfortunately this comparison could not be done at 45˚C due to insufficient data.

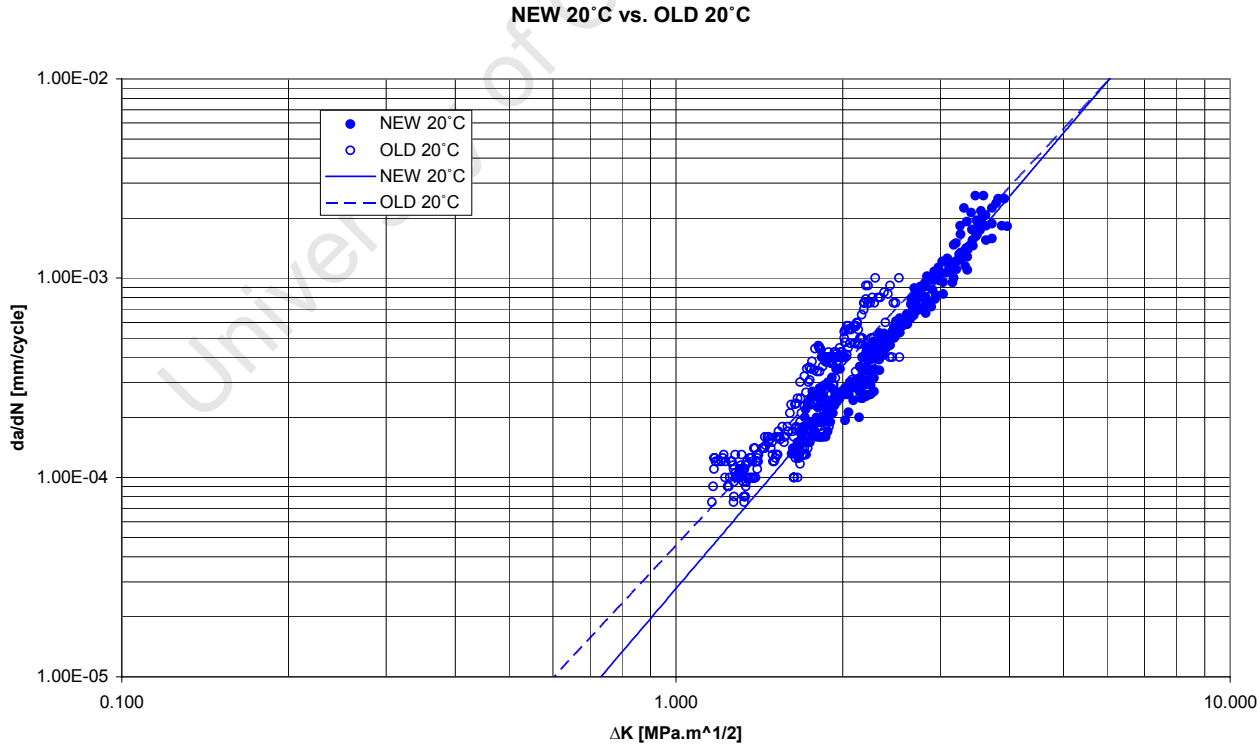

FIGURE 4.17: Paris curve for NEW and OLD material at 20˚C

The same method for calculating shown in Section 4.2.1 was followed. The results for the NEW 20˚C and OLD 20˚C are shown in Table 4.3. Again, a spread of three different but acceptably close trend lines was used.

TABLE 4.3: m and C values for NEW 20˚C and OLD 20˚C

Trend line	1	2	3
m - NEW20˚C	3.08	3.26	3.57
C - NEW20˚C	3.31E-08	2.71E-08	2.07E-08
m - OLD20˚C	2.58	2.99	3.72
C - OLD20˚C	6.40E-08	4.56E-08	3.23E-08

4.3 SUMMARY OF m AND C VALUES

The mean values for m and C are shown below. These include estimates of errors in the form of an approximate standard deviation.

NEW 20˚C:

- m = 3.26 ± 0.25
- C = 2.7 ± 0.6 * 10^{-8}

NEW 45˚C:

- m = 2.85 ± 0.3
- C = 8.55 ± 3.3 * 10^{-8}

OLD 20˚C:

- m = 3 ± 0.5
- C = 4.56 ± 1.5 * 10^{-8}

A means of indicating and calculating the relative differences between the material types can now be done by comparing the C-values for each grouping. For example, the difference in performance between NEW 20˚C and NEW 45˚C from the Paris constant C can be calculated by the following equation:

$$Temperature\ factor = \frac{C_1}{C_2} \qquad \text{[Equation 4.4]}$$

Therefore, to compare the fatigue life performance between NEW 20˚C and NEW 45˚C and thereby determine the relative temperature effect, the following process may be used:

$$Temperature\ factor = \frac{8.55 * 10^{-8}}{2.7 * 10^{-8}} = 3.17$$

$$Temperature\ factor = 3.17$$

Therefore, the temperature effect on crack growth rate is of the magnitude of approximately between 3 and 3.5 times effect for 20˚C versus 45˚C. Similarly, the ageing effect can be calculated using the data from NEW20˚C and OLD˚C. This ratio works out to be approximately 1.7.

Strictly, one would have to consider the exact level of ΔK being considered as the lines are not parallel (the slopes m are different). Nonetheless these values give an approximate estimate of the relative effect of temperature (20˚C to 45˚C) on fatigue life.

Therefore, in conclusion it is reasonable to say that there is a clear temperature effect on the fatigue life performance of the material of the order of 3 to 3.5 times. While there appears to be an ageing effect of approximately 1.5 times, it is reasonable that the effect is not as substantial as that of the temperature effect (3.2X). To return to the failure scenario of the pipes underground in the Madinat Jumeirah resort, the fatigue life performance and ultimate failure appears to be driven predominantly by a temperature effect.

4.4 COMPARISON OF SN AND PARIS GRAPHS

The values for m and C from Section 4.3 can be related to the corresponding slope and “intercept” (n and A) values for the SN graphs (Section 4.1.3). By calculating these and the values for the SN graphs (Table 4.1), a suitable comparison can be made between the different trends for each testing phase.

The temperature effect on lifetime from the SN data is of the order of 2.0 to 4.6 times (depending on stress level). This is further explained in Section 5.2.1. The effect on crack growth rate as monitored by the Paris formulation (above) is approximately 3.0 to 3.5 (for NEW material) times as shown above.

These trends are self consistent and of the same order, but do depend on rigorous values of stress and initial flaw size.

4.5 FRACTURE TOUGHNESS RESULTS

As shown in Section 2.7.2, according to LEFM – Linear Elastic Fracture Mechanics – fracture toughness values are necessary for the calculation of the fatigue lifetime in that the toughness value facilitates determination of the critical flaw size, which is used as the upper limit in the fatigue life integration (Equation 2.3).

The relevant dimensions of each specimen were measured, and those values used in toughness evaluation (Equations 3.17 – 3.22). Examples of toughness determination for SENB and C-shaped specimens, as well as a calculation of Crack-Tip Opening Displacement (CTOD) are presented below. Further details on specific specimens' geometries, as well as a summary of the individual values used for calculation, are given in Appendix H. The graphs containing the Load versus Crack extension plots are given in Appendix E.

24 specimens were tested for each of the SENB and C-Shaped tests. The 24 specimens included 12 NEW and 12 OLD types. However, not all samples were used for calculation of the fracture toughness as a few were excluded due to handling errors in ramping. Fracture toughness was measured in the standard units of MPa√m.

4.5.1 SENB SAMPLE CALCULATION

The ramping curve of SENB specimen 3PT2 is show in Figure 4.18. This is the specimen which will be used for the sample calculation.

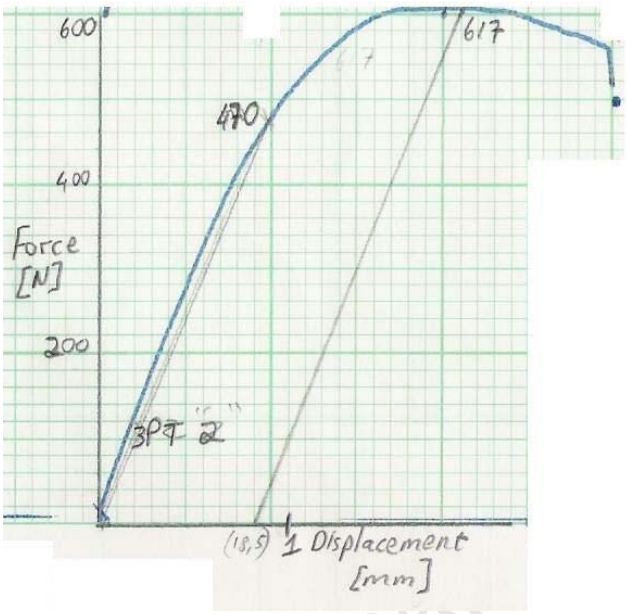

FIGURE 4.18: Force-Displacement curve of 3PT2

A 5% offset line was drawn, and the value for P_Q read – in this case = 470 N. When measuring the specimen, the values for B and W were 11.38 mm and 24.24 mm respectively. The crack length was measured by the process explained in Section 3.6.3.1, and found to be 13.08 mm; this gave an a/W value of 0.540. Reading from the codes [55], the value for f(a/W) was 3.04. A copy of this table for the reading of f(a/W) for SENB specimens can be found in Appendix D.

Using these values, and a span of 100 mm, K_q was calculated as follows using Equation 3.17:

$$K_q = \left(\frac{P_q S}{BW^{3/2}}\right) * f\left(\frac{a}{w}\right) \qquad \text{[Equation 3.17]}$$

$$K_q = (\frac{470 * 0.1}{0.01138 * 0.02424^{3/2}}) * (3.04)$$

$$K_q = 3.33 MPa\sqrt{m}$$

The above calculations were used to calculate the fracture toughness values for the OLD and NEW SENB specimens, in units of MPa√m. The relevant data used for the calculation of K_q for NEW and OLD type is shown in Table 4.4 and 4.5 respectively. Some of the values, for example V_p were not used for the fracture toughness calculation, but were however used for CTOD calculations and therefore included in the table of relevant data.

TABLE 4.4: Fracture toughness values for NEW SENB specimens

Specimen	a	W	B	z	a/w	f(a/w)	F_m	V_p	F_q	K_q
	[mm]	[mm]	[mm]	[mm]			[N]	[mm]	[N]	MPa√m
3PT1	13.66	24.45	10.98	3.01	0.56	3.19	606	0.857	440	3.34
3PT2	13.08	24.24	11.38	3.04	0.54	3.04	617	0.881	470	3.33
3PT3	13.39	24.55	11.03	3.10	0.55	3.14	650	0.810	400	2.96
3PT4	13.04	24.46	11.01	3.03	0.53	2.94	635	0.952	430	3.00
3PT5	12.50	24.21	11.32	3.06	0.52	2.84	757	1.119	460	3.06
3PT6	11.97	24.24	11.30	3.15	0.49	2.58	727	0.833	520	3.15
3PT7	12.50	24.37	11.33	3.01	0.51	2.75	745	0.905	460	2.93
3PT8	12.97	24.44	11.03	3.09	0.53	2.94	618	0.881	400	2.79
3PT9	12.65	24.22	11.34	3.01	0.52	2.84	670	0.929	440	2.92
3PT10	12.37	24.39	11.32	3.10	0.51	2.75	723	1.071	400	2.55
3PT11	13.14	24.44	11.28	3.09	0.54	3.04	704	1.167	500	3.53
3PT12	13.06	24.45	11.32	3.05	0.53	2.94	660	1.143	400	2.72
Mean	12.86	24.37	11.22	3.06	0.53	2.92	676	0.962	443	**3.02**
Std Dev	0.47	0.11	0.16	0.04	0.02	0.18	53	0.128	41	0.28

TABLE 4.5: Fracture toughness values for OLD SENB specimens

Specimen	a	W	B	z	a/w	f(a/w)	F_m	V_p	F_q	K_q
	[mm]	[mm]	[mm]	[mm]			[N]	[mm]	[N]	MPa√m
3PT20	12.20	24.26	11.13	2.98	0.50	2.66	605	0.500	470	2.97
3PT21	11.82	24.24	11.13	3.10	0.49	2.58	677	0.667	460	2.83
3PT22	12.44	24.24	11.21	3.01	0.51	2.75	603	0.524	460	2.99
3PT23	12.13	24.32	11.14	2.99	0.50	2.66	620	0.405	520	3.27
3PT24	12.04	24.24	11.19	3.04	0.50	2.66	618	0.429	500	3.15
3PT25	11.70	24.21	11.25	3.06	0.48	2.59	660	0.381	490	2.99
3PT26	12.34	24.23	11.16	3.14	0.51	2.75	640	0.619	500	3.27
3PT27	12.64	24.22	11.28	3.12	0.52	2.84	583	0.476	450	3.01
3PT28	12.62	24.22	11.18	3.18	0.52	2.84	573	0.524	420	2.83
3PT29	12.12	24.23	11.17	3.05	0.50	2.66	684	0.762	460	2.90
3PT30	12.00	24.23	11.23	2.99	0.50	2.66	663	0.524	500	3.14
3PT31	11.82	24.22	11.24	3.04	0.49	2.58	661	0.524	480	2.92
Mean	12.10	24.25	11.18	3.04	0.50	2.66	641	0.550	483	**3.05**
Std Dev	0.21	0.03	0.04	0.05	0.01	0.06	31	0.114	22	0.16

The samples 3PT25, 3PT27 and 3PT28 for the OLD type were excluded due to errors in handling procedure during the ramping stages and non-achievement of peak load.

The summary of values for the SENB specimens is presented in Table 4.6, showing the mean values for NEW, OLD, and the combination of NEW and OLD. The values indicate that there is no significant difference in toughness for OLD and NEW specimens (i.e.: with a circumferential crack orientation).

TABLE 4.6: K_{IC} fracture toughness values for SENB specimens

Sample	Mean	Std Deviation
NEW	3.02	0.28
OLD	3.05	0.16

4.5.2 C-SHAPE SAMPLE CALCULATION

The ramping curve of 3CUR11 is show in Figure 4.19. This is the specimen which will be used for the sample calculation.

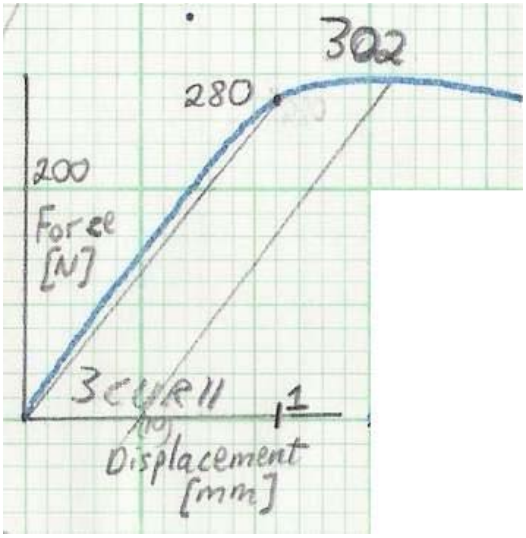

FIGURE 4.19: Force-Displacement curve of 3CUR11

A 5% offset line was drawn, and the value for F_q read – in this case = 280 kN. Measurements of the specimen were made, and the values for B and W were 15.82 mm and 13.64 mm respectively. The crack length was measured, and found to be 8.12 mm; this gave an a/W value of 0.595. Reading from the codes [52], the value for f(a/W) was 5.145. This value was also verified using Equation 3.21. A copy of this table for the reading of f(a/W) for the C-Shaped specimens can be found in Appendix D.

Ideally values for r_1 and r_2, the inner and outer radii of the C-shape specimens (Figure 3.5) should be approximately 110 mm and 97 mm according to the initial dimensions for the pipe (Figure 3.2). However, due to variations in fabrication, these cannot be taken as standard values for calculation purposes. Therefore, these values needed to be calculated to get the precise values for use in the fracture toughness evaluation.

To determine r_1 and r_2, X and L, the Loading hole offset and Length (Figure 3.32) were required, and in the case of 3CUR11 were 7.28 mm and 130.44 mm respectively. X and L could be used to calculate r_2, the outer radius, with equation 3.18. The ratio r_1/r_2 could then be calculated using Equation 3.19, and finally, as a check, r_1 could be calculated as a comparison to the ideal value for r_1.

Using the correct units, and Equation 3.18:

$$r_2 = \frac{L^2}{8(W+X)} + \frac{(W+X)}{2} \quad \text{[Equation 3.18]}$$

$$r_2 = \frac{(0.13046)^2}{8(0.01364+0.00728)} + \frac{(0.01364+0.00728)}{2}$$

$$\therefore r_2 = 0.112m$$

The ratio r_1/r_2 was then calculated using Equation 3.19:

$$r_1 / r_2 = 1 - \frac{W}{r_2} \quad \text{[Equation 3.19]}$$

$$r_1 / r_2 = 1 - \frac{0.01364}{0.112}$$
$$\therefore r_1 / r_2 = 0.878$$

$$\therefore r_1 = 0.878 * 0.112$$
$$r_1 = 0.098m$$
$$r_1 - r_2 = 0.112 - 0.098 = 0.014m$$

The above values are consistent with the actual nominal outer radius, inner radius and wall thickness of approximately 100, 97 and 13 mm respectively. These values were then substituted into Equation 3.20 to solve for K_q:

$$K_q = (\frac{P_q}{BW^{1/2}})[3\frac{X}{W} + 1.9 + 1.1\frac{a}{W}] * [1 + 0.25(1 - \frac{a}{W})^2(1 - \frac{r_1}{r_2})] * f(\frac{a}{W}) \quad \text{[Equation 3.20]}$$

$$K_q = (\frac{280}{0.01582 * 0.01364^{1/2}})[3\frac{0.007.28}{0.01364} + 1.9 + 1.1\frac{0.00812}{0.01364}] * [1 + 0.25(1 - \frac{0.00812}{0.01364})^2 *$$

$$(1 - 0.878)] * 5.145$$

$$\therefore K_q = 3.26MPa\sqrt{m}$$

The Fracture toughness values for the C-shaped specimens, in units of MPa√m, are shown in Tables 4.7 and 4.8 for NEW and OLD specimens respectively. 3CUR1 and 3CUR3 were excluded due to handling errors and non-achievement of peak load during the ramp testing process.

TABLE 4.7: Fracture toughness values for NEW C-shaped specimens

Specimen	a	W	B	z	a/w	f(a/w)	X	L	r1/r2	F_m	F_q	K_q
	[mm]	[mm]	[mm]	[mm]			[mm]	[mm]		[N]	[N]	MPa√m
3CUR1	8.61	13.53	15.00	2.90	0.636	6.054	8.38	130.16	0.874	303	280	4.35
3CUR2	8.25	14.52	15.89	2.82	0.568	4.662	6.59	128.44	0.866	471	380	3.62
3CUR3	8.30	12.99	15.00	2.92	0.639	6.120	8.29	131.28	0.884	260	-	-
3CUR4	7.33	13.71	15.81	2.87	0.535	4.162	7.95	130.99	0.875	450	340	3.25
3CUR5	7.08	12.89	15.90	2.85	0.549	4.368	7.88	130.22	0.885	322	280	2.96
3CUR6	7.81	13.58	15.75	2.89	0.575	4.778	7.55	128.39	0.874	410	340	3.74
3CUR7	7.41	13.66	15.80	2.81	0.542	4.270	7.25	128.48	0.875	461	380	3.62
3CUR8	8.13	13.70	15.80	2.72	0.593	5.109	7.22	130.32	0.878	384	320	3.67
3CUR9	7.47	12.95	15.81	2.82	0.577	4.807	8.13	130.93	0.885	276	250	2.97
3CUR10	7.80	13.98	15.87	2.64	0.558	4.499	6.92	130.93	0.876	414	320	3.09
3CUR11	8.12	13.64	15.82	2.97	0.595	5.145	7.28	130.46	0.878	302	280	3.26
3CUR12	7.84	13.51	14.86	2.83	0.580	4.868	7.95	129.90	0.876	276	250	3.05
Mean	7.72	13.61	15.73	2.82	0.567	4.667	7.47	129.91	0.877	377	314	**3.32**
Std Dev	0.39	0.47	0.31	0.09	0.021	0.338	0.51	1.071	0.005	77	48	0.31

TABLE 4.8: Fracture toughness values for OLD C-shaped specimens

Specimen	a	W	B	z	a/w	f(a/w)	X	L	r1/r2	F_m	F_q	K_q
	[mm]	[mm]	[mm]	[mm]			[mm]	[mm]		[N]	[N]	MPa√m
3CUR20	6.53	13.11	14.98	2.65	0.498	3.711	7.96	130.62	0.883	325	260	2.42
3CUR21	7.26	13.59	15.15	2.69	0.534	4.156	6.90	130.88	0.882	359	250	2.37
3CUR22	7.01	13.55	15.00	2.59	0.517	3.938	7.94	128.58	0.873	371	300	2.88
3CUR23	6.67	13.02	14.91	3.11	0.512	3.876	8.51	126.90	0.875	331	270	2.74
3CUR24	6.93	12.96	14.87	3.02	0.535	4.163	8.95	130.35	0.880	263	230	2.60
3CUR25	7.57	13.48	14.81	2.53	0.562	4.556	7.57	126.63	0.873	368	270	3.02
3CUR26	7.93	13.29	15.15	2.33	0.597	5.172	6.37	130.01	0.887	272	260	3.09
3CUR27	6.56	13.00	14.88	3.03	0.505	3.785	7.85	128.15	0.881	337	290	2.78
3CUR28	7.02	12.81	14.87	2.96	0.548	4.350	7.41	128.70	0.886	288	250	2.75
3CUR29	7.18	12.92	14.87	2.66	0.556	4.465	7.93	130.77	0.886	281	230	2.66
3CUR30	6.99	13.61	14.76	2.98	0.514	3.892	7.45	130.08	0.877	343	280	2.62
3CUR31	6.48	13.21	14.93	2.72	0.491	3.628	8.23	127.70	0.875	298	250	2.30
Mean	7.01	13.21	14.93	2.77	0.531	4.141	7.75	129.11	0.880	320	262	**2.69**
Std Dev	0.44	0.29	0.12	0.24	0.031	0.440	0.69	1.53	0.005	38	22	0.25

The summary of values for the C-shaped specimens is presented in Table 4.9, showing the mean values for NEW and OLD material type. While the toughness values for the SENB samples (i.e.: cracking circumferentially) were nominally identical (3.02 versus 3.05 for NEW and OLD respectively), the values for the C-Shape specimen (i.e.: cracking longitudinally) vary significantly; between NEW and OLD material types from 3.32 to 2.69 MPa√m. Thus, it is possible to conclude that not only is there a crack orientation effect but also an ageing effect in the C-shape specimens, from the samples tested.

TABLE 4.9: K_{IC} fracture toughness values for C-Shaped specimens

Sample	Mean	Std Deviation
NEW	3.32	0.31
OLD	2.69	0.25

4.5.3 CTOD SAMPLE CALCULATION

The methodology for calculating the CTOD was the similar to that employed for SENB and C-Shaped specimens. For the sample calculation, 3PT2 will again be used, referring to Figure 4.18.

A line was drawn parallel to the elastic region of the curve, from the point of maximum load (F_m = 617 N) to the zero load line. This then gave a value for V_p of 0.881 mm. Where applicable, the values used for calculating the fracture toughness for the SENB specimen are again used here. Values used for Poisson's ratio (ν), Yield strength (σ_{ys}) and Elastic modulus (E) were 0.41, 50 MPa and 3000 MPa respectively [24, 42]. The CTOD was calculated using Equation 3.22. The crack length was 13.08 mm, and z, the height of the knife edges used for the ramp tests was 3.04 mm. The span for SENB specimens was 100 mm.

$$\delta = [\frac{FS}{BW^{1/2}} * f(\frac{a_0}{W})]^2 \frac{(1-\nu^2)}{2\sigma_{YS}E} + \frac{0.4(W-a_0)V_p}{0.4W + 0.6a_0 + z} \qquad \text{[Equation 3.22]}$$

$$\delta = [\frac{617 * 0.1}{0.01138 * 0.02424^{1/2}} * 3.04]^2 \frac{(1 - 0.41^2)}{2 * 50 * 10^6 * 3000 * 10^6} + \frac{0.4(0.02424 - 0.01308) * 0.000881}{0.4 * 0.02424 + 0.6 * 0.01308 + 0.00304}$$

$$\therefore \delta = 0.031 * 10^{-6} + 0.191 * 10^{-3}$$

$$\delta = 0.191 * 10^{-3} mm$$

The CTOD values for the SENB and C-shaped specimens, for NEW and OLD are shown in Tables 4.10 – 4.13.

TABLE 4.10: CTOD for NEW SENB specimens

Specimen	Elastic [µm]	Plastic [mm]	CTOD [mm]	% Elastic	% Plastic
3PT1	0.0352	0.176	0.176	0.02	99.98
3PT2	0.0311	0.191	0.191	0.02	99.98
3PT3	0.0387	0.172	0.172	0.02	99.98
3PT4	0.0326	0.211	0.211	0.02	99.98
3PT5	0.0413	0.259	0.259	0.02	99.98
3PT6	0.0315	0.204	0.204	0.02	99.98
3PT7	0.0372	0.212	0.212	0.02	99.98
3PT8	0.0308	0.196	0.196	0.02	99.98
3PT9	0.0322	0.212	0.212	0.02	99.98
3PT10	0.0351	0.254	0.254	0.01	99.99
3PT11	0.0408	0.254	0.254	0.02	99.98
3PT12	0.0333	0.252	0.252	0.01	99.99
Mean	0.0350	0.216	**0.216**	0.016	99.98
Std dev	0.00374	0.031	0.031	0.003	0.003

(Again 3PT25, 3PT27 and 3PT28 were excluded as for the fracture toughness calculations)

TABLE 4.11: CTOD for OLD SENB specimens

Specimen	Elastic	Plastic	CTOD	% Elastic	% Plastic
	[µm]	[mm]	[mm]		
3PT20	0.0239	0.121	0.121	0.02	99.98
3PT21	0.0282	0.167	0.167	0.02	99.98
3PT22	0.0250	0.123	0.123	0.02	99.98
3PT23	0.0250	0.099	0.099	0.02	99.98
3PT24	0.0247	0.105	0.105	0.02	99.98
3PT25	0.0264	0.096	0.096	0.02	99.98
3PT26	0.0285	0.145	0.146	0.02	99.98
3PT27	0.0247	0.108	0.108	0.02	99.98
3PT28	0.0243	0.119	0.119	0.02	99.98
3PT29	0.0304	0.184	0.184	0.02	99.98
3PT30	0.0282	0.129	0.129	0.02	99.98
3PT31	0.0264	0.131	0.131	0.02	99.98
Mean	0.0267	0.134	**0.134**	0.02	99.98
Std dev	0.00220	0.028	0.028	0.000	0.000

(3CUR1 and 3CUR3 were again omitted)

TABLE 4.12: CTOD for NEW C-shape specimens

Specimen	Elastic	Plastic	CTOD	% Elastic	% Plastic
	[um]	[mm]	[mm]		
3CUR1	3.35E-06	0.058	0.058	0.01	99.99
3CUR2	3.66E-06	0.129	0.129	0.00	100.00
3CUR3	-	-	-	-	-
3CUR4	3.23E-06	0.130	0.130	0.00	100.00
3CUR5	2.48E-06	0.088	0.088	0.00	100.00
3CUR6	3.40E-06	0.107	0.107	0.00	100.00
3CUR7	3.40E-06	0.133	0.133	0.00	100.00
3CUR8	3.38E-06	0.119	0.119	0.00	100.00
3CUR9	2.35E-06	0.069	0.069	0.00	100.00
3CUR10	3.17E-06	0.107	0.107	0.00	100.00
3CUR11	2.68E-06	0.077	0.077	0.00	100.00
3CUR12	2.48E-06	0.098	0.098	0.00	100.00
Mean	3.00E-06	0.103	**0.103**	0.00	100.00
Std dev	4.98E-07	0.022	0.022	0.00	0.00

TABLE 4.13: CTOD for OLD C-shape specimens

Specimen	Elastic	Plastic	CTOD	% Elastic	% Plastic
	[um]	[mm]	[mm]		
3CUR20	2.24E-06	0.127	0.127	0.00	100.00
3CUR21	2.69E-06	0.106	0.106	0.00	100.00
3CUR22	2.67E-06	0.107	0.107	0.00	100.00
3CUR23	2.40E-06	0.103	0.103	0.00	100.00
3CUR24	2.06E-06	0.098	0.098	0.00	100.00
3CUR25	3.11E-06	0.095	0.095	0.00	100.00
3CUR26	2.57E-06	0.070	0.070	0.00	100.00
3CUR27	2.40E-06	0.066	0.066	0.00	100.00
3CUR28	2.37E-06	0.067	0.067	0.00	100.00
3CUR29	2.37E-06	0.095	0.095	0.00	100.00
3CUR30	2.47E-06	0.120	0.120	0.00	100.00
3CUR31	2.01E-06	0.102	0.102	0.00	100.00
Mean	2.45E-06	0.096	**0.096**	0.00	100.00
Std dev	2.96E-07	0.0198	0.0198	0.00	0.00

A summary of the CTOD mean values and standard deviations for NEW and OLD type material is shown in Table 4.14 for SENB and C-shaped specimens. For all of the calculations for the specimens, CTOD was almost entirely essentially plastic, with minimal contribution from elastic sources for the C-shaped specimens.

Values differed from the NEW to the OLD specimen types for the SENB specimens, with a CTOD of almost 40% less for the OLD than for the NEW. However, for the C-shaped specimens where the cracking is longitudinal, the CTOD was almost identical. Both sets of specimens had similar standard deviations.

TABLE 4.14: CTOD fracture toughness values for C-Shaped specimens

Sample	Mean	Std Deviation
	[mm]	[mm]
SENB NEW	0.216	0.031
SENB OLD	0.134	0.028
C-SHAPE NEW	0.103	0.022
C-SHAPE OLD	0.096	0.020

The values from Table 4.14 and those for the elastic K_{IC} fracture toughness, Tables 4.6 and 4.9 would seem, at first glance, to be contradictory. The SENB K_{IC} toughness values (Table 4.6) between the NEW and OLD SENB specimens differed marginally (3.02 to 3.05 MPa$\sqrt{m}$) while the C-shape values (Table 4.9) showed a significant difference between the NEW and OLD (3.32 to 2.69 MPa$\sqrt{m}$). For CTOD values, the SENB (Table 4.14) showed a marked difference between those values for NEW and OLD (0.216 to 0.134 mm), while the values for CTOD C-shaped specimens (Table 4.14) showed a small difference between the NEW and OLD (0.103 to 0.096 mm). A suggested difference is ductility (and hence V_P)

It should however be noted that cracking in the longitudinal direction (i.e.: C-Shaped specimens) generally yielded lower CTOD fracture toughness than circumferential cracking (i.e.: SENB specimens), as might be expected.

4.6 SUMMARY

Chapter 4 presented all the data from testing. Each phase of testing was analysed to determine trends and noticeable characteristics.

The SN curves showed a decrease in performance from 20˚C to 45˚C, a relationship which was also apparent for the fatigue cracking. Ageing effects were noticeable, but they were not as substantial as the temperature effect. Gradients and “intercepts” in the form of ‘n’ and ‘A’ were calculated, for use in equations to predict the cycle count for any particular stress, or vice-versa.

The fracture surfaces were examined, and it was determined that up until 25 MPa, normal crack growth was apparent. At higher stresses, crack growth was rapid and shorter, with failure occurring sometimes from very small thumb-nail cracks, as was often the case for OLD type material.

Paris fatigue results of truncated data confirmed the temperature effect on the material, in the case of NEW 20˚C to 45˚C, the temperature effect on reducing

the fatigue life was between 3 and 3.5. Gradients and intercepts (m and C) were calculated for each of the test groups. 3 Trend lines were used to present a spread of possible values for m and C. An ageing effect was also confirmed by Paris testing, but this was only by a factor of approximately 1.7 times.

The SN curves similarly showed a decrease in fatigue lifetime with temperature of approximately 1.6 to 4.6 times (depending on stress level) and this is discussed in more detail in the following Chapter.

Fracture toughness results showed a higher toughness value for both K_{IC} and CTOD fracture toughness values for the SENB samples, than for the C-Shaped specimens, consistent with longitudinal cracking occurring more readily than circumferential cracking. All of the values used for K_{IC} and CTOD fracture toughness calculations were presented.

CHAPTER 5. DISCUSSION

5.1 INTRODUCTION

This Chapter evaluates all the results from each of the testing phases. The test results and the comparison between the test data from testing and comparative data from literature are also discussed. Where applicable, conclusions are drawn about the implications of the final results, and the impact and benefit in engineering solutions, and how the results apply in real-life scenarios. Finally, a lifetime prediction is made, using conventional engineering values.

5.2 SN DISCUSSION

The key findings of the research in this thesis were the decrease in fatigue life as the temperature increased from 20˚C to 45˚C, which was shown in Figure 4.1 (reproduced here as Figure 5.1). In addition, there was also some lifetime effect due to ageing of the pipe material, as shown in Figure 4.3 (reproduced here as Figure 5.2). Figure 4.4 also illustrated ageing effects at 45˚C.

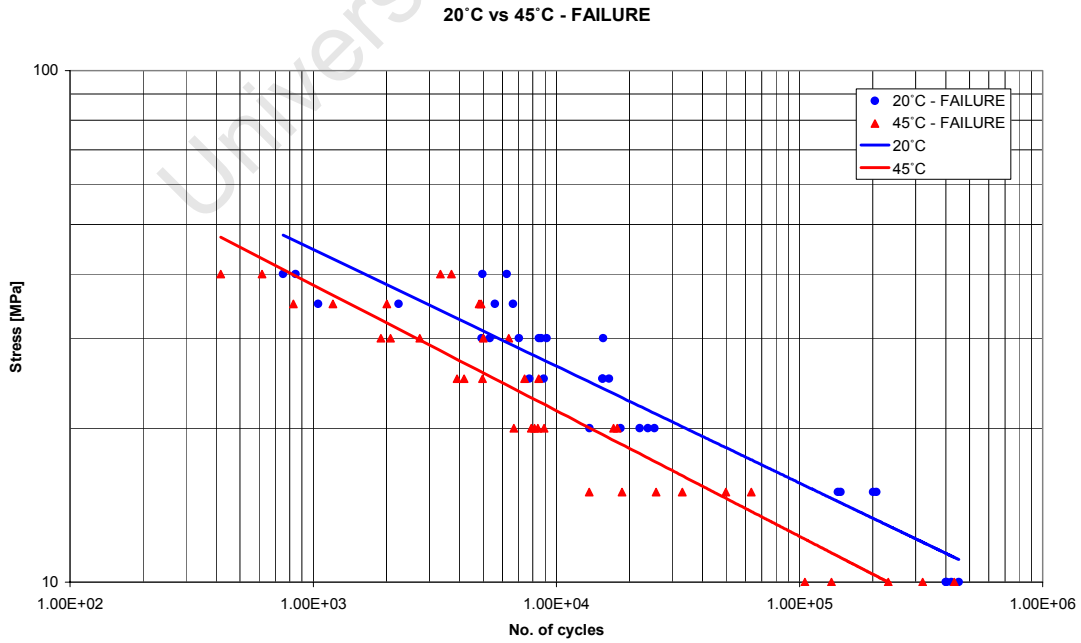

FIGURE 5.1: SN curve of failure for 20˚C vs. 45˚C

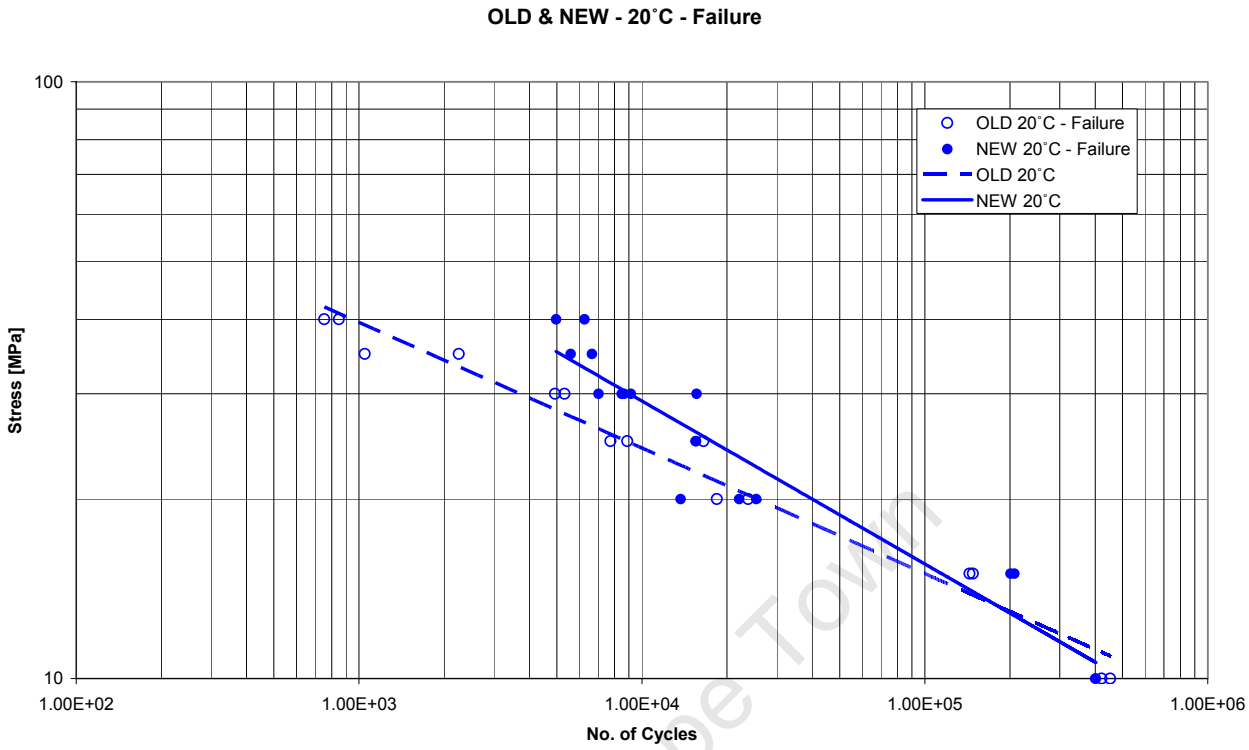

FIGURE 5.2: SN curve of OLD vs. NEW for 20˚C

It was noted that in addition to a decrease in lifetime performance, there was a similar decrease in lifetime for first crack between 45˚C and 20˚C. The gradients (n), and "intercepts" (A) for each of the failure trend lines were calculated to be used as a means of comparison between trend lines (Table 4.1). Furthermore, equations for predicting the failure lifecycle (N), or if re-arranged, the Stress (S), were also produced. These equations, while proving useful for the SN lifetime prediction, could also be used as a means of comparison between the SN and fracture mechanics Paris data, which was discussed in Section 4.4.

By using the equations and calculating the cycle count at each stress level, a "fatigue performance factor", similar to the "temperature factor" of Section 4.3, could be calculated. This factor reflected by how much the fatigue life was different in one condition (e.g.: NEW20˚C) versus a similar, but different, corresponding condition (e.g.: NEW45˚C) at the same stress level. These

performance factors could also provide an insight into the trends for temperature and ageing effects.

5.2.1 SN TEMPERATURE COMPARISON

Referring to Figure 5.1, the decrease in performance between 20˚C and 45˚C is clearly apparent. When comparing cycle counts at the test stress ranges of 10 – 40 MPa, it was found that there was a drop in performance by a mean factor of 2.4 between the 20˚C and 45˚C data, including both NEW and OLD in each temperature division. The drop in performance between NEW20˚C and NEW45˚C specimens, was 2, while for OLD20˚C and OLD45˚C specimens, the difference was approximately 2.6. The cycle counts according to the constants calculated in Section 4.1.3, and the relevant fatigue performance factors for each stress level tested are shown in Table 5.1.

TABLE 5.1: Temperature performance ratios

Condition		NEW20˚C	NEW45˚C	OLD20˚C	OLD45˚C
		Cycle count		Cycle count	
Stress	10	526030	257047	695314	151530
Performance factor		2.0		4.6	
Stress	15	118472	59156	100844	30126
Performance factor		2.0		3.3	
Stress	20	41142	20860	25627	9576
Performance factor		2.0		2.7	
Stress	25	18113	9294	8856	3936
Performance factor		1.9		2.2	
Stress	30	9266	4801	3717	1904
Performance factor		1.9		2.0	
Stress	35	5257	2746	1784	1030
Performance factor		1.9		1.7	
Stress	40	3218	1693	945	605
Performance factor		1.9		1.6	
Mean performance factor		**2.0**		**2.6**	

When plotted graphically on an axis of Stress vs. Fatigue performance factor (Figure 5.3) the role of temperature in the fatigue life over the stress ranges becomes apparent. Over the stress ranges, the NEW material differed only slightly in its fatigue life, from 20˚C to 45˚C conditions. In fact, the factors only differed from 1.9 to 2. This means that at any given stress, the fatigue life for a NEW 20˚C specimen will have a lifetime of approximately double that of the NEW 45˚C.

However, the OLD material did not show such a consistent fatigue lifetime performance, with a performance factor ranging from 1.6 to 4.6. At the high stress levels, the performance of the OLD material was somewhat comparable to the NEW material, however at loads of increased cycle counts, this difference grew. So much so, that at 10 MPa tests, the OLD 20˚C was outperforming OLD 45˚C specimens by a factor of 4.6. This clearly shows that the temperature effect was more significant for the OLD than the NEW material.

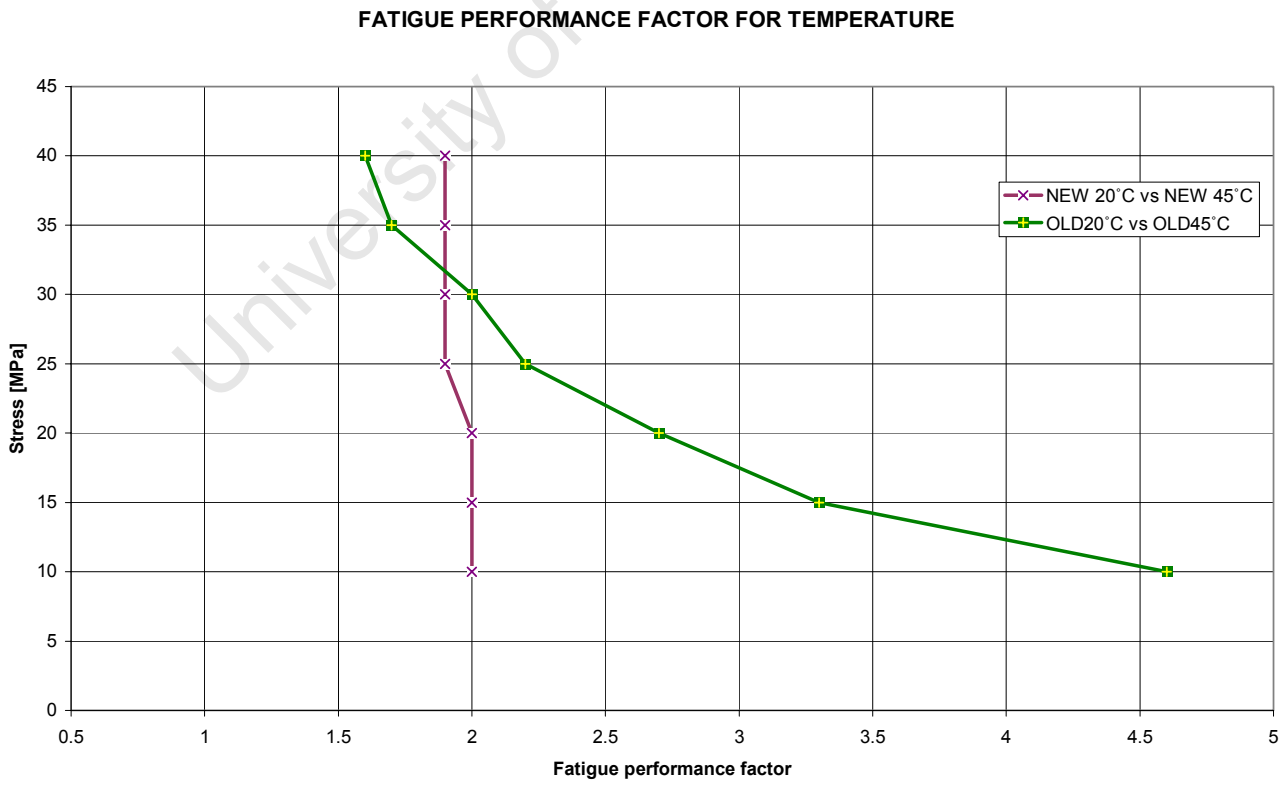

FIGURE 5.3: Fatigue performance factor for temperature (20˚C/45˚C)

It is interesting to note that at the stress levels of 35 and 40 MPa, the OLD material had a performance factor closer to unity than that of the NEW material. A possible reason for this could be the mode of failure in each of the material types. For the NEW material, there was fatigue crack initiation and propagation, accompanied by stress whitening, and ultimately failure by crack growth along the length of the pipe and an inability to maintain the required load due to deformation of the pipe. The OLD material, however, had very little crack propagation at high stresses. There was crack initiation, normally at an inclusion site, and then fast and often catastrophic brittle failure. These differences of crack length were shown in Section 4.1.4. Therefore, as the mode of failure for OLD material was one of brittle rather than the fatigue of NEW material, the performance factors are closer to unity than that for NEW type material.

At the low stress levels, some of the tests ran for approximately 74 hours (~400 000 cycles at a frequency of 1.5 Hz), and these extended tests allowed for the material to degrade of perhaps even soften. At these lower stress levels, even for the OLD type material, the failure mode was one of fatigue. And in terms of critical flaw size, as the mode was fatigue, this meant that fatigue lifetime was dependent on fracture toughness. Fracture toughness for the NEW material was 3.32 MPa√m in the direction of crack propagation (C-Shape specimens) while for the OLD material it was 2.69 MPa√m. This is further discussed in Section 5.4.

5.2.2 SN AGEING EFFECT

As shown in Figure 5.2, there was an ageing effect between the NEW and OLD type material when compared within temperature tests. This effect however was not as significant as that of temperature.

When observing Figure 5.2, it could be argued that OLD and NEW material types had a similar fatigue lifetime at 20˚C as their trend lines appear to intersect. This was however not the case. Rather, the lines appear to intersect as the NEW

material tests were halted at approximately 400 000 cycles, with no failure recorded for the NEW type at this temperature. Had tests run to failure, this would have perhaps given a truer representation, however it was felt that there was insufficient time for this as a single specimen test could have taken a number of days.

5.2.3 SN LITERATURE COMPARISON

All of the SN data from the literature surveyed and the test data for both 20˚C and 45˚C are summarised in one graph in Figure 5.4. The 20˚C test data covered almost the full corridor of results from Joseph and Leevers and Marshall *et al*, and had a lesser slope, indicating a far greater projected fatigue lifetime at lower stresses. The 45˚C data differed significantly from the literature data, which was to be expected as it was the only data set which was generated at this temperature.

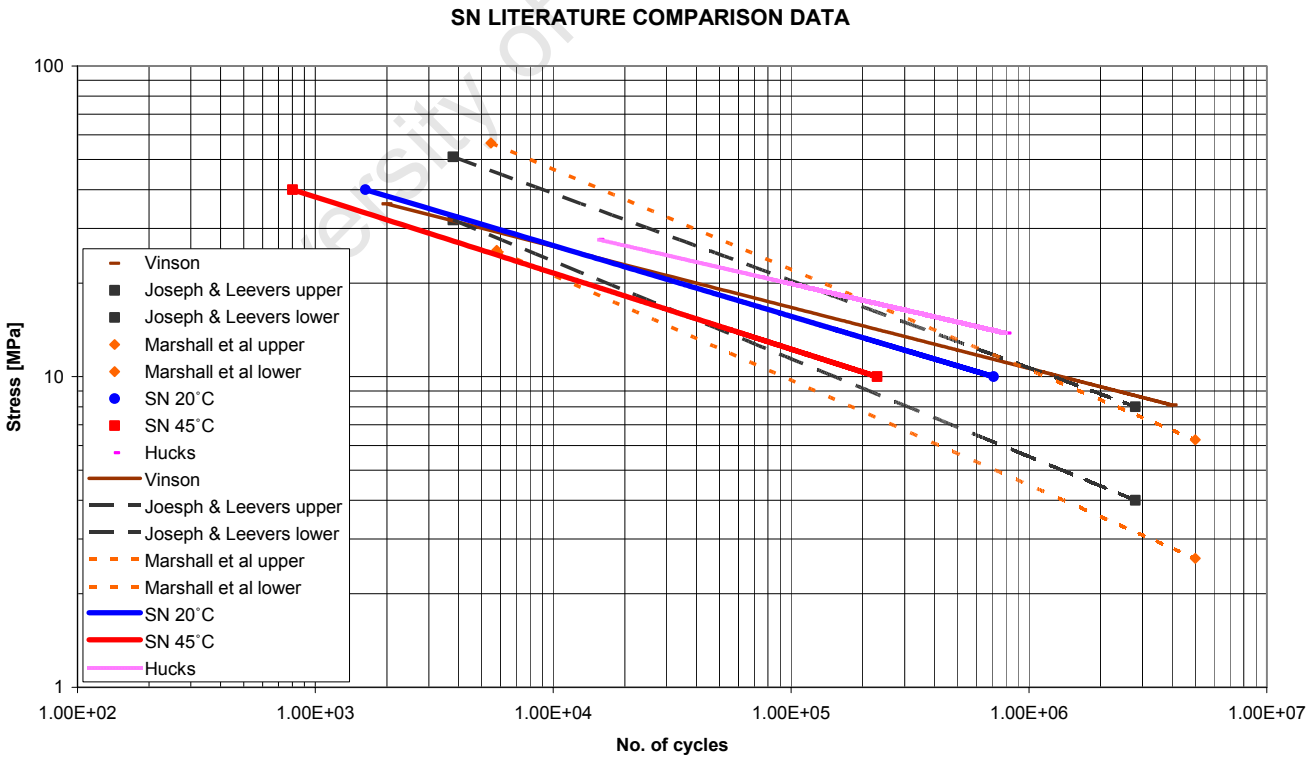

FIGURE 5.4: Comparative SN curves from test and literature data

The experimental data from the 20˚C and 45˚C tests, confirmed the testing performed by Whittle and Teo [47] of 20˚C, 30˚C and 40˚C, and which showed that there is a decrease in fatigue lifetime with increased temperature.

5.2.4 SN FOR ON-SITE SCENARIO

According to the report prepared for Africon by Origen Engineering in September 2005 [1], the actual maximum stresses experienced by the underground piping in the Madinat Jumeirah resort are approximately 6 MPa. Therefore, using 6 MPa as the reference stress, the expected lifetimes between 20˚C and 45˚C can be calculated for both NEW and OLD type material.

As mentioned in Chapter 1, the Madinat Jumeirah resorts boasts two hotels of 300 rooms each, 340 cluster rooms and suites, as well as 120 shops, cafes and restaurants [3], all using water. This therefore means that there will be pressure spikes throughout the day when valves are opened and closed during peak times. These pressure surges could be estimated to be 500 times a day, based on the size of the resort and the requirement not only for ablution purposes, but also for watering the landscaped gardens.

These 500 cycles a day, and taking into account the peak and low tourist seasons compensating for each other, this would imply 182 500 cycles a year (assuming a non leap year). The projected lifetimes for each pipe type can then be calculated based on the estimated cycles to failure at 6 MPa. These predictions are shown in Table 5.2 in units of years to failure, after applying a safety factor of 2.

TABLE 5.2: Years to failure for pipes at real life stress of 6 MPa

Condition	NEW20˚C	NEW45˚C	OLD20˚C	OLD45˚C
	Cycle count		Cycle count	
Stress 6	18 years, 10 months	8 years, 11 months	43 years, 4 months	6 years, 4 months

As mentioned in Section 5.2.2, the low stress levels of the NEW 20˚C are not truly representative of the fatigue lifetime. If a comparison between NEW 20˚C and OLD 20˚C were made a medium stress level (~25 MPa), as shown in Figure 5.2, this would give a performance factor of approximately 2 (18113 vs. 8856 cycles) in favour of the NEW type material. However, even this would be a conservative estimate, as were full tests run to failure for the NEW type, the slope of the NEW 20˚C would not be as high as it is. Using the conservative performance factor estimate of 2 for the NEW and OLD material at temperature for 20˚C, this would give a life cycle rather of 86 years and 8 months for the NEW material at 20˚C.

This would be vastly superior to the fatigue life at 45˚C, for both NEW and OLD. Ideally temperatures closer to 20˚C would provide a far longer fatigue lifetime, and therefore perhaps a step towards decreasing the temperature of the desalinated water flowing through the pipes should be taken to ensure long lasting underground water systems.

The results are merely indicative of sensitivities to temperature and other inputs. For a truly rigorous fatigue lifetime analysis one would need a detailed load history as well as reliable input values for initial flaw sizes, and until this is undertaken, the speculation is only of interest in that it highlights the sensitivities issues.

5.3 PARIS DISCUSSION

General trends for the da/dN vs. ΔK Paris curves showed a similar behaviour to the SN curves in the difference in crack growth rate between NEW20˚C and NEW45˚C, as shown in Figure 4.8, reproduced here as Figure 5.5. A higher growth rate was experienced during testing of the NEW 45˚C than for the NEW20˚C at the same given ΔK value. This would indicate that, as for the SN

tests, there is indeed a significant temperature effect, extending earlier studies such as Whittle and Teo [47].

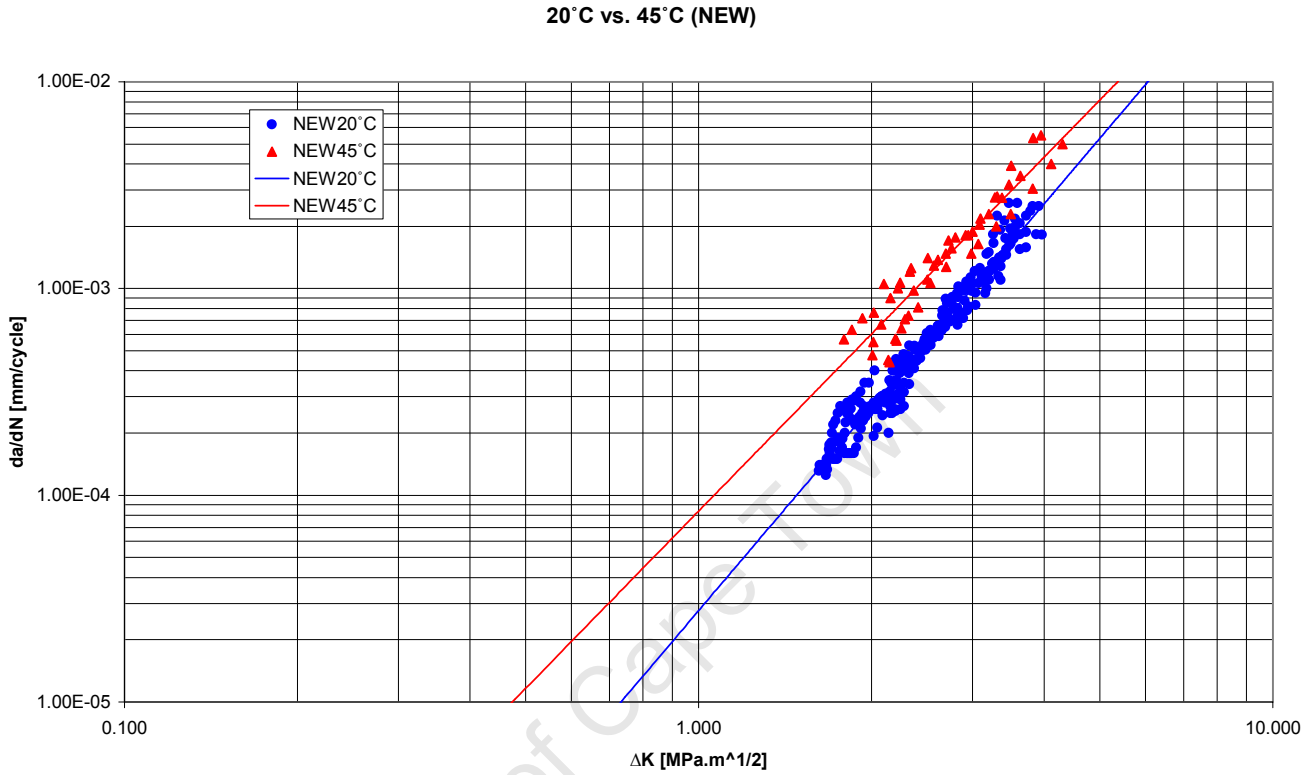

FIGURE 5.5: Paris curve for 20˚C vs. 45˚C

Crack growth data from an undergraduate thesis investigation into the crack growth rate of OLD type material [54] was incorporated into the NEW type results. However, the large amount of scatter implied that the OLD20˚C results could not be classed as definitive, and were only used as a means of comparison to determine, or confirm from SN tests, if there was an ageing effect. The OLD 45˚C results were unable to be used, as the amount of data was insufficient to draw any conclusions.

The constants m and C were calculated for each of the sets of data. In a similar way that the constants n and A were used for comparison purposes for the SN curves, so could m and C be used for the Paris results. Ultimately, these

constants could be used as comparison between each type of testing, to confirm the apparent trends.

5.3.1 PARIS TEMPERATURE COMPARISON

Referring to Figure 5.6, the Paris curve for 20˚C vs. 45˚C (for NEW), there is a clear distinction between the data points of 20˚C and those for 45˚C. This shows that at any given stress intensity (ΔK) value the 45˚C testing produced a higher crack growth rate, and ultimately a shorter operational lifetime until failure.

A comparison between the C values for two temperatures tests for NEW showed a lifetime performance factor of between 3 and 3.5 in favour of the 20˚C tests.

5.3.2 PARIS LITERATURE COMPARISON

While there was no extensive data with which to compare the 45˚C results, the Paris results from the NEW20˚C tests could be compared to those of Maddox and Manteghi [28] as their tests were conducted at temperatures of 20˚C. The Maddox and Manteghi envelope [28] is consistent with the current data obtained from 20˚C testing and is shown in Figure 5.6. The curve for 45˚C from the present study is also included as a means of comparison.

The envelope for fatigue (by Kim, Mai and Cotterell [49]) of PVC *in water* at 20˚C is also shown and its position is consistent with the 45˚C data (in water) from the present study.

It should be recalled from Section 2.8.2 that Maddox and Manteghi used SENB and not Compact Tension specimens [28]. Joseph and Leevers also did not use CT specimens for their Paris characterisation, but rather rectangular flat plates [25], and this difference reportedly slightly lowers measured values of toughness for a given load [59] but its effect on fatigue crack growth rate is unclear. By far

the dominant effect, however, is that of a temperature rise leading to an increase in crack growth rate and a shorter fatigue lifetime.

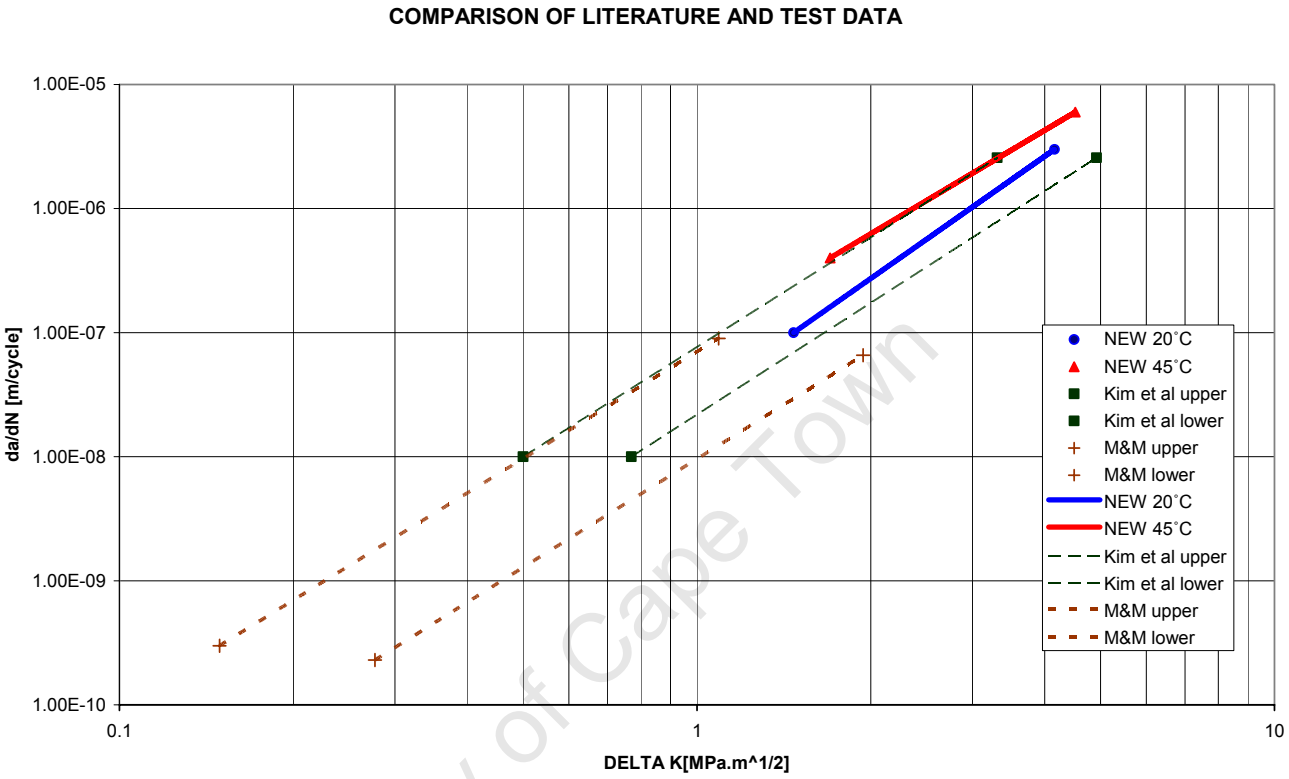

FIGURE 5.6: Test Paris curves vs. Maddox and Manteghi

5.4 FRACTURE TOUGHNESS COMPARISON

The fracture toughness can be characterised by LEFM (the K_{IC} parameter) or CTOD (δ parameter). For LEFM the so-called "valid thickness" criterion is given by [55]:

$$a, B, W - a \geq 2.5\left(\frac{K_{IC}}{\sigma_y}\right)^2 \qquad \text{[Equation 5.1]}$$

This equation yields valid thickness values of approximately 7 to 11 mm which is of the same order of the actual crack sizes and pipe thickness. Thus it appears just acceptable to characterise the toughness in LEFM (K_{IC}) terms as well as in CTOD (δ terms).

K_{IC} Fracture toughness values for the SENB specimens were 3.02 MPa√m for the NEW type, and 3.05 MPa√m for the OLD type material. This can be regarded as near identical values. However, the CTOD fracture toughness value for the NEW SENB material was 0.216 mm versus the 0.134 mm for the OLD SENB type.

For the C-Shaped specimens, the NEW K_{IC} fracture toughness was 3.32 MPa√m, while for the OLD type it was 2.69 MPa√m. However, the CTOD fracture toughness value differed from the trend of the NEW K_{IC} fracture toughness, and was nearly identical, with values of 0.103 mm for the NEW type, and 0.096 mm for the OLD type.

The above difference and spread of values is believed to be due to ductility during testing. It was noted that overall the C-Shaped specimens (longitudinal cracking direction) had lower toughness values overall than the SENB specimens (circumferential cracking direction).

5.5 CRITICAL FLAW SIZES

By considering the stress, geometric factor (Y) and material fracture toughness, the critical flaw size can be calculated. This is the flaw size at which failure will occur by fast fracture. By reorganising Equation 2.1, it is possible to solve directly for the flaw size, a:

$$K = \sigma Y \sqrt{\pi a} \qquad \text{[Equation 2.1]}$$

$$a = \frac{1}{\pi}\left(\frac{K_{IC}}{Y\sigma}\right)^2 \qquad \text{[Equation 5.2]}$$

For example, the OLD 30 MPa test at 45˚C, shown in Figure 4.11 (and reproduced here as Figure 5.7) is considered.

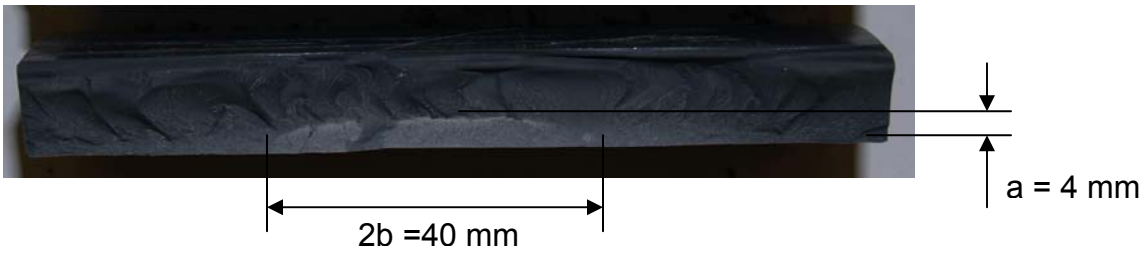

FIGURE 5.7: Fracture surface of OLD specimen at 30 MPa and 45˚C

The crack profile is approximately 40 x 4 mm, that is, the aspect ratio, a/2b is 0.1 (4/40) with a normalised depth ratio, a/t of 0.3 (4/13). These values allow an assumption for Y to be made (bearing in mind that this thumbnail crack is *not* in an infinite sheet), assumed in this case to be 0.8 [60]. Therefore, using Equation 5.2 and a fracture toughness of 2.69 MPa√m and substituting in the necessary values:

$$a = \frac{1}{\pi}\left(\frac{2.69}{0.8*30}\right)^2$$

$$a = 4.03mm$$

This calculated critical flaw size is comparable to the *actual* size of flaw at fracture, Figure 5.8. The flaw sizes of the other fatigue specimens were broadly compatible with these fracture mechanics predictions, but perhaps more precision could be obtained using CTOD methods and PD6493 [38] or BS7910 [61], but this was considered beyond the scope of the present thesis focusing on fatigue.

5.6 LIFETIME PREDICTION

Having ascertained the Paris equation material fatigue properties for the different uPVC pipes and conditions, a lifetime prediction is able to be made. In Section 2.7.4, Equation 2.3 was presented for predicting the fatigue lifetime given an

initial and critical flaw size, the geometric correction factor Y, and the material Paris parameters m and C.

$$N_f = \int_{a_i}^{a_{critical}} \frac{da}{C(Y\Delta\sigma\pi)^m a^{m/2}} \qquad \text{[Equation 2.3]}$$

Using an approach due to Joseph and Leevers [25] and integrating between the limits of a_i and $a_{critical}$ (where $a_{critical}$ was taken as half the wall thickness [25]):

$$N_f = \left(\frac{1}{[1-\frac{m}{2}]C(Y)^m \pi^{\frac{m}{2}} (\Delta\sigma)^m}\right) * (a_{critical}{}^{1-\frac{m}{2}} - a_i{}^{1-\frac{m}{2}}) \qquad \text{[Equation 5.3]}$$

Where Y = 1.20 for semi-elliptical cracks with an aspect ratio approaching 0.1 [62]. Using NEW 20˚C as an example, with m = 3.26 and C = 2.7 * 10^{-8}, Equation 5.3 becomes:

$$N_f = (5.02*10^6)(\Delta\sigma)^{-3.26}(a_i{}^{-0.63} - a_{critical}{}^{-0.63}) \qquad \text{[Equation 5.4]}$$

Equation 5.4 can now provide a whole range of cycles to failure depending on the cyclic stress amplitude chosen, as well as the initial and critical flaw sizes. Indeed, Equation 5.4 can be used to predict fatigue lifetimes according to the m and C values.

Using an assumed initial flaw size of 300 μm (which is plausible from the manufacturing inclusions), a final flaw size of 6.75 mm, and an assumed stress of 20 MPa, the fatigue lifetime is therefore:

$$N_f = (5.02*10^6)(20)^{-3.26}((0.0003)^{-0.63} - 0.00675^{-0.63})$$

$$\therefore N_f = 4.1*10^4 \, cycles$$

The above process was used to predict the number of cycles to failure for the NEW 20˚C and NEW 45˚C material. These temperature case stress level fatigue life prediction lines are shown (dotted) in Figure 5.8 together with actual fatigue data. The correlation between predicted and actual data is not perfect, but is considered acceptable, at both 20˚C and 45˚C.

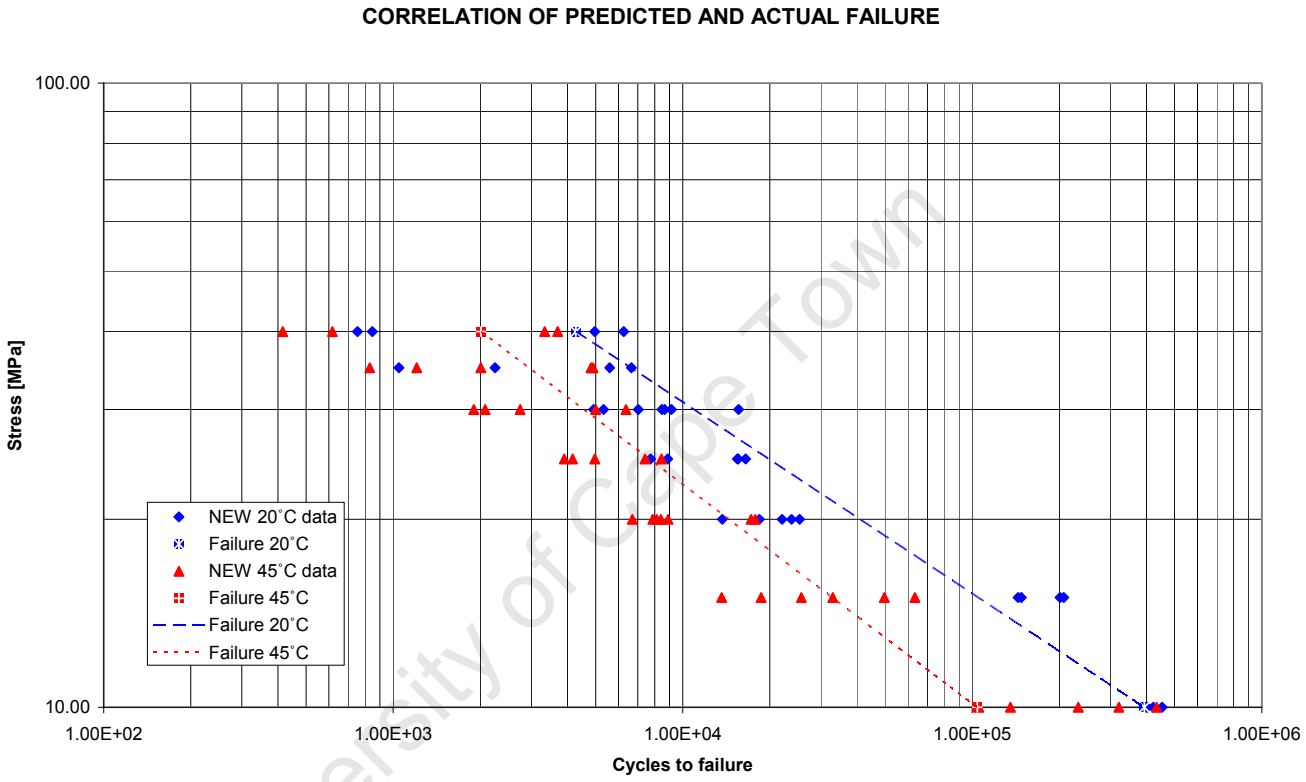

FIGURE 5.8: Correlation of predicted and actual failure for NEW 20˚C and 45˚C material

CHAPTER 6. CONCLUSIONS AND RECOMMENDATIONS

This Chapter presents the conclusions garnered from the research project, and presents recommendations based on the findings.

Premature failures of underground, desalinated water-carrying uPVC pipes in the luxury resort of Madinat Jumeirah in Dubai stimulated research into the fatigue behaviour of such PVC piping. This research aimed to establish the fatigue behaviour of the uPVC piping material at temperatures of 20˚C and 45˚C, while also investigating if there was an ageing effect experienced by comparing so-called “OLD” and “NEW” pipes. The OLD pipes were pipes which had transported the desalinated water throughout the resort and had been excavated for testing.

6.1 CONCLUSIONS

Two types of fatigue testing were carried out – traditional SN and the more comprehensive fracture mechanics approach. SN tests used sections of pipe from the resort at 20˚C and 45˚C, and testing both OLD and NEW, unused pipes. Fracture mechanics testing established the Paris equation from crack growth data of Compact Tension (CT) specimens, both at 20˚C and 45˚C, although this was only for the NEW type material.

Fracture toughness tests on SENB and C-Shaped specimens were carried out to determine if there was an orientation effect on the fracture toughness. The SENB specimens tested the fracture toughness in a circumferential direction, while the C-Shaped specimens tested the fracture toughness in the longitudinal direction (i.e.: the direction of crack growth on failed specimens from the resort). There was indeed a slight reduction in longitudinal cracking toughness.

All of the testing phases were successful. Test data for all phases supplemented existing literature data, particularly in the 45˚C data range. The following conclusions were able to be made with regards to each phase of testing:

SN

- A decrease in performance was noticeable from 20˚C to 45˚C reducing fatigue lifetime by between 4.6 and 1.6 times (for OLD material) depending on stress levels, but only approximately 2 times for new material.
- There was a decrease in performance from NEW to OLD material type; however this decrease in performance was not as substantial as that for the temperature effect (typically in the range of 1.0 to 2.5 times). While the ageing effects are recognised as important, they were beyond the scope of the thesis, although future work could focus on this phenomenon.
- Fracture surface fractography showed stable crack growth for the lower stress levels, while the higher stress level tests were often characterised by fast brittle fracture, particularly for the OLD type specimens.
- Specimens tested at 45˚C exhibited a “whiter” fracture surface, suggesting that there is some environmental degradation due to temperature effects.
- The fracture surface sizes were consistent with the fracture mechanics inter-relationship between stress, flaw size and toughness, as characterised by the “triangle of integrity”.

PARIS

- An increase in crack growth rate of between 3 and 3.5 times was shown to exist between NEW 20˚C and NEW 45˚C specimens, with a consequent reduction in fatigue lifetime.
- The trend lines for NEW type material at 20˚C and 45˚C could be summarised by the following Paris equations:

$$20°C: \frac{da}{dN} = 2.7 * 10^{-8} \Delta K^{3.26}$$

$$45°C: \frac{da}{dN} = 8.55 * 10^{-8} \Delta K^{2.85}$$

- The ageing effect was approximately a factor of 1.7, i.e.: less than the temperature effect.

FRACTURE TOUGHNESS

- K_{IC} and CTOD fracture toughness values differed for each material type and could be characterised by both K_{IC} and CTOD (δ). The orientation perpendicular (SENB) and parallel (C-Shape) to actual cracking direction.
- The toughness values were:

Fracture toughness	K_{IC}		CTOD (δ)	
	[MPa√m]		[mm]	
Specimen type	SENB	C-Shape	SENB	C-Shape
OLD	3.05	2.69	0.103	0.096
NEW	3.02	3.32	0.216	0.134

- Generally speaking, the C-Shaped specimens had lower fracture toughness values than those for the SENB specimens, both for K_{IC} and CTOD values, consistent with the fabrication direction being less tough.

6.2 RECOMMENDATIONS

With regard to the research undertaken, several recommendations can also be made:

- Extended low-level stress tests – more data needs to be generated for final failure at the low stress levels of 10 MPa. In addition, it would be beneficial to run tests at 6 MPa, the actual stress experienced by the pipes. However, given the time required to run a single test (potentially

months) and given the need to be able to show repeatability, this is admittedly not an easy task to accomplish.

- More comprehensive data for Paris of the OLD material, both at 20˚C and 45˚C is required.
- Fracture toughness values at 45˚C – fracture toughness tests were only run at 20˚C, and while the tests were successful in showing an orientation effect, for completeness sake, full K_{IC} and CTOD fracture toughness tests should be performed at 45˚C on both the OLD and NEW material.
- Ageing effects should be further investigated, and a more complete understanding of the term “ageing” should be obtained. This could perhaps include the deliberate and controlled exposure of uPVC piping to not only the harsh and searing hot climate of Dubai, but also to climates around the world. After the controlled exposure, a more thorough comparison can be made on the ageing effects of UV exposure on uPVC piping.
- The effect of water/UV on uPVC fatigue crack growth should be further investigated.
- On-site pipe-stress surveys should be ascertained for a complete and rigorous lifetime prediction of the PVC pipes.

Several recommendations can be made from the results of this thesis, pertaining to the PVC piping usage at the Madinat Jumeirah resort:

- In order to minimise the temperature effect and subsequent premature pipe failure, an effort should be made to cool the desalinated water entering the underground piping. Even a few degrees would have a beneficial affect on the fatigue lifetime.
- In addition to lowering the effect of the temperature, an effort should be made, in future installations, to properly compact the soil around the pipes, thereby lowering the effective stress experienced by the pipes, and also extending the fatigue life.

- Efforts should be made where to possible to reduce the peak stress from valves opening and closing, as the fatigue cracking is driven by the cyclic fatigue stress amplitude. Therefore measures should be taken to smooth the stress peaks by installing surge tanks which would help to lower and smooth the stress peaks.

REFERENCES

1 – R.B Tait and J Press, Cape Residual Stress
"Madinat Jumeriah: PVC pipe failures"
Origen failure analysis report for Africon
September 2005

2 – http://www.damnfunnypictures.com/html/The-Burj-Al-Arab-Hotel.html
The only 7 Star Hotel in the world
Accessed: 25 July 2007

3 – http://www.hotelmanagement-network.com/projects/madinat/
Madinat Jumeirah Resort, United Arab Emirates
Accessed: 25 July 2007

4 – http://www.trekearth.com/gallery/Middle_East/United_Arab_Emirates/photo623223.htm
Madinat Jumeirah
Accessed: 2 August 2007

5 – http://www.dubai.fi/image/albums/userpics/10001/Dubaimap.swf
Map of Dubai beachfront
Accessed: 10 December 2007

6 – http://www.desware.net/
DESWARE – Encyclopaedia of Desalination and Water Resources
Accessed: 10 December 2007

7 – R.B Tait and L von Zwiklitz
"Hot fatigue failure of PVC piping"
Engineering Failure Analysis Conf, Toronto, June 2006

8 – http://matse1.mse.uiuc.edu/polymers/polymers.html
History of Polymers
Department of Materials Science and Engineering, University of Illinois Urbana-Champaign
Accessed: 5 September 2006

9 – http://worldaccount.basf.com/
Accessed: 25 January 2007

10 – http://www.jhu.edu/~matsci/what-is-materials-science/
What is Materials Science? – John Hopkins University: Department of Materials Science and Engineering
Accessed: 25 January 2007

11 – http://www.globalpolymerscorp.com/technical.htm
Global Polymers Corp – Technical Service
Accessed: 25 January 2007

12 – M.M Carroll
Polyvinylchloride (PVC) pipe reliability and failure modes
Reliability Engineering, vol 13, part 1 (1985) pp 11–21

13 – Engineers technical handbook: Book 1
Phoenix Technical Publications CC, Gauteng, South Africa, 2007

14 – J.C Radon and L.E Culver
“Effect of temperature and frequency in fatigue of polymers”
Polymer, vol 16 July (1975) pp 539–544

15 – M.F Ashby and D.R.H Jones
Engineering Materials 2, International Series on Material Science
Pergamon, 1986 pp 202–237

16 – A.W Birley, B Haworth and J Batchelor
Physics of Plastics – Processing, Properties and Materials Engineering
Carl Hanser Verlag, 1992

17 – P.C Powell
Engineering with Polymers
Chapman and Hall Ltd. 1983

18 – W.D Callister
Materials Science and Engineering – an Introduction, Fourth Edition
John Wiley and Sons Inc 1997

19 – N.J Mills
Plastics – Microstructure, Properties and Applications
Edward Arnold (Publishers) 1986

20 – C Hall
Polymer materials – An introduction for technologists and scientists
Macmillan Press LTD, 1981

21 – O Schwarz
Poly(vinyl chloride) – PVC – Polymer Materials Handbook
Natal Witness Printing and Publishing Company (Pty) Ltd 1995 pp 69–76

22 – M.A Osry
PVC pipes for life – Modern developments and design criteria: PVC-U, PVC-M and PVC-O
DPI Plastics (Pty) Ltd., South Africa

23 – http://www.vinyl.org.au/building/pipes.cfm
Pipes and Conduits
Vinyl council of Australia, 2003
Accessed: 27 September 2006

24 – V John
Introduction to Engineering Materials – 3rd Edition
Macmillan Education Ltd, 1992

25 – S.H. Joseph and P.S. Leevers
"Failure mechanics of uPVC cyclically pressurized water pipelines"
Journal of Materials Science 20 (1985) pp 237–245

26 – E.J Hearn
Mechanics of Materials 1 – Third Edition
Butterworth-Heinemann, 1997

27 – Failure Analysis of Polymers
Metals Handbook Ninth Edition
Vol 11 – Failure Analysis and Prevention pp 758–765
American Society for Metals, November 1986

28 – S.J Maddox and S Manteghi
"The fatigue design of uPVC water pipe with consideration of environmental effects"
Plastics, Rubber and Composites Processing and Applications 17 (1992) pp 5–18

29 – S Kaang, Y.W Jin, Y.I Huh, W.J Lee, W.B Im
"A test method to measure fatigue crack growth rate of rubbery materials"
Polymer Testing 25 (2006) pp 347–352

30 – D.R Moore and S Turner
Deformation and strength in plastics
Plastics Division, ICI Ltd, Welwyn Garden City, Hertfordshire
pp 177 – 185, 1974

31 – A Roulin-Maloney
Fractography and Failure Mechanisms of Polymers and Composites
Elsevier, 1989

32 – http://www.plastics.org.nz/pipa
Handling and Storage of PVC Pipes
Marley New Zealand, Plastics Industry Pipe Association New Zealand
Accessed: 8 February 2008

33 – Vinidex Systems and Solutions
Fatigue design and fatigue thresholds for PVC, PVC-M and PVC-O
North Rocks, NSW, Australia
Number VX-TN-4K.0, December 2001

34 – JT Barnby
Fatigue
Mills and Boon Limited, 1972

35 – G.G Garrett,
Failure by fatigue, Johannesburg 1980
Fracture 79, Pergamon press

36 – S. Suresh
Fatigue of materials
Cambridge University Press 1991

37 – R.B Tait
Materials selection in the mining industry
SAIMechE conf Johannesburg
21 August – 2 September 1982

38 – PD6493 – “Guidance on methods for answering the acceptability of flaws in fusion welded structure
British Standards, 1991

39 – T.L Anderson
Fracture Mechanics – Fundamentals and Applications, Second Edition
CRC Press, Inc, 1995

40 – R.B. Tait
Fracture mechanics short course, University of Cape Town, 27 – 29 Jan 2008

41 – R.T Hucks
Design of PVC water-distribution pipe
Civil Engineering ASCE 42, no. 6:70-73, 1972

42 – J.D Jeffery, Northprop Grumman Missions Systems
A.P Moser, Utah State University
S.L. Folkman, Utah State University
Long term cyclic testing of PVC pipe
Final report: Revised – 26 February, 2004

43 – H Vinson, "Response of PVC pipe to large, repetitive surges" – Proceedings of the international conference on underground plastic pipe held in New Olreans 30 March – 1 April 1981
Edited by B. Jay Schrock, 485 – 494. New York: American Society of Civil Engineers

44 – J.A Bowman, 1990
The fatigue response of polyvinyl chloride and polyethylene pipe systems
Buried plastic pipe technology. ASTM STP 1093

45 – A.O Moser
Cyclic life of PVC pipe
Logan, UT: Utah State University, College of Engineering, 2001

46 – G.P Marshall, S Brogden, M.A Shepherd
Evaluation of the surge and fatigue resistance of PVC and PE pipeline materials for use in the U.K. water industry
London, UK, 1998

47 – A.J. Whittle and A. Teo
Resistance of PVC-U and PVC-M to cyclic fatigue
Plastics, Rubbers and Composites, vol 34, No 1, 2005 pp 40 – 46

48 – R.B Tait and J Press
Madinat Pipe Fatigue Testing: Report on Comparative Fatigue Tests of existing (underground) and new pipe materials.
Origen Engineering Solutions
2 March 2006

49 – H.S Kim, Y.W Mai and B Cotterell
Effect of water on fatigue crack growth in uPVC
Mechanics in Engineering practice, Australian Fracture group, Melbourne University, November 1988

50 – H.S Kim, Y.W Mai and B Cotterell
Fatigue crack propagation in unplasticised poly (vinyl chloride) (uPVC) – Effect of mean stress
Polymer, 29, 1998 pp 268 – 276

51 – H.S Kim, Y.W Mai and B Cotterell
Fatigue crack propagation in unplasticised poly (vinyl chloride) (uPVC) – Near threshold fatigue crack growth
Polymer, 29, 1998 pp 277 – 285

52 – Annual book of ASTM Standards – Metals test methods and analytical procedures
E399 – Plain-strain fracture toughness of metallic materials, 1987

53 – Annual book of ASTM Standards – Metals test methods and analytical procedures
E647 – Measurement of fatigue crack growth rates, 1987

54 – G Izaaks
Hot fatigue failure of PVC pipes
Undergraduate thesis, prepared for Professor R.B Tait, University of Cape Town
October 2007

55 – BS7448: Fracture mechanics toughness tests
Part 1: Method for determination of K_{IC}, critical CTOD and critical *J* values of metallic materials, 1991

56 – P.P Benham, R.J Crawford and C.G Armstrong,
Mechanics of Engineering Materials
Maskew Miller, 1996

57 – J.W Dally, W.F Riley and K.G McConnell,
Engineering Measurements
J Wiley, 1984

58 – J.R Haigh and C.E Richards
ESH testing limited private report, 1979

59 – J.F Knott and D Elliot
Worked examples in Fracture Mechanics
Institute of Metallurgy Monograph 4, 1979

60 – O.S Rambocus amd R.B Tait
"An experimental study of the stress intensity factors of semi-elliptical thumbnail and crescent moon surface fatigue cracks in round bars"
MSc Thesis, University of Cape Town, 2006

61 – BS7910-2005
"Guide to methods for assessing the acceptability of flaws in metallic structures"
British Standards Institute

62 – D.P Rooke and D.J Cartwright
Compendium of stress intensity factors
HMSO, London, 1976

63 – Y Mai and P.R Kerr
Effect of processing on fracture toughness and fatigue crack propagation in uPVC
Journal of Vinyl technology, 7, 1985, pp 130 – 9

TABLE OF APPENDIX CONTENTS

APPENDIX A – SPECIMEN DRAWINGS

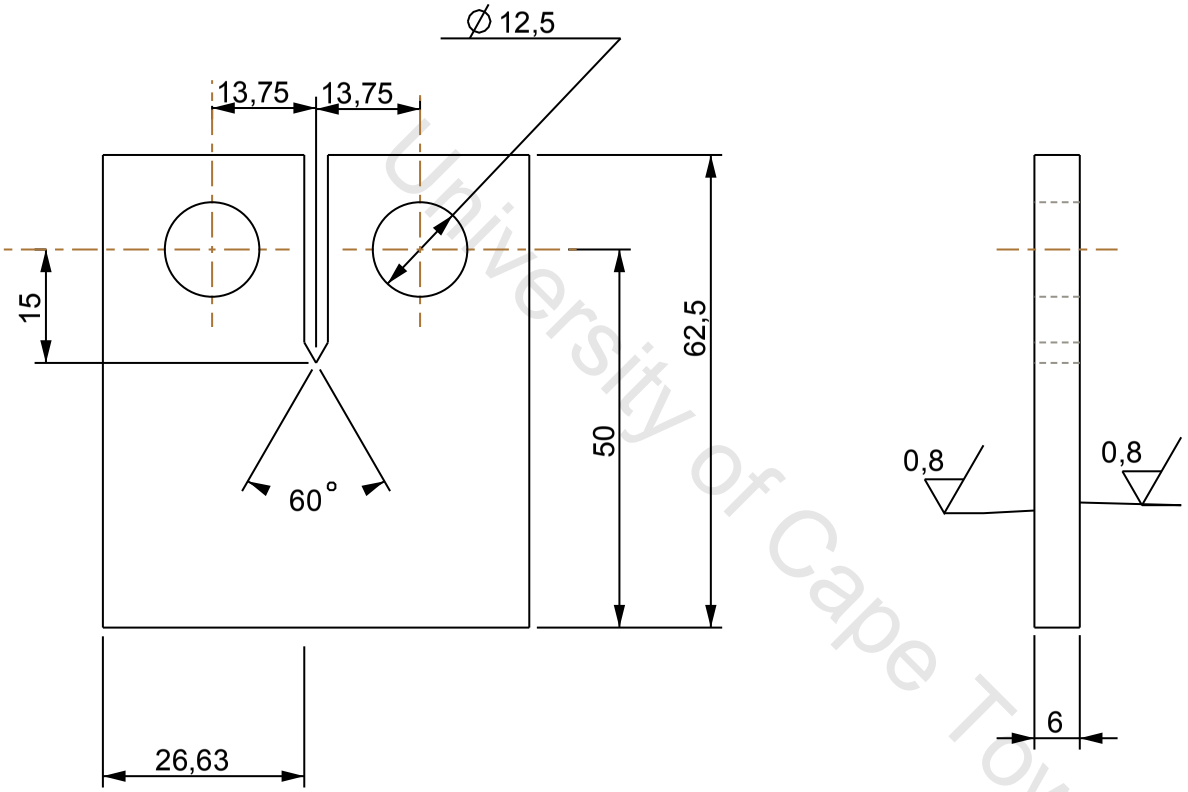

Item	Name	Qty	Material

University of Cape Town
Department of Mechanical Engineering

Title
Compact Test Specimen

Dimensions in mm Tolerance U.O.S.	Scale	Date	Sheet	of
	1,000	30-Oct-2007		
	Drawn By		Drawing Number	
0.1	G.S. Izaaks			

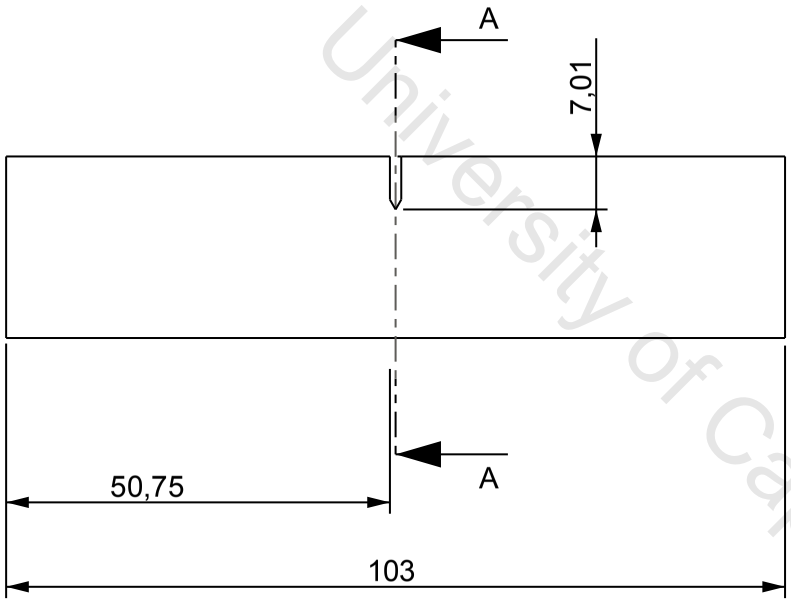

SECTION A-A

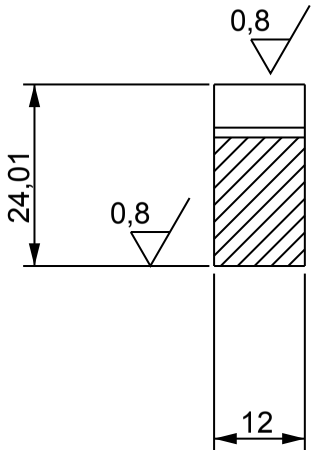

Item	Name	Qty	Material
	University of Cape Town Department of Mechanical Engineering		
	Title SENB Specimen		
Dimensions in mm Tolerance U.O.S. 0.1	Scale 1,000	Date 30-Oct-2007	Sheet / of
	Drawn By G.S. Izaaks		Drawing Number

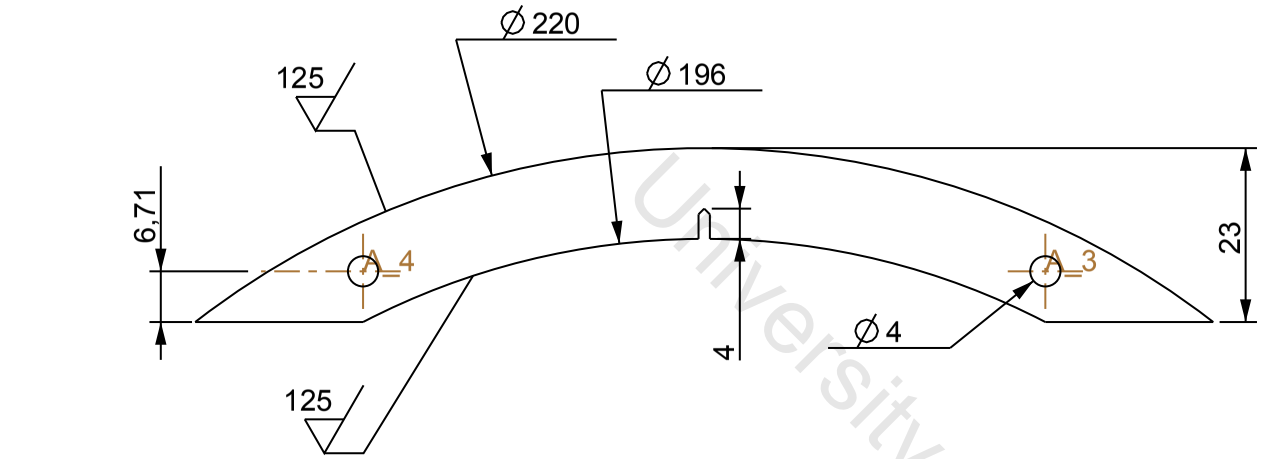

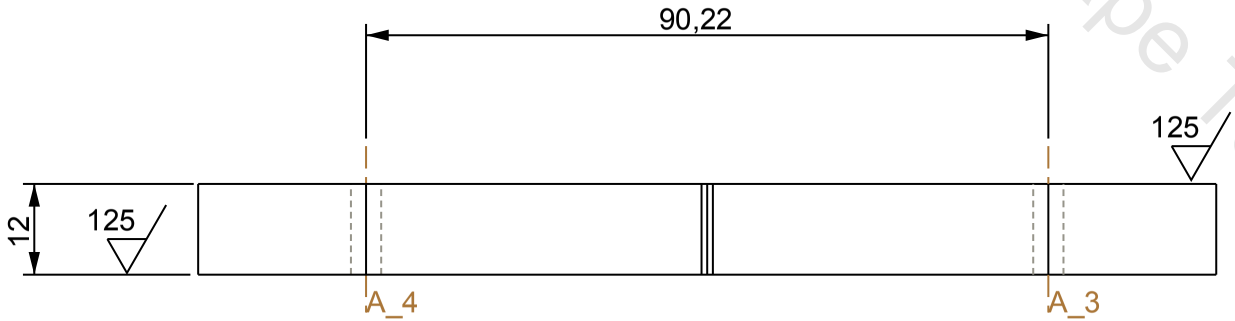

Item	Name	Qty	Material

University of Cape Town
Department of Mechanical Engineering

Title: Arc shape specimen

Dimensions in mm Tolerance U.O.S.	Scale	Date	Sheet	of
	1,000	30-Oct-2007		
	Drawn By		Drawing Number	
0.1	G.S. Izaaks			

APPENDIX B – MANUFACTURING DRAWINGS

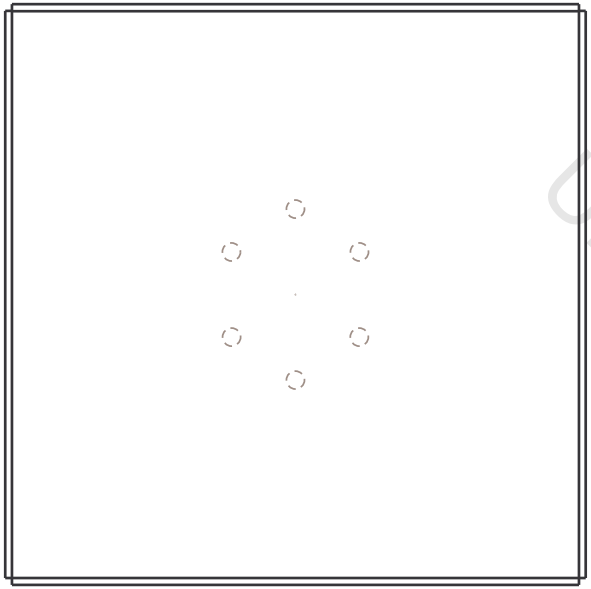

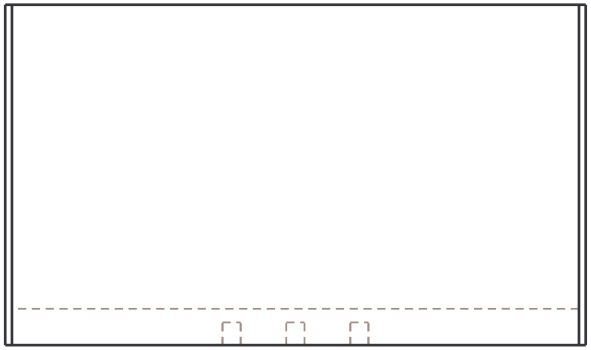

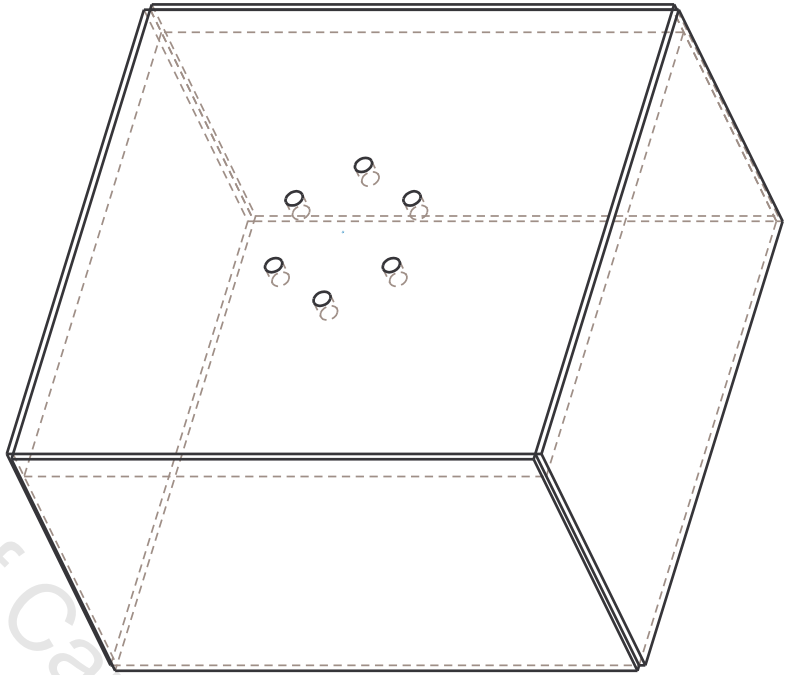

2	BOX_SIDE	4	STEEL_LC
1	BOX	1	STEEL_LC
Item	Name	Qty	Material

University of Cape Town
Department of Mechanical Engineering

Title
BATH ASSEMBLY

Dimensions in mm Tolerance U.O.S. 0.1	Scale 0,300	Date 15-Aug-05	Sheet 1	of 4
	Drawn By von Zwiklitz, L		Drawing Number	

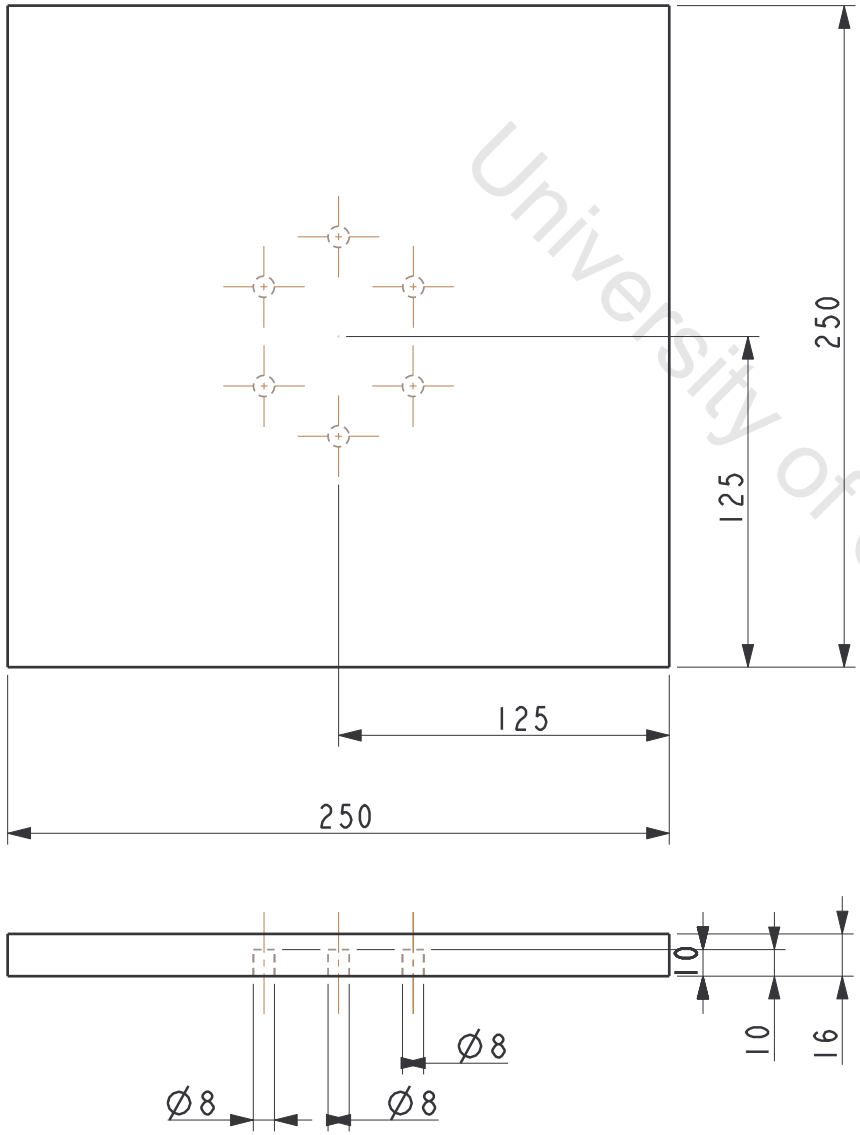

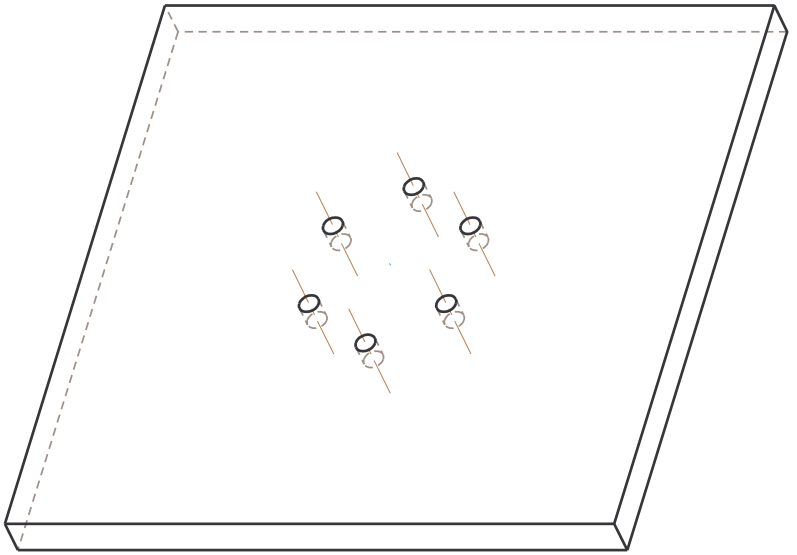

Item	Qty	Name	Material
		University of Cape Town Department of Mechanical Engineering	
		Title: Base of box	
Dimensions in mm Tolerance U.O.S. ±0.1		Scale: 0,350 / Date: 04-Feb-05 / Sheet: 2 / of: 4 Drawn By: von Zwiklitz, L	Drawing Number

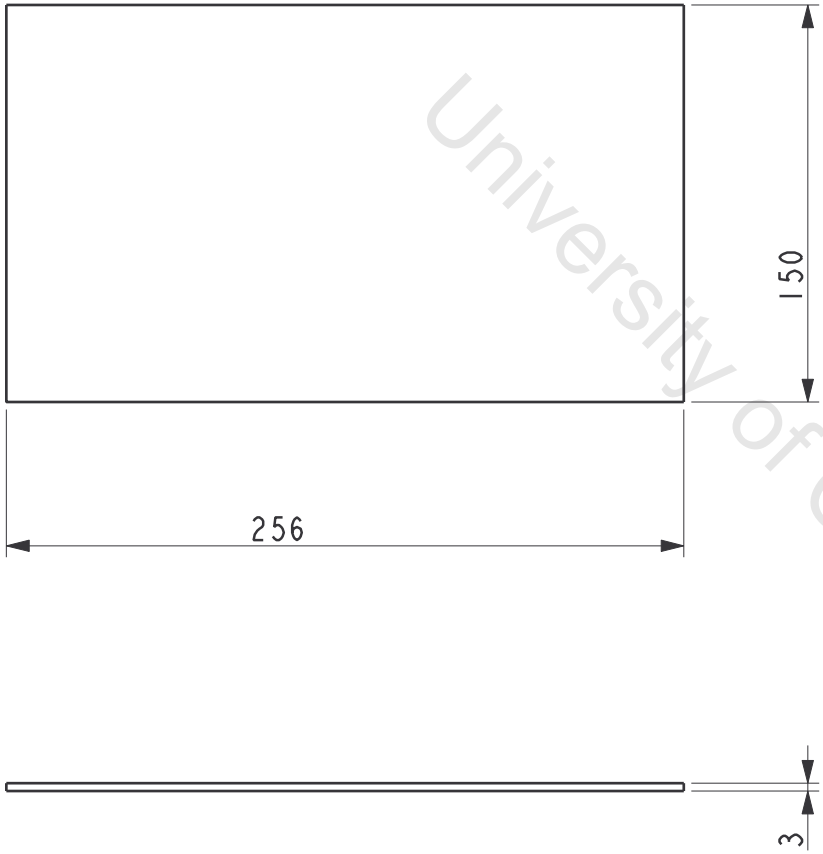

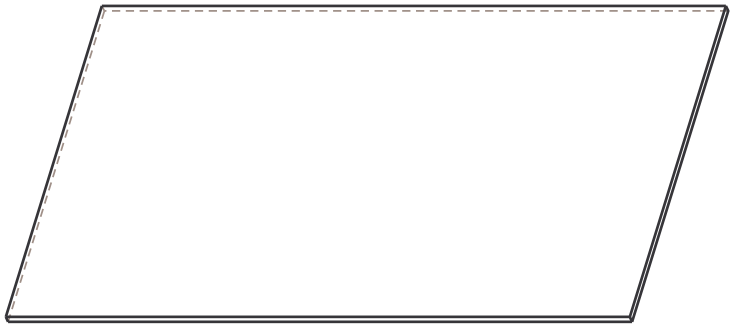

Item	Qty	Name	Qty	Material
		University of Cape Town Department of Mechanical Engineering		
		Title: SIDE OF BATH		
Dimensions in mm Tolerance U.O.S. ±0.1		Scale: 0,350	Date: 04-Feb-05	Sheet: 3 of 4
		Drawn By: von Zwiklitz, L		Drawing Number:

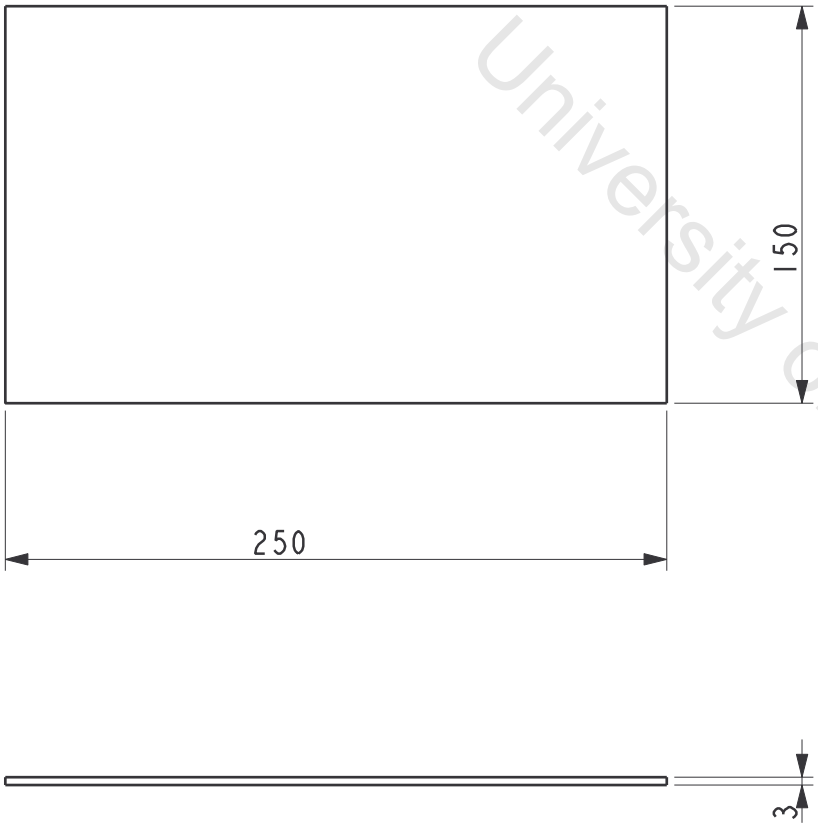

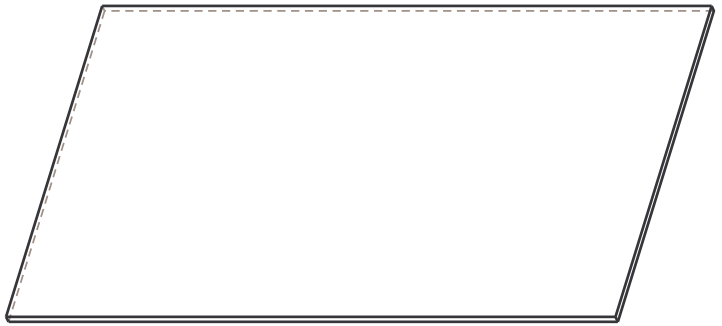

Item	Qty	Name	Material

University of Cape Town
Department of Mechanical Engineering

Title: SIDE OF BATH

Dimensions in mm Tolerance U.O.S.	Scale	Date	Sheet	of
±0.1	0,350	04-Feb-05	4	4

Drawn By: von Zwiklitz, L

Drawing Number:

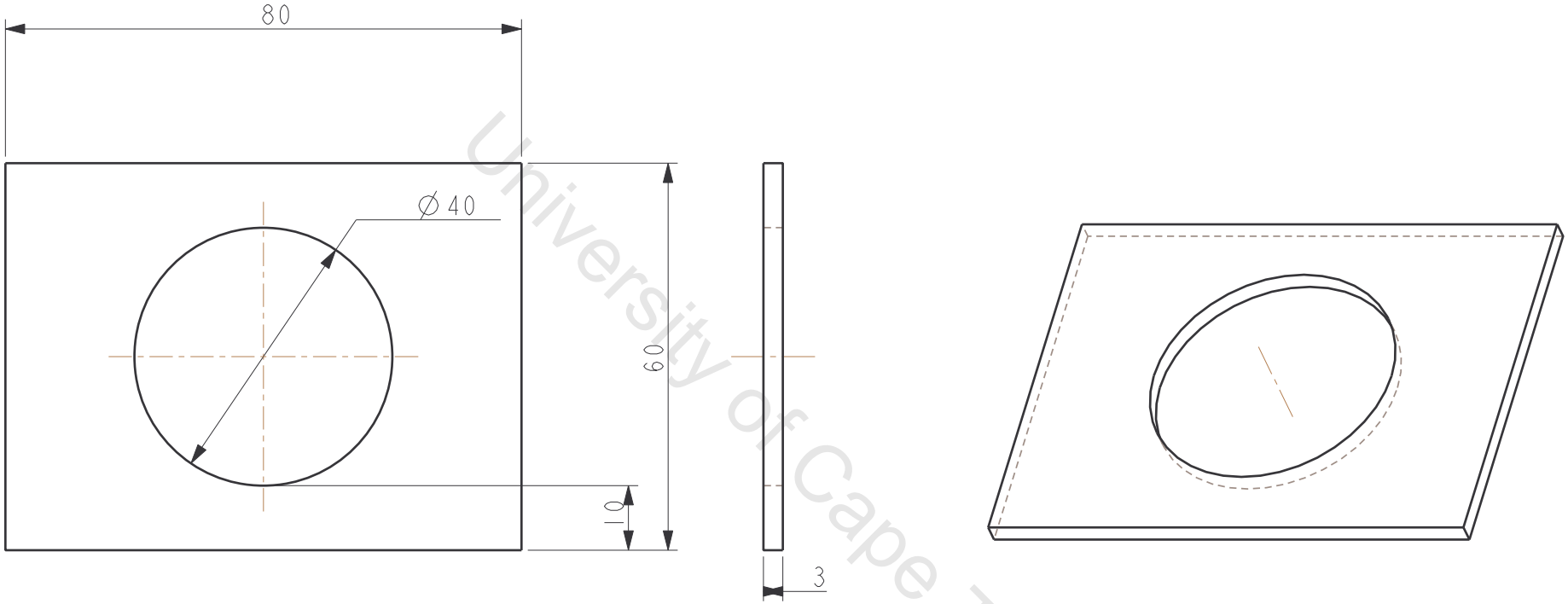

Item	Name	Qty	Material

University of Cape Town
Department of Mechanical Engineering

Title: Base of holder

Dimensions in mm Tolerance U.O.S.	Scale	Date	Sheet	of
0.1	1,000	15-Aug-05	1	2

Drawn By	Drawing Number
von Zwiklitz, L	HOLD02

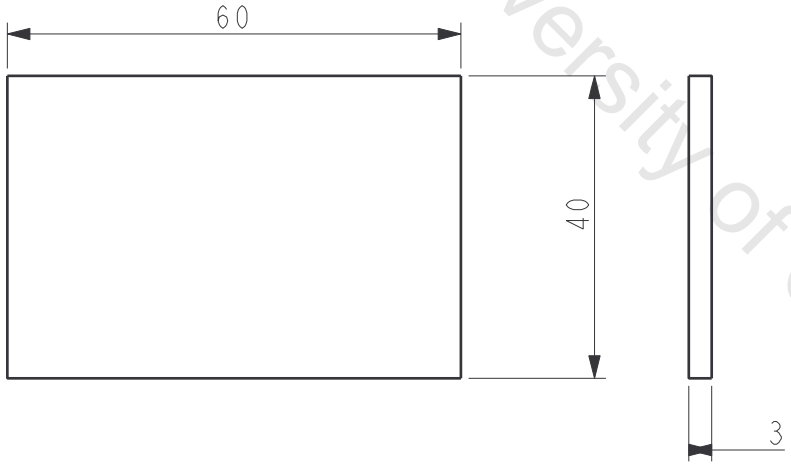

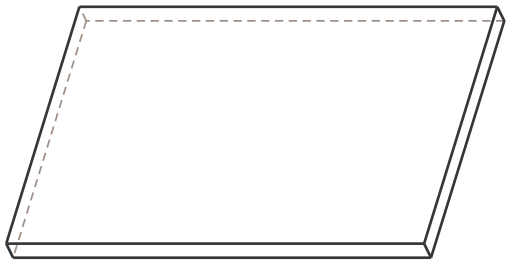

Item	Name	Qty	Material

University of Cape Town
Department of Mechanical Engineering

Title: Short side plate

Dimensions in mm Tolerance U.O.S.	Scale	Date	Sheet	of
0.1	1,000	15-Aug-05	2	2
	Drawn By: von Zwiklitz, L		Drawing Number: HOLD03	

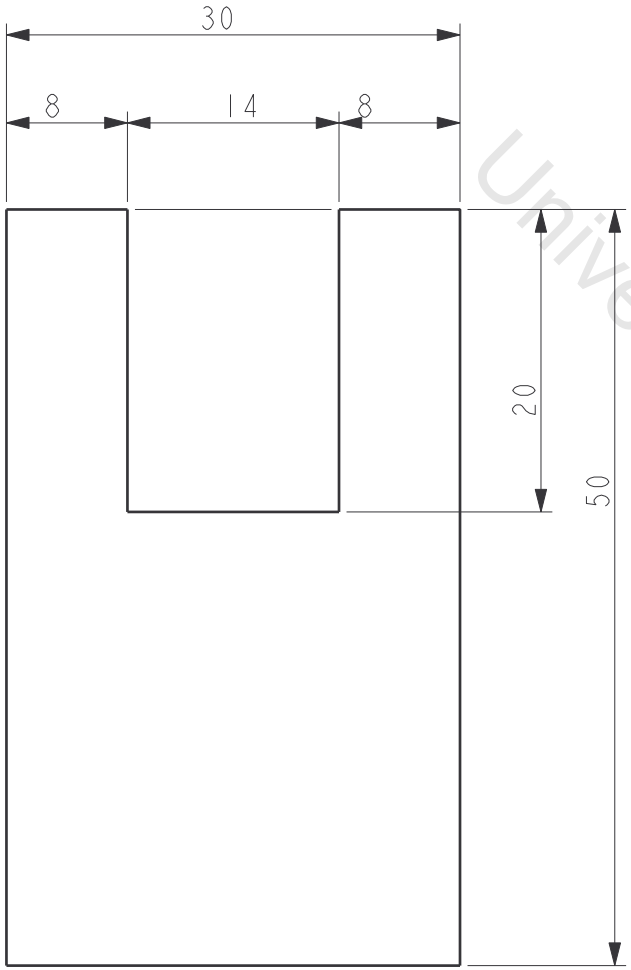

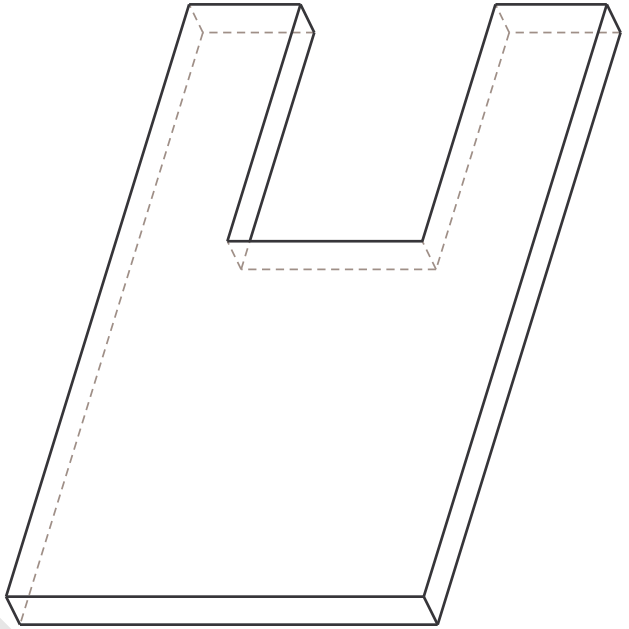

Item	Name	Qty	Material

University of Cape Town
Department of Mechanical Engineering

Title: Float Holder

Dimensions in mm Tolerance U.O.S.	Scale	Date	Sheet	of
0.1	2,000	15-Aug-05	1	1
	Drawn By: von Zwiklitz, L		Drawing Number:	

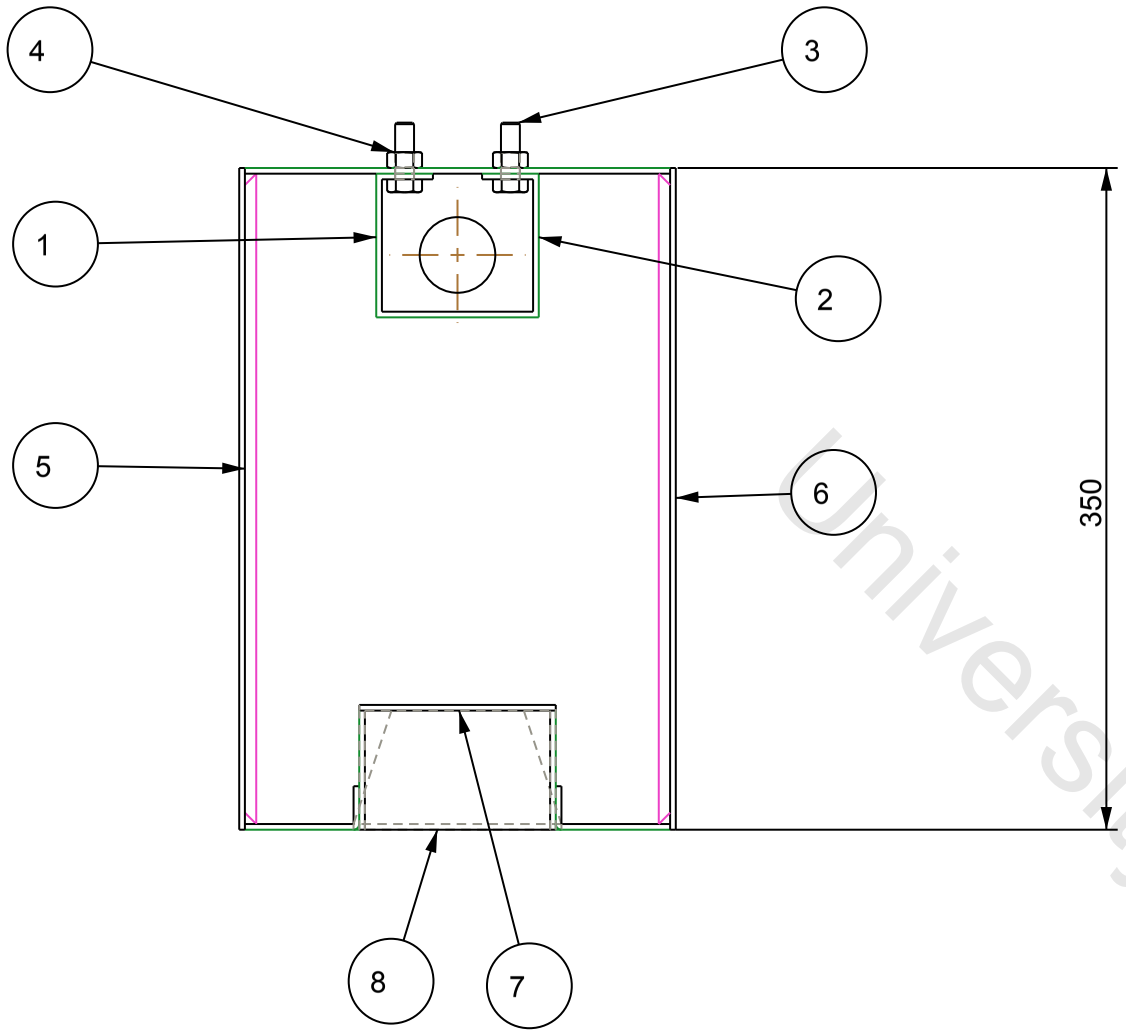

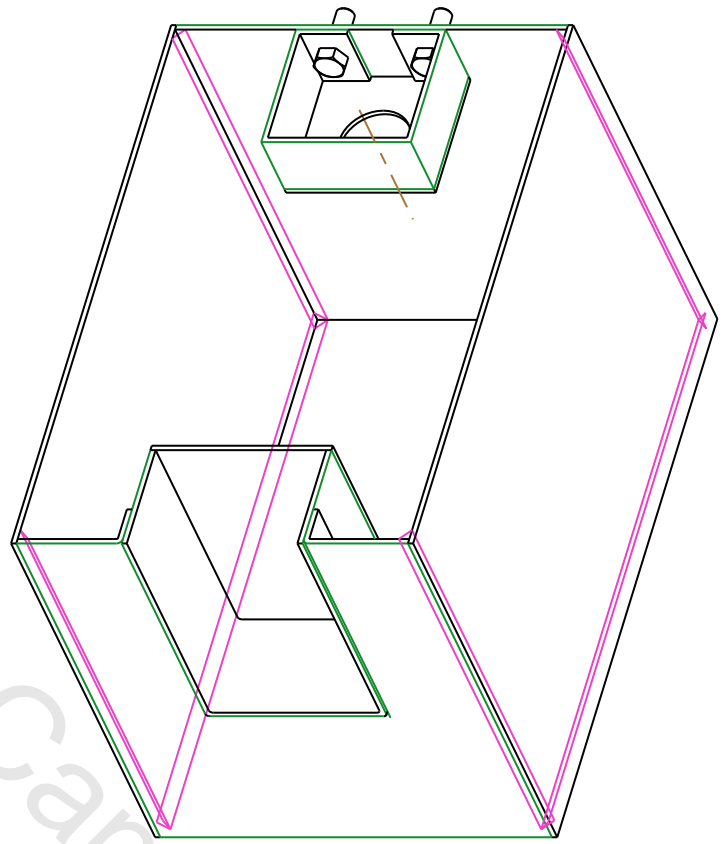

All Welds

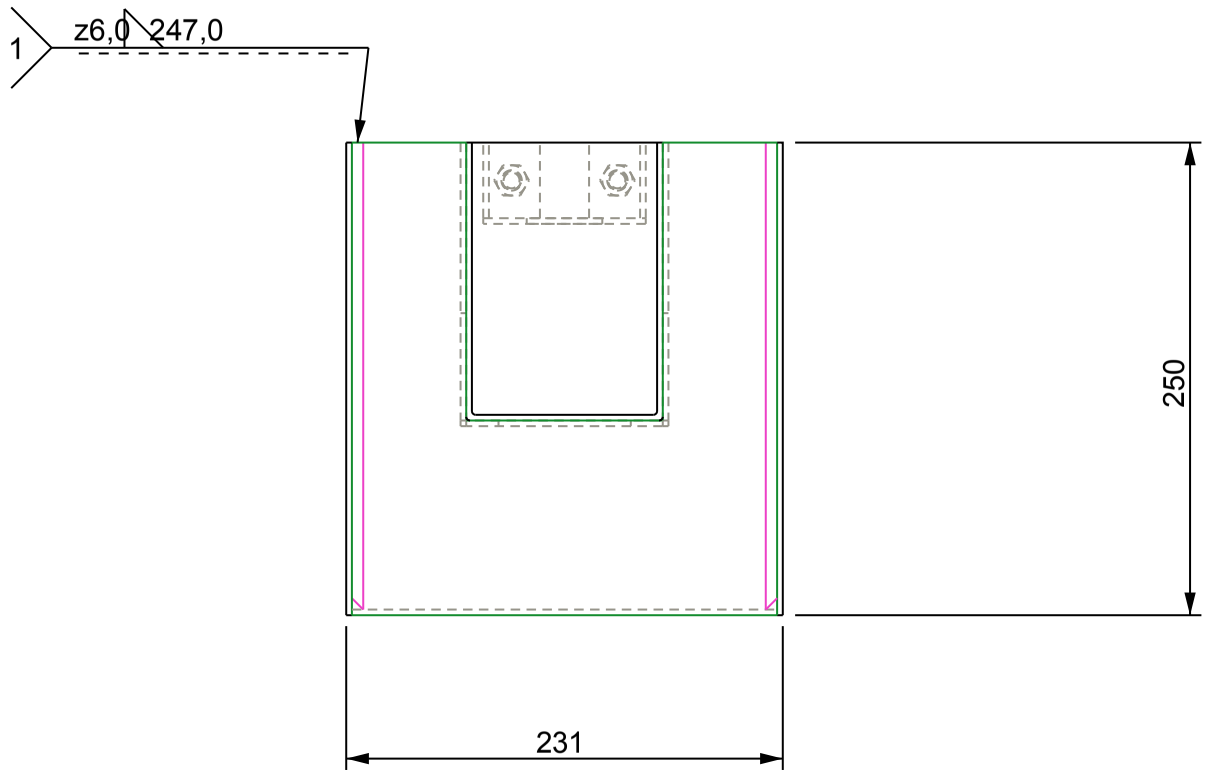

Item	Name	Qty	Material	Remarks
8	VIEW_BOX_COVER	1		Perspex
7	VIEW_BOX_BACK_COVER	1	STEEL_LC	Perspex
6	TEST_RIG_SIDE_COVER	2		Steel
5	TEST_RIG_FLOOR_SHEET	1		Steel
4	INHF102	2		Standard Part
3	IHBC04	2		Standard Part
2	HEAT_ELEMENT_HOLDER	1		Steel
1	H_E_HOLDER_FLOOR	1	STEEL_LC	Steel

University of Cape Town
Department of Mechanical Engineering

Title
Test Rig Assembly

Dimensions in mm Tolerance U.O.S.	Scale	Date	Sheet	of
0.1	0,250	June-2007	1	7
	Drawn By: G.S. Izaaks		Drawing Number: 1	

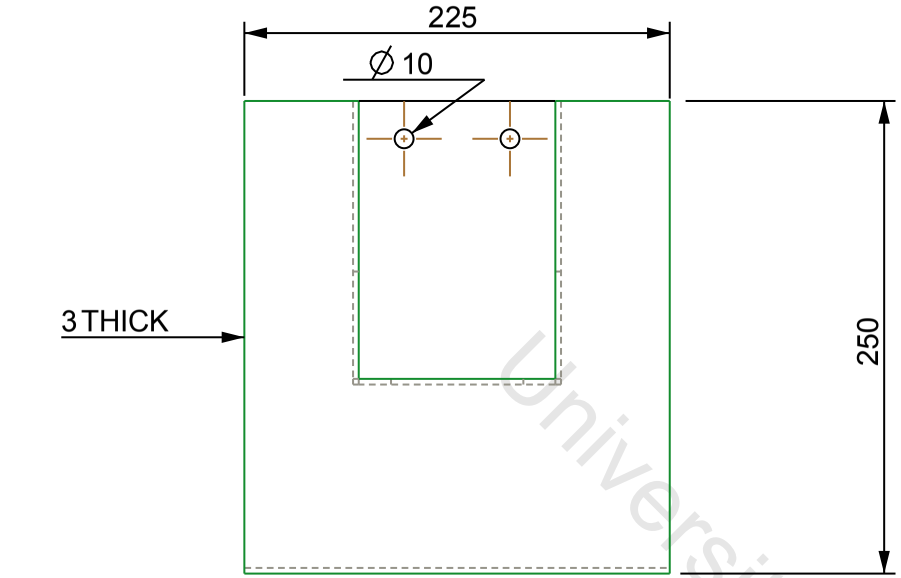

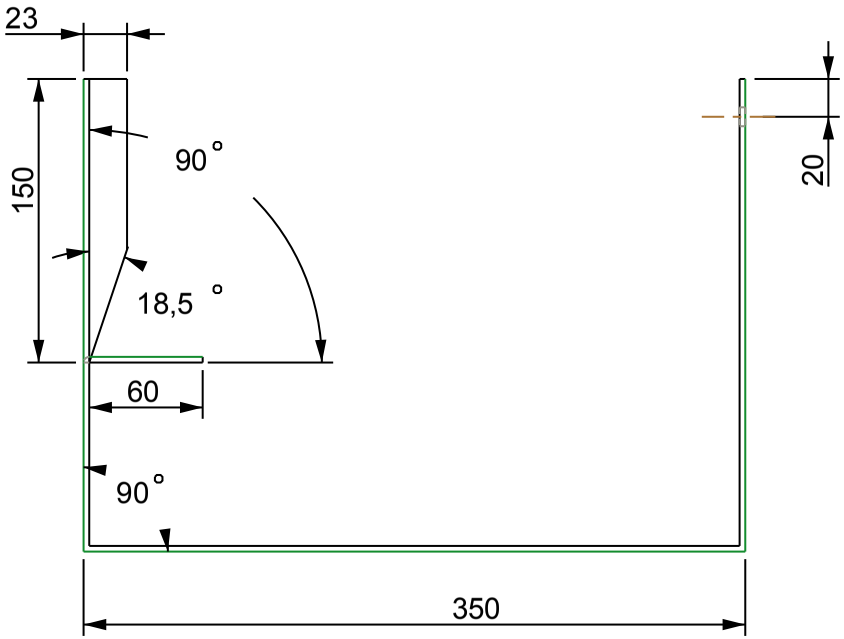

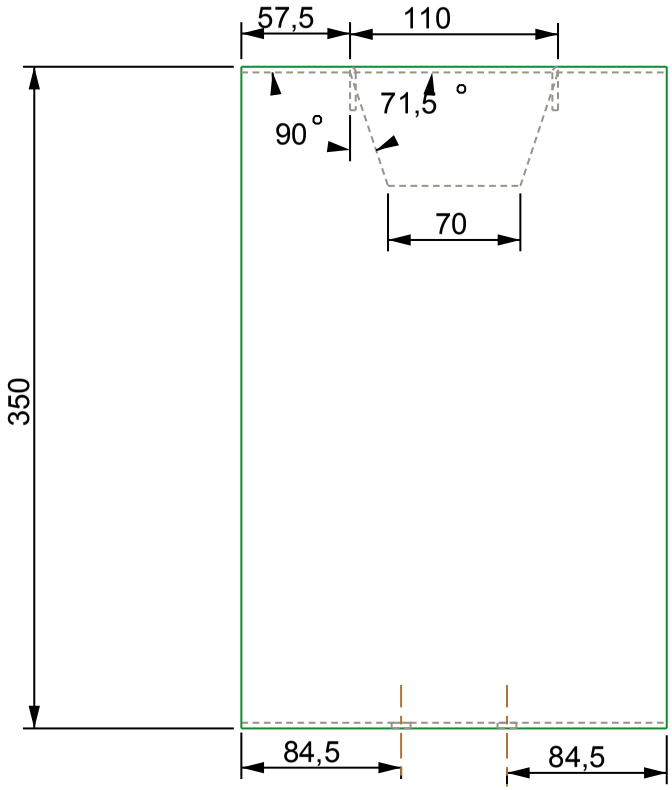

Item	Name	Qty	Material

University of Cape Town
Department of Mechanical Engineering

Title: Front Side of Rig

Dimensions in mm Tolerance U.O.S.	Scale	Date	Sheet	of
0.1	0,250	June-2007	2	7

Drawn By	Drawing Number
G.S. Izaaks	2

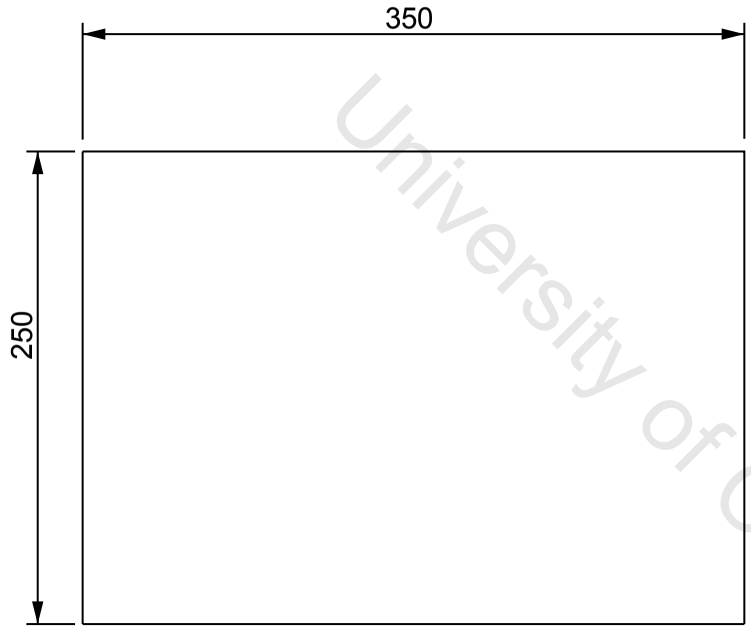

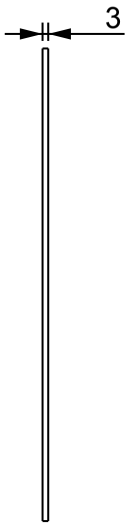

Item	Name	Qty	Material

University of Cape Town
Department of Mechanical Engineering

Title
Test Rig's Side cover

Dimensions in mm Tolerance U.O.S.	Scale	Date	Sheet	of
	0,250	June-2007	3	7
	Drawn By		Drawing Number	
0.1	G.S. Izaaks		3	

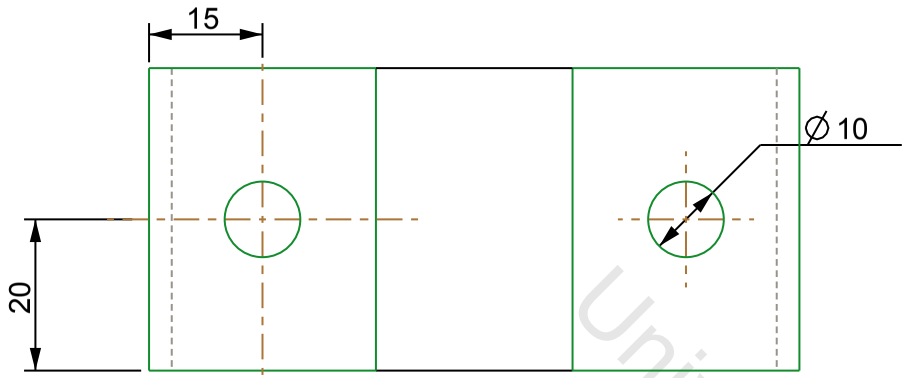

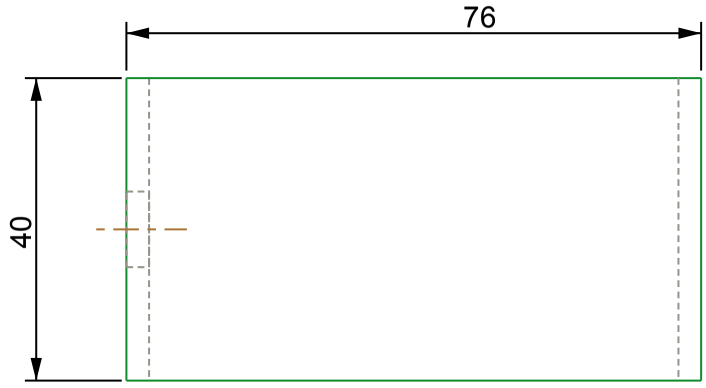

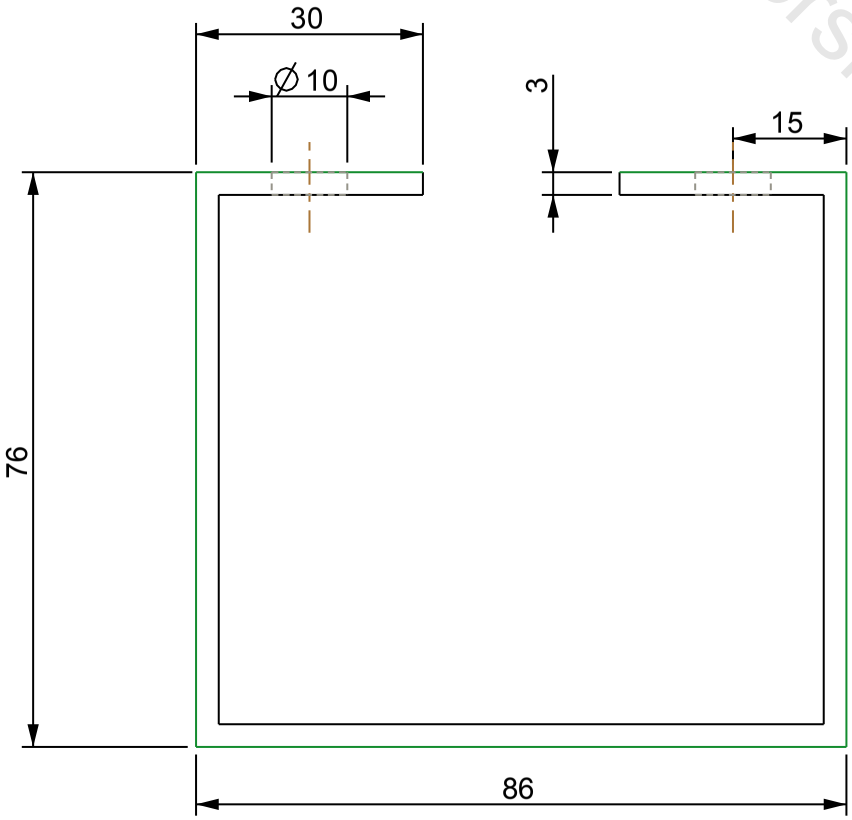

All bends at ∠ 90

Item	Name	Qty	Material

University of Cape Town
Department of Mechanical Engineering

Title: Heat Element holder_wall

Dimensions in mm Tolerance U.O.S.	Scale	Date	Sheet	of
0.1	1,000	June-2007	4	7

Drawn By	Drawing Number
G.S. Izaaks	4

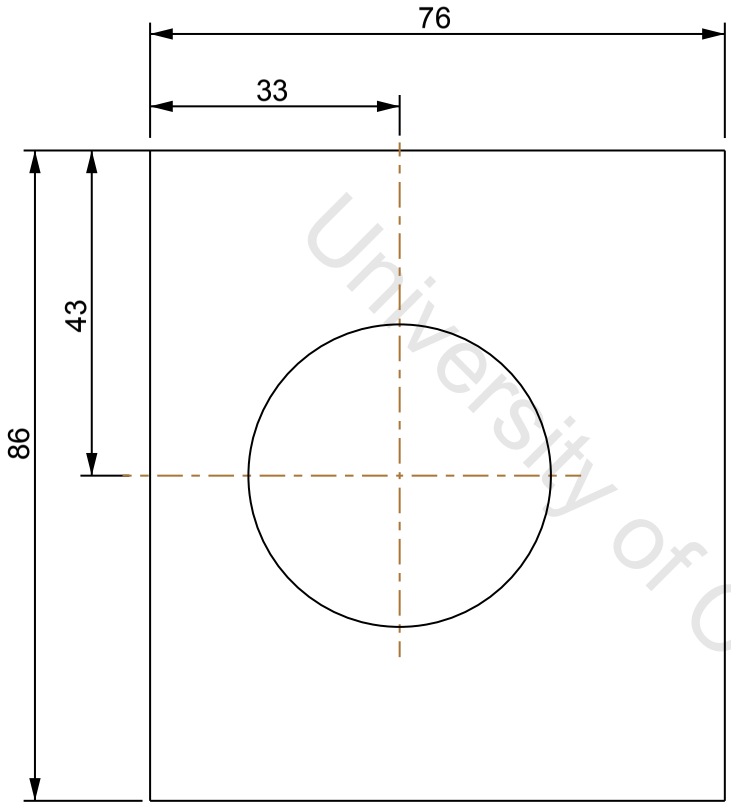

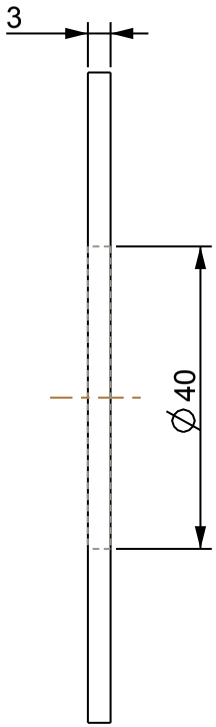

Item	Name	Qty	Material

University of Cape Town
Department of Mechanical Engineering

Title: Holder's Floor

Dimensions in mm Tolerance U.O.S.	Scale	Date	Sheet	of
0.1	1,000	June-2007	5	7
	Drawn By: G.S. Izaaks		Drawing Number: 5	

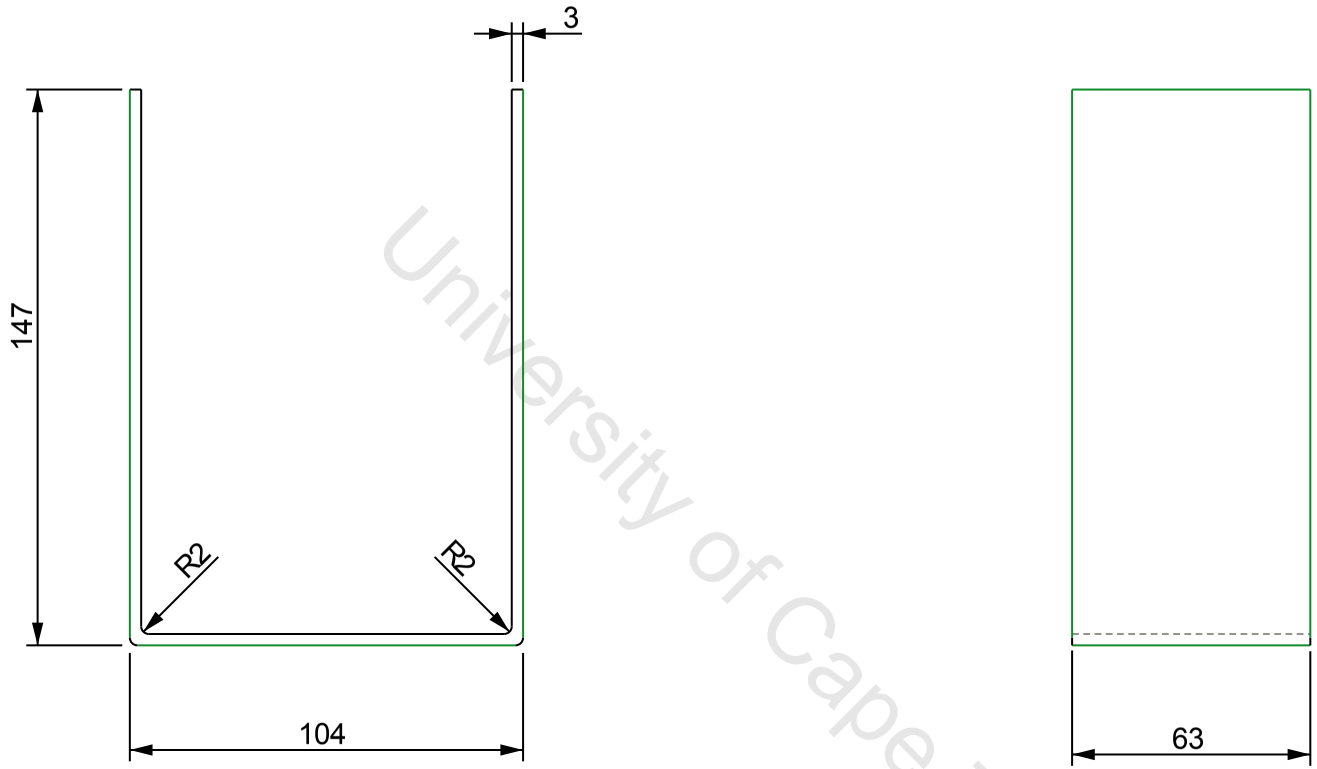

Item	Name	Qty	Material

University of Cape Town
Department of Mechanical Engineering

Title
View Box Sides

Dimensions in mm Tolerance U.O.S.	Scale	Date	Sheet	of
0.1	0,500	June-2007	6	7

Drawn By	Drawing Number
G.S. Izaaks	6

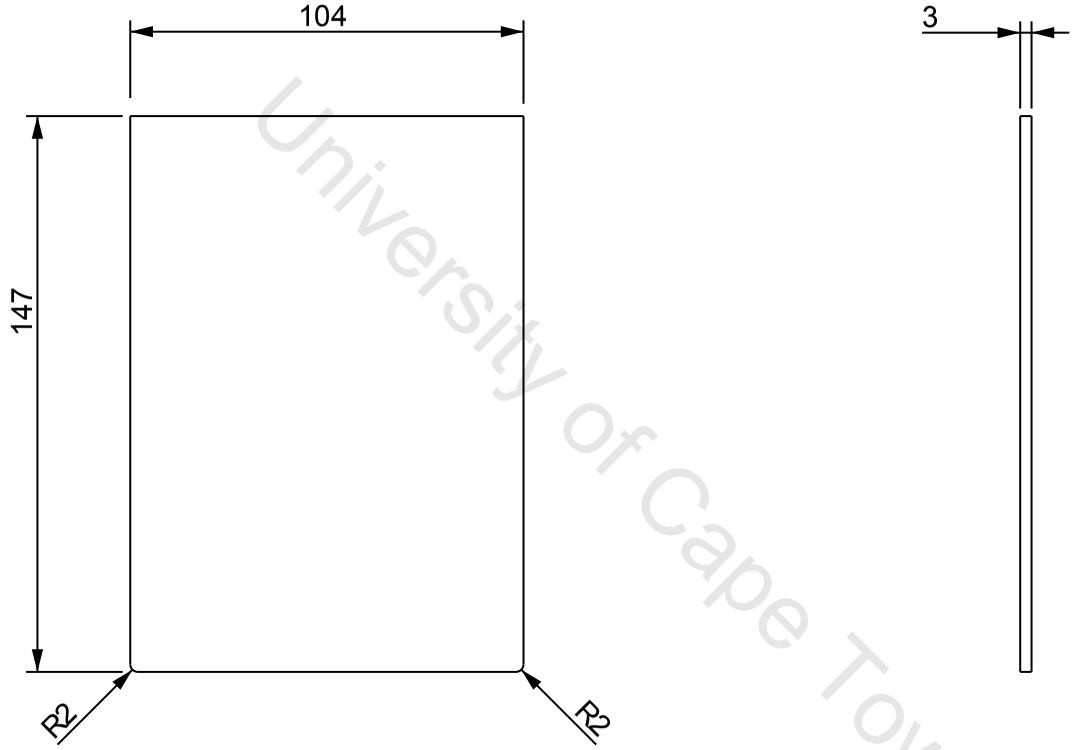

Item	Name	Qty	Material

University of Cape Town
Department of Mechanical Engineering

Title
View Box Back Cover

Dimensions in mm Tolerance U.O.S.	Scale	Date	Sheet	of
0.1	0,500	June-2007	7	7
	Drawn By		Drawing Number	
	G.S. Izaaks		7	

APPENDIX C – THERMO-CONTROLLER INSTRUCTIONS

4-2 Auto Tuning

During PID operation (on the REX-P90F or REX-P90D): An optimum PID constant is automatically calculated and set during Auto Tuning. Use the following procedure when the operator uses the system first time or when the system control is unstable.

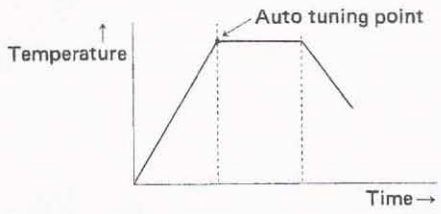

Key operations **On-screen display**

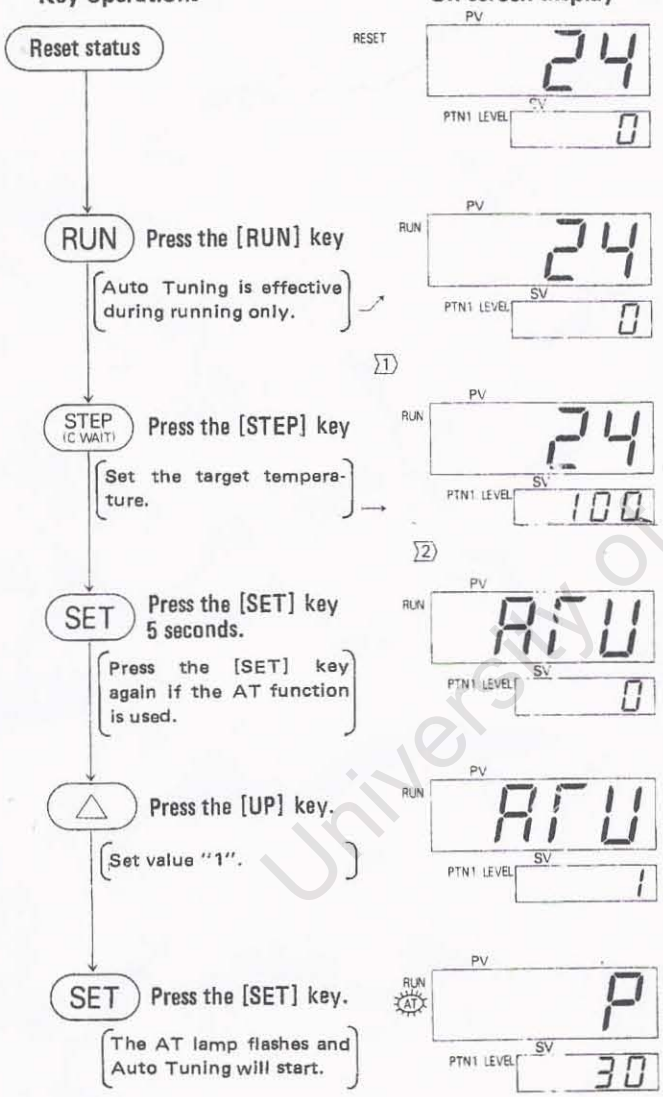

After Auto Tuning, the signal waves are generated for three cycles around the set value as shown in the figure. Then, PID control starts automatically.

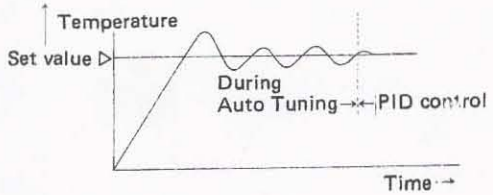

Note:
If you start Auto Tuning when the set value is being changed (during ramp control), the change of set value stops immediately and the appropriate PID constant is calculated at this point.

4-3 Auto Tuning for Level PID

Up to three PID constants can be set according to the temperature level. The level PID is useful if the load characteristics change due to the temperature.

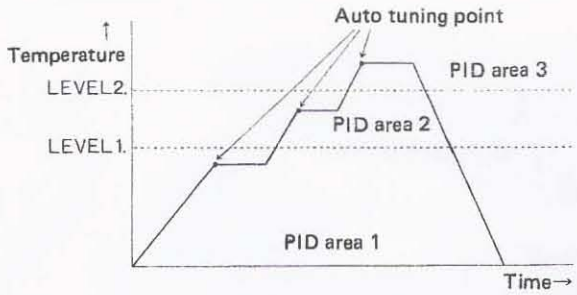

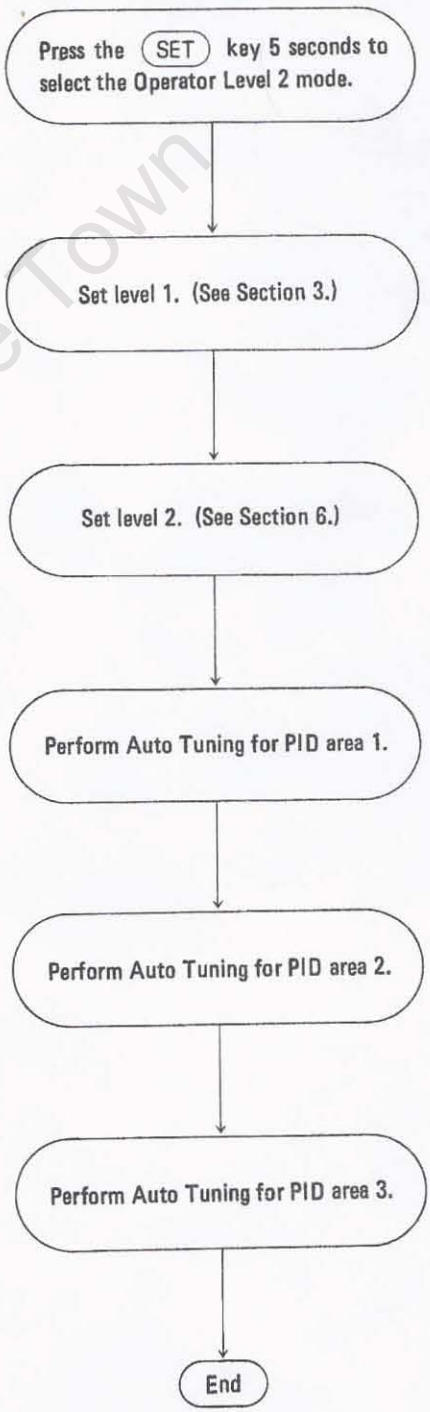

APPENDIX D – TABLES FOR f(a/W)

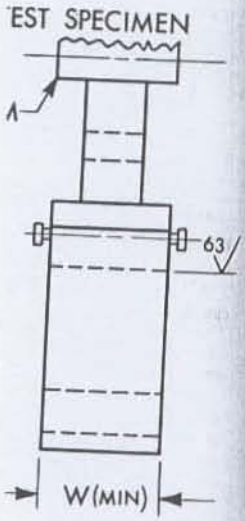

OR
OR
NDS

ithin 0.002 W.

SPECIMENS

is designs may be used
hey will accomplish the
ı.
ıces and suggested pro-
are given in Fig. A4.2.
specimens having W/
) and W/B = 4 for B ≦
)-psi (1930-MPa) yield
or the clevis and pins,
ed for testing the spec-
en in 7.1.3. If lower-
if substantially larger
σ_{YS}/E ratio than those
s will be required. As
orners may be cut off
ing of the clip gage in
mm) thick.
hould be given to
ssible through careful
g fixtures.
or generally applica-

ble details concerning the displacement gage see 6.3. For the compact specimen the displacements will be essentially independent of the gage length up to 1.2 W.

A4.4 Procedure

A4.4.1 *Measurement*—For a compact specimen measure the width, W, and the crack length, a, from the plane of the centerline of the loading holes (the notched edge is a convenient reference line but the distance from the centerline of the holes to the notched edge must be subtracted to determine W and a). Measure the width, W, to the nearest 0.001 in. (0.025 mm) or 0.1 %, whichever is larger, at not less than three positions near the notch location, and record the average value.

A4.4.1.1 For general requirements concerning specimen measurement see 8.2.

A4.4.2 *Compact Specimen Testing*—When assembling the loading train (clevises and their attachments to the tensile machine) care should be taken to minimize eccentricity of loading due to misalignments external to the clevises. To obtain satisfactory alignment keep the centerline of the upper and lower loading rods coincident within 0.03 in. (0.76 mm) during the test and center the specimen with respect to the clevis opening within 0.03 in. (0.76 mm).

A4.4.2.1 Load the compact specimen at such a rate that the rate of increase of stress intensity is within the range 30 to 150 ksi·in.$^{1/2}$/min (0.55 to 2.75 MPa·m$^{1/2}$/s) corresponding to a loading rate for a standard (W/B = 2) 1-in. thick specimen 4500 and 22 500 lbf/min (0.34 to 1.7 kN/s).

A4.4.2.2 For details concerning recording of the test record see 8.4.

A4.5 Calculations

A4.5.1 For general requirements and procedures in interpretation of the test record see 9.1.

A4.5.2 For a description of the validity requirements in terms of limitations on P_{max}/P_Q and the specimen size requirements see 9.1.2 through 9.1.3.

A4.5.3 *Calculation of K_Q*—For the compact specimen calculate K_Q in units of ksi·in.$^{1/2}$ (MPa·m$^{1/2}$) from the following expression (Note A4.1)

$$K_Q = (P_Q/BW^{1/2}) \cdot f(a/W)$$

where:

$$f(a/W) = \frac{(2 + a/W)(0.886 + 4.64a/W - 13.32a^2/W^2 + 14.72a^3/W^3 - 5.6a^4/W^4)}{(1 - a/W)^{3/2}}$$

where:

P_Q = load as determined in 9.1.1, klbf (kN),
B = specimen thickness as determined in 8.2.1, in. (cm),
W = specimen width, as determined in A4.4.1, in. (cm), and
a = crack length as determined in 8.2.2 and A4.4.1, in. (cm).

To facilitate calculation of K_Q, values of $f(a/W)$ are tabulated below for specific values of a/W.

Compact Specimens

a/W	$f(a/W)$	a/W	$f(a/W)$
0.450	8.34	0.500	9.66
0.455	8.46	0.505	9.81
0.460	8.58	0.510	9.96
0.465	8.70	0.515	10.12
0.470	8.83	0.520	10.29
0.475	8.96	0.525	10.45
0.480	9.09	0.530	10.63
0.485	9.23	0.535	10.80
0.490	9.37	0.540	10.98
0.495	9.51	0.545	11.17
		0.550	11.36

NOTE A4.1—The expression in A4.5.3 is considered to be accurate within ±0.5 % over the range of a/W from 0.2 to 1 **(12)** **(13)**.

4.5.4 *Calculation of R_{sc}*—For the compact specimen calculate the specimen strength ratio (which is dimensionless and has the same value in any consistent system of units):

$$R_{sc} = \frac{2P_{max}(2W + a)}{B(W - a)^2\sigma_{YS}}$$

where:

P_{max} = maximum load that the specimen was able to sustain,
B = thickness of specimen as determined in 8.2.1,
W = width of the specimen as determined in A4.4.1,
a = crack length as determined in 8.2.2 and A4.4.1, and
σ_{YS} = yield strength in tension (offset = 0.2 %) (see Methods E 8).

ate that the overall
t the requirements
test method.
s conducted at a

temperature T_1 and testing at a different temperature T_2, K_{max} must not exceed 0.6 $(\sigma_{YS1}/\sigma_{YS2})K_Q$, where σ_{YS1} and σ_{YS2} are the yield strengths at the respective temperatures T_1 and T_2.

IIREMENTS FOR THE TESTING OF BEND SPECIMENS

en is a single edge-
ided in three-point
ominally equal to
ral proportions of
n in Fig. A3.1.
have $1 \le W/B \le$
nominal support

pecifications con-
n see Section 7.
ck the bend spec-
will be tested so
nown. However,
ked in cantilever
ease of reversed
-point bending is
ig moments for a
7). While fatigue
yield satisfactory
ie crack tip stress
crack orientation

eneral principles
n Fig. A3.2. This
tional effects by
and move apart
s permitting roll-
are allowed lim-
el to the notched
positively posi-
n length and are
(such as rubber

enerally applica-
nt gage see 6.3.
nts will be essen-
to a gage length

specimen meas-
c length, a, from
he opposite side

oncerning spec-

t up the test fix-
plied load shall
centers within
rs (for example,

within 0.04 in. (1.0 mm) for a 4-in. (100-mm) span). Measure the span to within 0.5 % of nominal length. Locate the specimen with the crack tip midway between the rolls to within 1 % of the span, and square to the roll axes within 2°. Seat the displacement gage on the knife edges to maintain registry between knife edges and gage grooves. In the case of attachable knife edges, seat the gage before the knife edge positioning screws are tightened.

A3.4.2.1 Load the specimen at a rate such that the rate of increase of stress intensity is within the range 30 to 150 ksi·in.$^{1/2}$/min (0.55 to 2.75 MPa·m$^{1/2}$/s), corresponding to a loading rate for the standard (B = 0.5 W) 1-in. (25.4-mm) thick specimen between 4000 and 20 000 lbf/min (0.30 to 1.5 kN/s).

A3.4.3 For details concerning recording of the test record see 8.4.

A3.5 Calculations

A3.5.1 *Interpretation of Test Record*—For general requirements and procedures in interpretation of the test record see 9.1.

A3.5.2 *Validity Requirements*—For a description of the validity requirements in terms of limitations on P_{max}/P_Q and the specimen size requirements, see 9.1.2 through 9.1.3.

A3.5.3 *Calculation of K_Q*—For the bend specimen calculate K_Q in units of ksi·in.$^{1/2}$ (MPa·m$^{1/2}$) as follows (Note A3.1):

$$K_Q = (P_Q S/BW^{3/2}) \cdot f(a/w)$$

where:

$$f(a/W) = \frac{3(a/W)^{1/2}[1.99 - (a/W)(1 - a/W) \times (2.15 - 3.93a/W + 2.7a^2/W^2)]}{2(1 + 2a/W)(1 - a/W)^{3/2}}$$

where:

P_Q = load as determined in 9.1.1, klbf (kN),
B = specimen thickness as determined in 8.2.1, in. (cm),
S = span as determined in A3.4.2, in. (cm),
W = specimen depth (width) as determined in A3.4.1, in. (cm), and
a = creak length as determined in 8.2.2, in. (cm).

To facilitate calculation of K_Q, values of $f(a/W)$ are tabulated in the following table for specific values of a/W.

Bend Specimens

a/W	$f(a/W)$	a/W	$f(a/W)$
0.450	2.29	0.500	2.66
0.455	2.32	0.505	2.70
0.460	2.35	0.510	2.75
0.465	2.39	0.515	2.79
0.470	2.43	0.520	2.84
0.475	2.46	0.525	2.89

Bend Specimens

a/W	$f(a/W)$	a/W	$f(a/W)$
0.480	2.50	0.530	2.94
0.485	2.54	0.535	2.99
0.490	2.58	0.540	3.04
0.495	2.62	0.545	3.09
		0.550	3.14

NOTE A3.1—The expression in A3.5.3 is considered to be accurate within ±0.5 % over the entire range of a/W from 0 to 1 for an S/W = 4 (12).

A3.5.4 *Calculation of R_{sb}*—For the bend specimen calculate the specimen strength ratio (which is dimensionless and has the same value in any o of units):

$$\rightarrow R_{sb} = \frac{6P_{max}W}{B(W - a)^2\sigma_{YS}}$$

where:

P_{max} = maximum load that the specir sustain,
B = thickness of specimen as detern
W = width (depth) of specimen, a: A3.4.1,
a = crack length as determined in 8
σ_{YS} = yield strength in tension (offs Methods E 8).

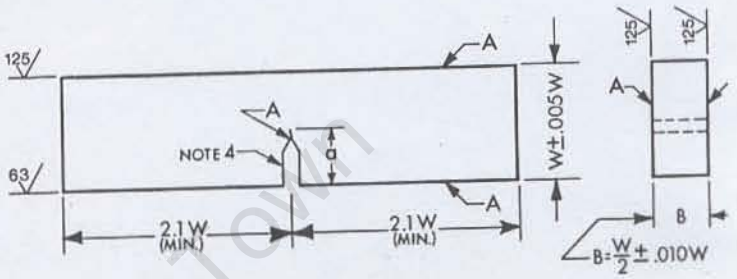

NOTE 1—*A* surfaces shall be perpendicular and parallel as applicable within 0.001 W TIR.
NOTE 2—Crack starter notch shall be perpendicular to specimen surfaces to within ±2°.
NOTE 3—Integral or attachable knife edges for clip gage attachment may be used (see Figs. 5 an
NOTE 4—For starter notch and fatigue crack configurations see Fig. 7.

FIG. A3.1 Bend Specimen SE (B)—Standard Proportions and Toler

ible, determine the average value of r_2 Note A5.1): Measure within 5 % the cord of the outer surface, which cord e loading hole centers (see Fig. A5.3). rement, calculate

$$\frac{L^2}{8(W+X)} + \frac{(W+X)}{2}$$

W/r_2.

. 10 % variation of the ratio r_1/r_2 will f the stress intensity factor by 1 % or t the relative crack length a/W is not vever, the stress analysis is based on at the specimens are to be cut from axisymmetric cross section. If inspec- ie stock deviates from axisymmetry %, it should be reworked to within

fracture measure the crack length in .2.2 but a special procedure is neces- aped specimen due to its curvature. surement, m, made from a reference the crack mouth to a point on the greater than the corresponding dis- ual point of intersection between the e inside circumference of the speci- 3). The error, e, may be computed expression:

$$= r_1 - \left[r_1^2 - \frac{g^2}{4}\right]^{1/2}$$

ance across the crack mouth at the r measurement of the crack length. that g may be equal to N (Fig. 7) or ichined knife edges are used to hold cample, $g = 0.25$ in. (2.5 mm) as in ve error $e/m < 0.01$, then record m ; otherwise e should be subtracted ult recorded as the crack length.

ed Specimen Testing—When as- ng train (clevises and their attach- n machine) care should be taken to ity of loading due to misalignments vises. To obtain satisfactory align- rline of the upper and lower loading hin 0.03 in. (0.76 mm) during the specimen with respect to the clevis 3 in. (0.76 mm).

the arc-shaped specimen at such a increase of stress intensity is within ksi·in.$^{1/2}$/min (0.55 to 2.75 MPa· onding loading rates for a standard k specimen are: (*1*) for the specimen between 2800 and 14 000 lbf/min id (*2*) for the specimen with an $X/$ 0 and 22 500 lbf/min (0.34 to 1.7

ails concerning recording of the test

al requirements and procedures in test record see 9.1.

C-Shape

A5.5.2 For a description of the validity requirements in terms of limitations on P_{max}/P_Q and the specimen size requirements see 9.1.2 through 9.1.3.

A5.5.3 *Calculation of K_Q*—For the arc-shaped specimen calculate K_Q in units of ksi·in.$^{1/2}$ (MPa·m$^{1/2}$) from the following expression (Note A5.2):

$$K_Q = (P_Q/BW^{1/2})[3X/W + 1.9 + 1.1a/W] \times [1 + 0.25(1 - a/W)^2(1 - r_1/r_2)]f(a/W) \quad (11)$$

where

$$f(a/W) = [(a/W)^{1/2}/(1 - a/W)^{3/2}] \times [3.74 - 6.30a/W + 6.32(a/W)^2 - 2.43(a/W)^3]$$

where:

P_Q = load as determined in 9.1.1, klbf (kN),
B = specimen thickness as determined in 8.2.1, in. (cm),
X = loading hole offset as determined in A5.4.1, in. (cm),
W = specimen width as determined in A5.4.1, in. (cm),
a = crack length as determined in 8.2.2 and A5.4.1.1, in. (cm), and
r_1/r_2 = ratio of inner to outer radii as determined in A5.4.1.

To facilitate calculation of K_Q, values of $f(a/W)$ are tabulated in the following table for specific values of a/W:

a/W	$f(a/W)$	a/W	$f(a/W)$
0.450	3.23	0.500	3.73
0.455	3.27	0.505	3.79
0.460	3.32	0.510	3.85
0.465	3.37	0.515	3.91
0.470	3.42	0.520	3.97
0.475	3.47	0.525	4.03
0.480	3.52	0.530	4.10
0.485	3.57	0.535	4.17
0.490	3.62	0.540	4.24
0.495	3.68	0.545	4.31
...	...	0.550	4.38

NOTE A5.2—The accuracy of the expression in A5.5.3 for all values of r_1/r_2 is considered to be as follows: (*1*) ±1 % for $0.45 \le a/W \le 0.55$ and X/W of 0 or 0.5, (*2*) ±1.5 % for $0.2 \le a/W \le 1$ and X/W of 0 or 0.5, and (*3*) ±3 % for $0.2 \le a/W \le 1$ and $0 \le X/W \le 1$ **(14)**.

A5.5.4 *Calculation of R_{ss}*—For the arc-shaped specimen calculate the specimen strength ratio (which is dimensionless and has the same value in any consistent system of units) as follows:

$$R_{ss} = \frac{2P_{max}(3X + 2W + a)}{B(W - a)^2\sigma_{YS}}$$

where:

P_{max} = maximum load that the specimen was able to sustain,
B = thickness of the specimen as determined in 8.2.1,
X = loading hole offset as determined in A5.4.1,
W = width of the specimen as determined in A5.4.1,
a = crack length as determined in 8.2.2 and A5.4.1.1, and
σ_{YS} = yield strength in tension (offset = 0.2 %) (see Methods E 8).

APPENDIX E – RAMPING GRAPHS

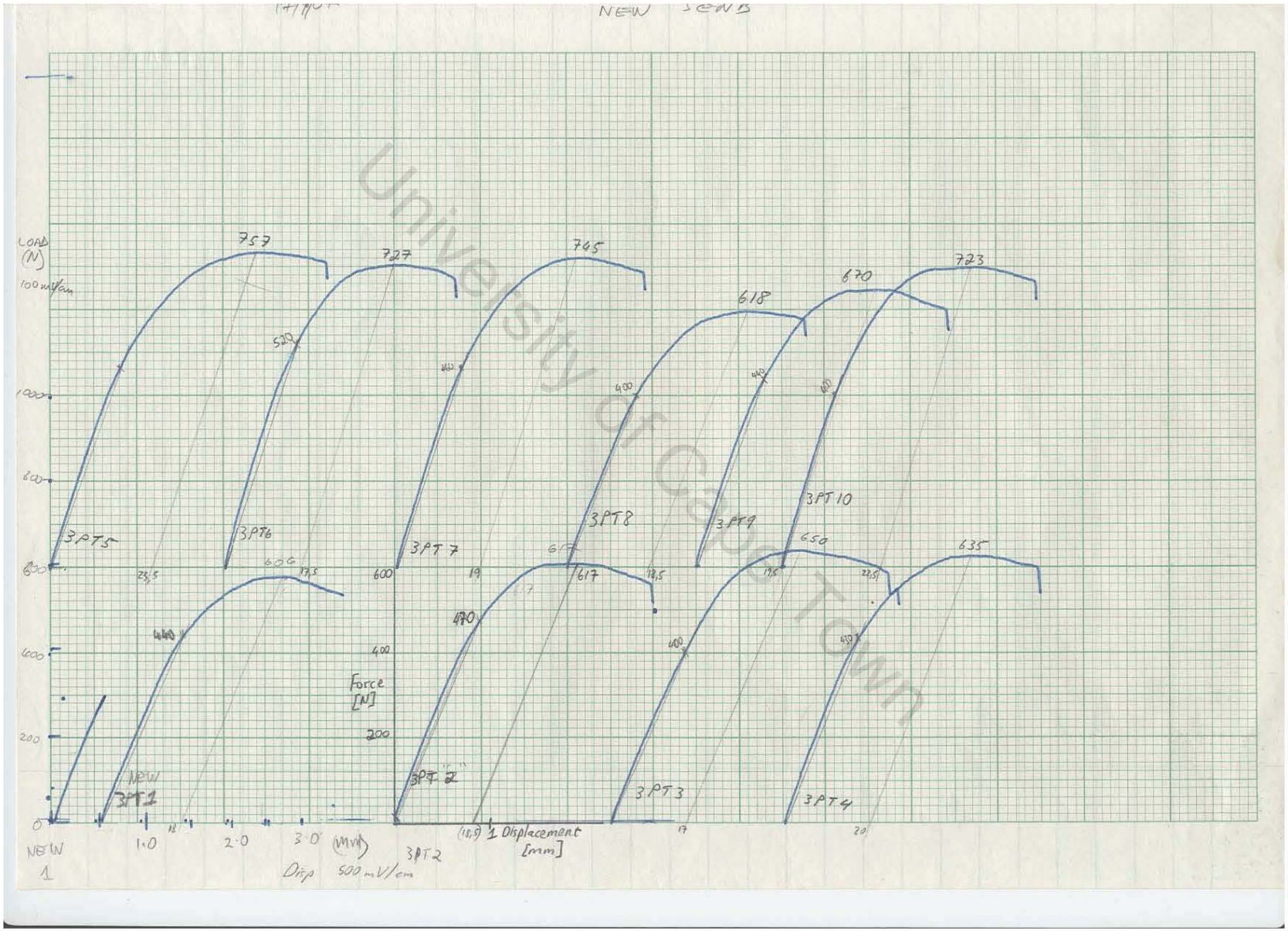

17/09/07 SENB - NEW

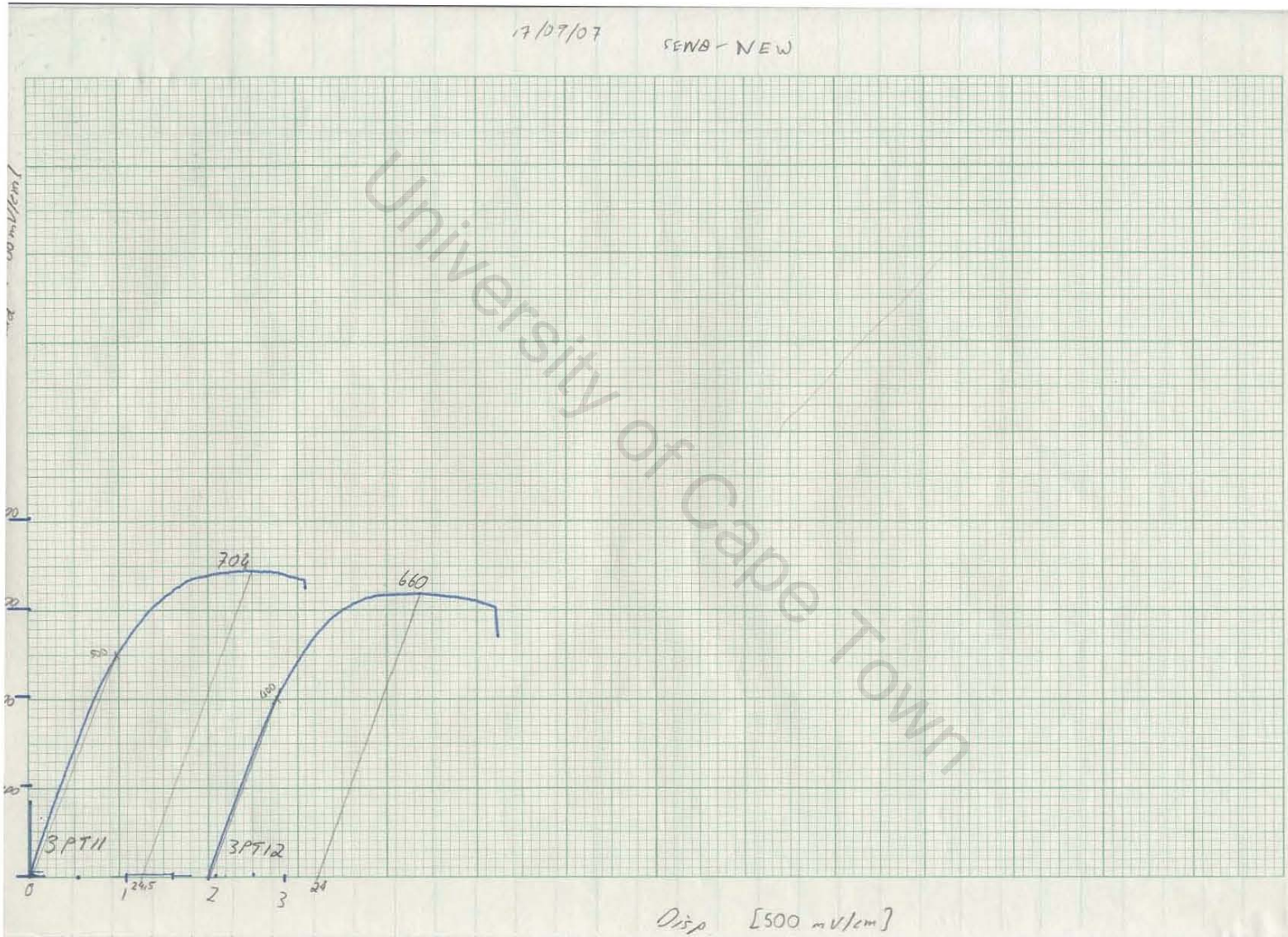

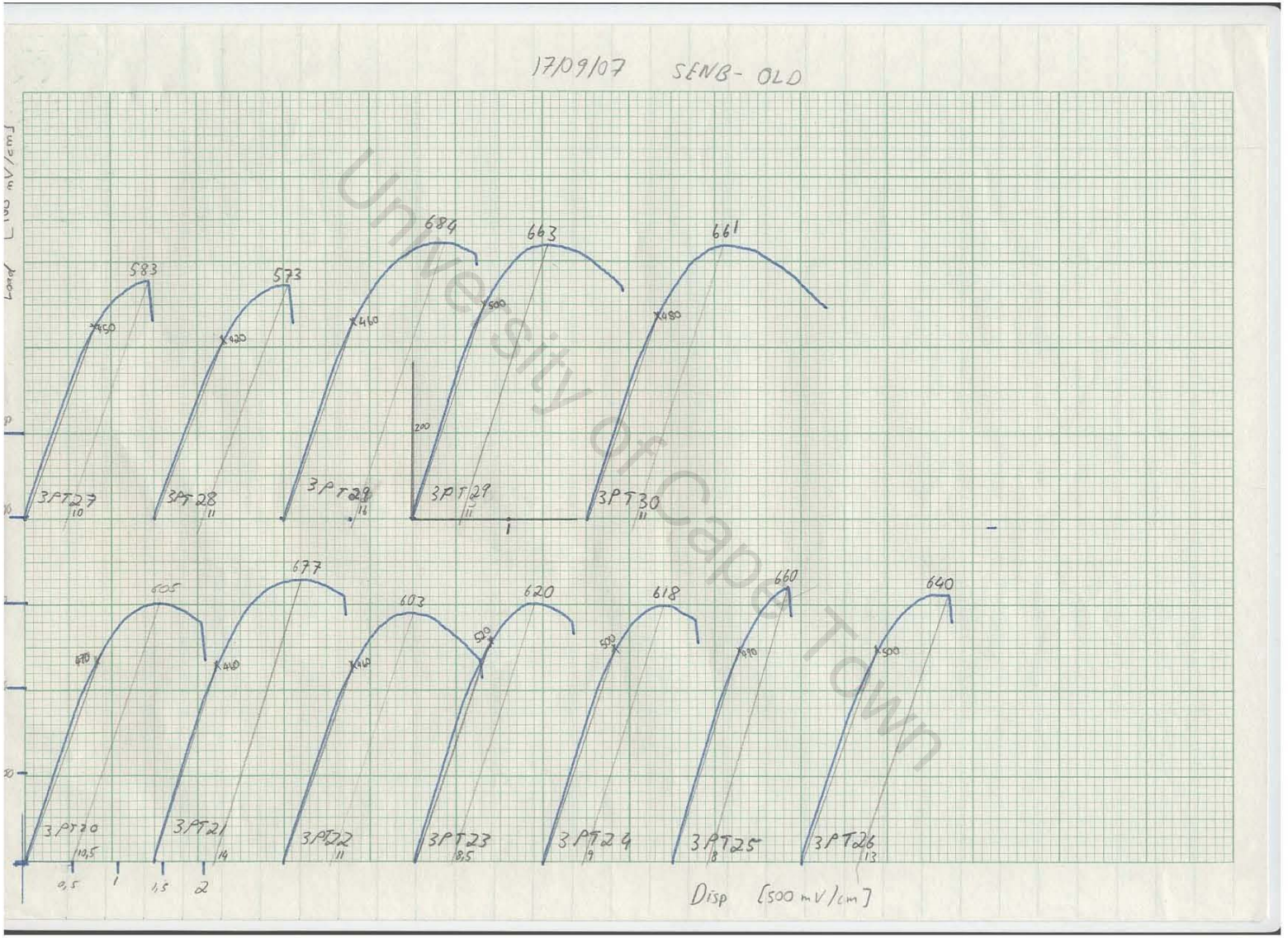
17/09/07 SENB- OLD
583
573
684
663
661
605
677
603
620
618
660
640
3PT27
3PT28
3PT29
3PT29
3PT30
3PT20
3PT21
3PT22
3PT23
3PT24
3PT25
3PT26
Disp [500 mV/cm]

NEW C-Shape (08/10/07)

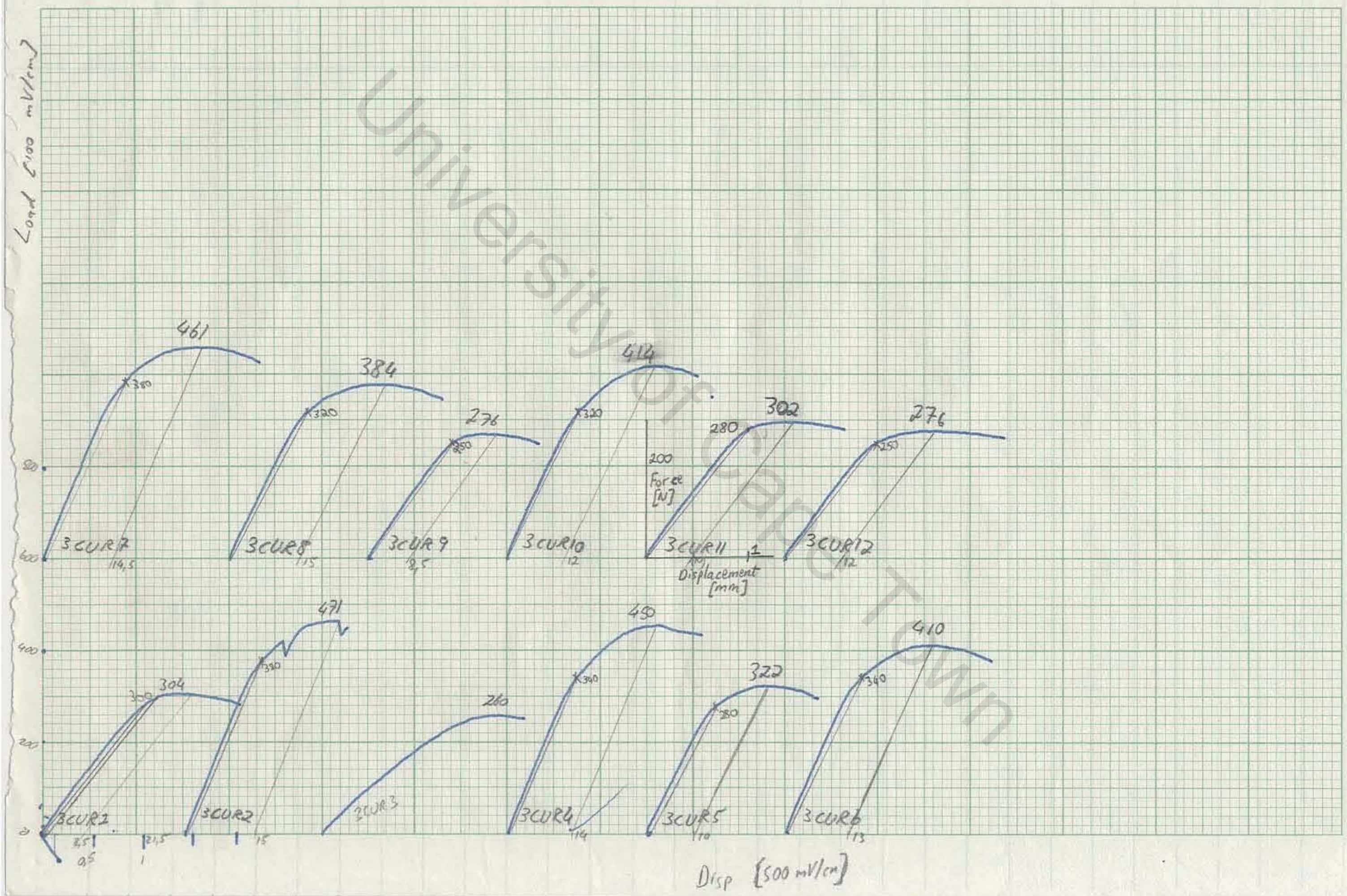

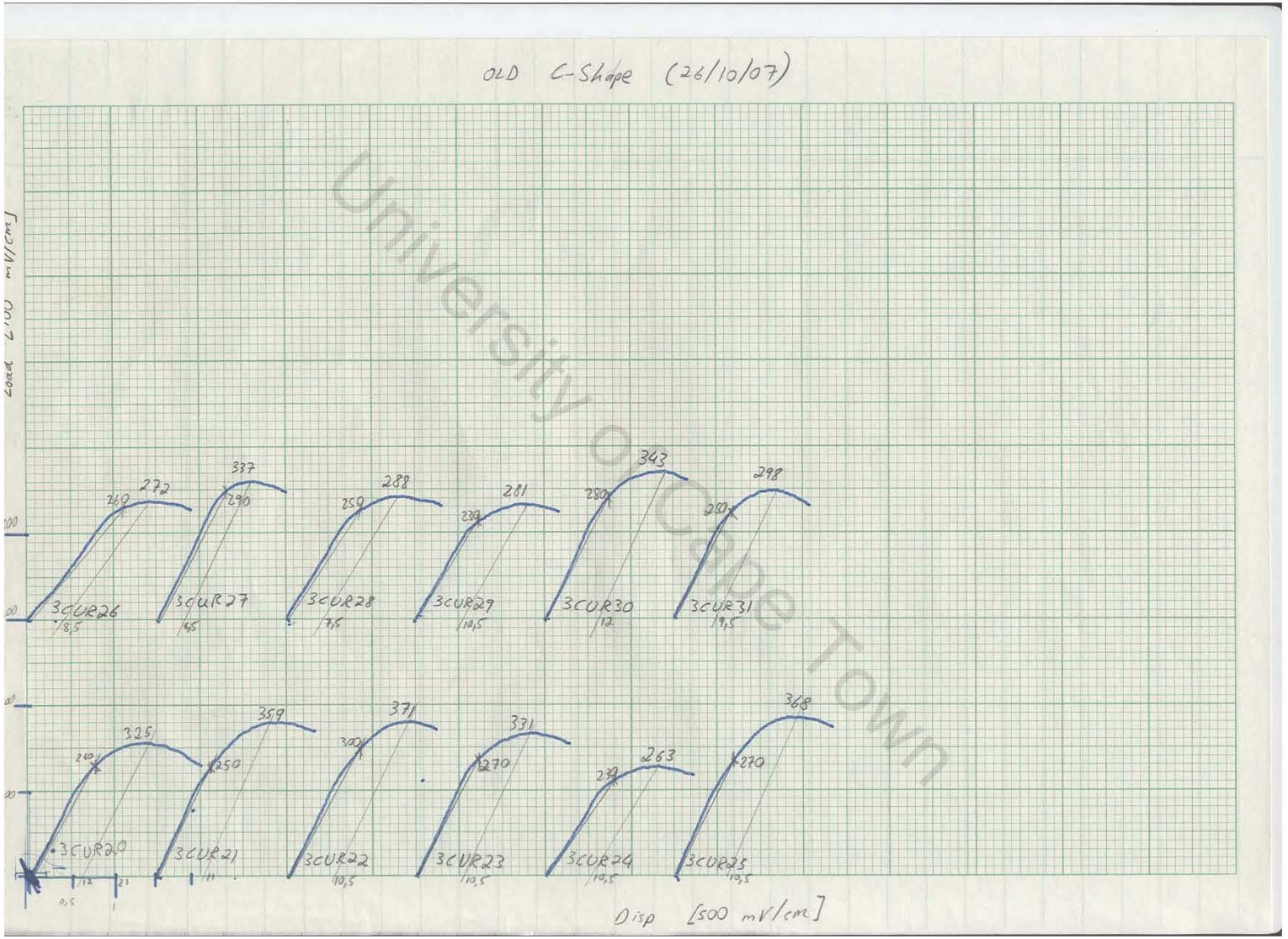

APPENDIX F – RAMPING EQUIPMENT MANUFACTURING DRAWINGS

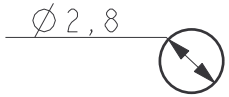

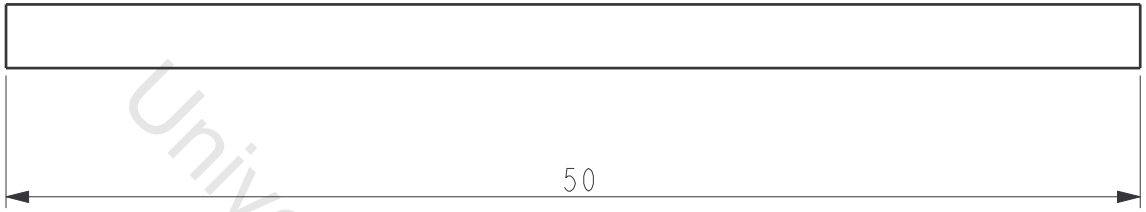

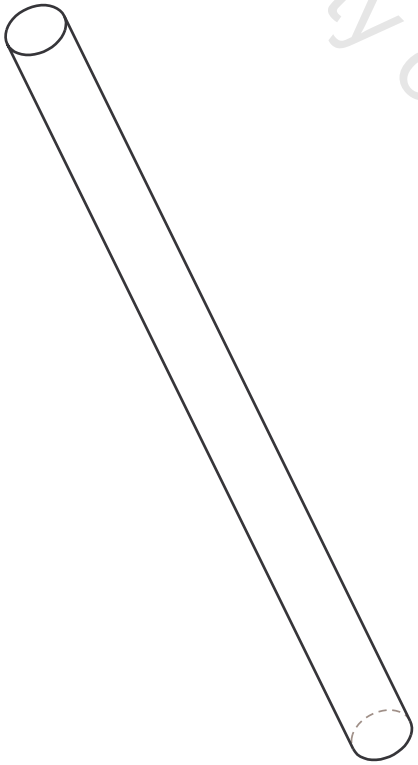

Item	Name	Qty	Material
	University of Cape Town Department of Mechanical Engineering		
	Title: ROD		
Dimensions in mm Tolerance U.O.S. 0.1	Scale: 3,000	Date: 15-Aug-05	Sheet: 1 of 2
	Drawn By: L von Zwiklitz		Drawing Number: xx

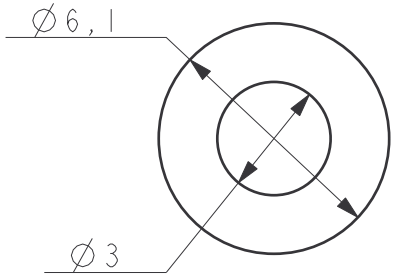

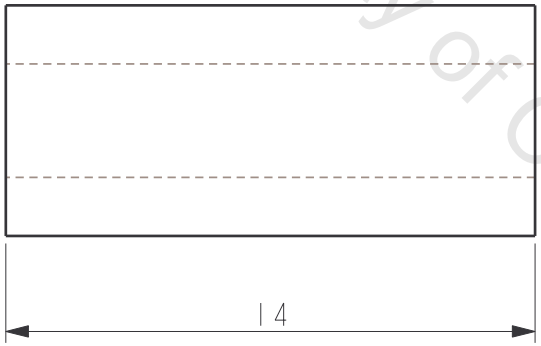

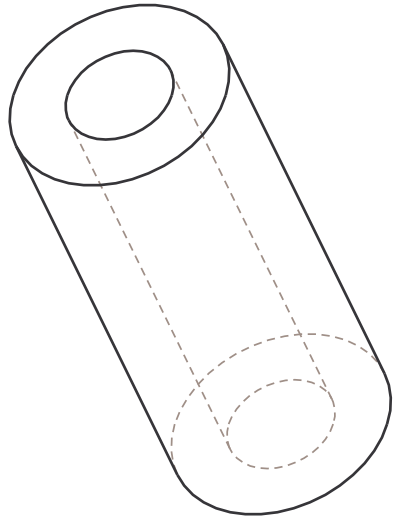

Item	Name	Qty	Material
	University of Cape Town Department of Mechanical Engineering		
	Title BUSH FOR RAMPING		

Dimensions in mm Tolerance U.O.S.	Scale	Date	Sheet	of
0.1	5,000	15-Aug-05	2	2
	Drawn By von Zwiklitz, L		Drawing Number xx	

APPENDIX G – SN CYCLE COUNT

10 MPa

Sample Number	Temperature	First Crack	Failure	
OLD86	20	403092	421745	
OLD92	20	-	452683	++++
NEW85	20	-	400000	++++
NEW107	20	-	402575	++++
OLD100	45	90500	135500	
OLD101	45	89800	105326	
NEW96	45	289400	320700	
NEW98	45	203600	232226	
NEW122	45	-	433000	++++

15 MPa

Sample Number	Temperature	First Crack	Failure
OLD108	20	92900	144000
OLD109	20	102300	147853
NEW95	20	143000	207165
NEW111	20	140150	200918
OLD78	45	15500	18661
OLD79	45	35400	63333
OLD105	45	-	25688
OLD106	45	11206	13631
NEW84	45	28750	49701
NEW134	45	24000	33000

20 MPa

Sample Number	Temperature	First Crack	Failure
OLD22	20	19000	23762
OLD132	20	14000	18400
NEW42	20	9000	13700
NEW71	20	16400	25346
NEW112	20	16100	22051
OLD75	45	11000	17213
OLD103	45	7300	8127
OLD118	45	5600	6700
NEW41	45	12600	17800
NEW82	45	-	8410
NEW83	45	-	7874
NEW117	45	8150	8900

25 MPa

Sample Number	Temperature	First Crack	Failure
FW21	20	8240	16500
OLD51	20	6100	8878
OLD72	20	3300	7740
NEW53	20	-	15455
NEW113	20	8550	15540
OLD64	45	-	4966
OLD124	45	-	3900
OLD129	45	-	4165
NEW70	45	-	8450
NEW81	45	4800	7410

30 MPa

Sample Number	Temperature	First Crack	Failure
OLD23	20	3750	4926
OLD139	20	4350	5325
N24	20	2560	7021
NEW52	20	6300	15590
NEW58	20	-	8651
NEW59	20	5300	8482
NEW120	20	6900	9135
OLD62	45	-	2747
OLD125	45	2078	2078
OLD126	45	1850	1900
NEW61	45	2500	6370
NEW93	45	4000	5000

35 MPa

Sample Number	Temperature	First Crack	Failure
OLD49	20	2150	2250
OLD140	20	1047	1047
NEW55	20	2300	6646
NEW56	20	3800	5600
OLD68	45	2009	2009
OLD128	45	830	830
OLD137	45	1205	1205
NEW69	45	-	4900
NEW94	45	840	4823

40 MPa

Sample Number	Temperature	First Crack	Failure
OLD88	20	753	753
OLD89	20	848	848
NEW73	20	4000	4967
NEW133	20	4650	6260
OLD91	45	617	617
OLD136	45	416	416
NEW99	45	2350	3337
NEW104	45	3050	3700

APPENDIX H – SENB AND C-SHAPE DIMENSIONS

NEW SENB:

3PT1:

Reading	1	2	3	4	Mean
Thickness, B [mm]	10.90	11.00	11.00	11.00	**10.98**
Width, W [mm]	24.40	24.40	24.50	24.50	**24.45**
Knife edges to back face, W [mm]	3.02	2.98	3.01	3.01	**3.01**

	min	max	0.25%B	0.5%B	0.75%B	Mean
Total crack length [mm]	12.48	12.04	14.13	14.26	13.97	**13.66**

3PT2:

Reading	1	2	3	4	Mean
Thickness, B [mm]	11.40	11.40	11.30	11.40	**11.38**
Width, W [mm]	24.30	24.20	24.30	24.20	**24.25**
Knife edges to back face, W [mm]	3.03	3.05	3.03	3.06	**3.04**

	min	max	0.25%B	0.5%B	0.75%B	Mean
Total crack length [mm]	11.49	12.07	13.26	13.68	13.58	**13.08**

3PT3:

Reading	1	2	3	4	Mean
Thickness, B [mm]	11.00	11.00	11.10	11.00	**11.03**
Width, W [mm]	24.80	24.44	24.38	24.58	**24.55**
Knife edges to back face, W [mm]	3.12	3.08	3.08	3.12	**3.10**

	min	max	0.25%B	0.5%B	0.75%B	Mean
Total crack length [mm]	12.45	11.73	13.77	13.97	13.70	**13.39**

3PT4:

Reading	1	2	3	4	Mean
Thickness, B [mm]	11.00	11.02	11.00	11.00	**11.01**
Width, W [mm]	24.46	24.48	24.44	24.46	**24.46**
Knife edges to back face, W [mm]	3.10	3.00	3.00	3.00	**3.03**

	min	max	0.25%B	0.5%B	0.75%B	Mean
Total crack length [mm]	11.82	11.98	13.17	13.54	13.53	**13.04**

3PT5:

Reading	1	2	3	4	Mean
Thickness, B [mm]	11.30	11.31	11.33	11.34	**11.32**
Width, W [mm]	24.23	24.22	24.20	24.20	**24.21**
Knife edges to back face, W [mm]	3.04	3.02	3.10	3.06	**3.06**

	min	max	0.25%B	0.5%B	0.75%B	Mean
Total crack length [mm]	11.59	10.88	13.07	13.10	12.59	**12.50**

3PT6:

Reading	1	2	3	4	Mean
Thickness, B [mm]	11.28	11.30	11.32	11.30	**11.30**
Width, W [mm]	24.25	24.25	24.24	24.22	**24.24**
Knife edges to back face, W [mm]	3.16	3.13	3.17	3.14	**3.15**

	min	max	0.25%B	0.5%B	0.75%B	Mean
Total crack length [mm]	10.64	10.55	12.50	12.70	12.09	**11.97**

3PT7:

Reading	1	2	3	4	Mean
Thickness, B [mm]	11.35	11.35	11.32	11.30	**11.33**
Width, W [mm]	24.40	24.36	24.40	24.33	**24.37**
Knife edges to back face, W [mm]	3.00	3.00	3.04	3.00	**3.01**

	min	max	0.25%B	0.5%B	0.75%B	Mean
Total crack length [mm]	11.02	11.69	12.56	13.03	13.06	**12.50**

3PT8:

Reading	1	2	3	4	Mean
Thickness, B [mm]	11.00	11.00	11.00	11.12	**11.03**
Width, W [mm]	24.39	24.56	24.40	24.40	**24.44**
Knife edges to back face, W [mm]	3.16	3.07	3.06	3.08	**3.09**

	min	max	0.25%B	0.5%B	0.75%B	Mean
Total crack length [mm]	11.76	11.62	13.34	13.53	13.30	**12.97**

3PT9:

Reading	1	2	3	4	Mean
Thickness, B [mm]	11.28	11.36	11.34	11.38	**11.34**
Width, W [mm]	24.22	24.26	24.20	24.18	**24.22**
Knife edges to back face, W [mm]	3.02	3.00	3.02	3.00	**3.01**

	min	max	0.25%B	0.5%B	0.75%B	Mean
Total crack length [mm]	11.46	11.29	12.87	13.41	12.97	**12.65**

3PT10:

Reading	1	2	3	4	Mean
Thickness, B [mm]	11.28	11.34	11.34	11.32	**11.32**
Width, W [mm]	24.52	24.52	24.26	24.26	**24.39**
Knife edges to back face, W [mm]	3.21	3.06	3.07	3.06	**3.10**

	min	max	0.25%B	0.5%B	0.75%B	Mean
Total crack length [mm]	11.25	11.53	12.45	12.86	12.79	**12.37**

3PT11:

Reading	1	2	3	4	Mean
Thickness, B [mm]	11.28	11.30	11.30	11.24	**11.28**
Width, W [mm]	24.42	24.48	24.40	24.44	**24.44**
Knife edges to back face, W [mm]	3.15	3.08	3.06	3.08	**3.09**

	min	max	0.25%B	0.5%B	0.75%B	Mean
Total crack length [mm]	12.35	11.59	13.61	13.74	13.23	**13.14**

3PT12:

Reading	1	2	3	4	Mean
Thickness, B [mm]	11.28	11.37	11.30	11.34	**11.32**
Width, W [mm]	24.45	24.47	24.45	24.42	**24.45**
Knife edges to back face, W [mm]	3.04	3.03	3.08	3.06	**3.05**

	min	max	0.25%B	0.5%B	0.75%B	Mean
Total crack length [mm]	12.06	11.82	13.50	13.64	13.16	**13.06**

OLD SENB:

3PT20:

Reading	1	2	3	4	Mean
Thickness, B [mm]	11.14	11.14	11.14	11.10	**11.13**
Width, W [mm]	24.28	24.28	24.26	24.22	**24.26**
Knife edges to back face, W [mm]	3.00	2.94	2.94	3.02	**2.98**

	min	max	0.25%B	0.5%B	0.75%B	Mean
Total crack length [mm]	11.86	11.45	12.36	12.60	12.20	**12.20**

3PT21:

Reading	1	2	3	4	Mean
Thickness, B [mm]	11.06	11.18	11.16	11.10	**11.13**
Width, W [mm]	24.20	24.30	24.24	24.20	**24.24**
Knife edges to back face, W [mm]	3.12	3.10	3.08	3.10	**3.10**

	min	max	0.25%B	0.5%B	0.75%B	Mean
Total crack length [mm]	10.91	11.42	11.76	12.16	12.20	**11.82**

3PT22:

Reading	1	2	3	4	Mean
Thickness, B [mm]	11.14	11.20	11.22	11.28	**11.21**
Width, W [mm]	24.22	24.24	24.30	24.20	**24.24**
Knife edges to back face, W [mm]	3.04	3.00	2.98	3.00	**3.01**

	min	max	0.25%B	0.5%B	0.75%B	Mean
Total crack length [mm]	11.89	11.42	12.59	12.94	12.59	**12.44**

3PT23:

Reading	1	2	3	4	Mean
Thickness, B [mm]	11.12	11.16	11.16	11.13	**11.14**
Width, W [mm]	24.22	24.48	24.32	24.24	**24.32**
Knife edges to back face, W [mm]	3.00	3.00	2.98	2.98	**2.99**

	min	max	0.25%B	0.5%B	0.75%B	Mean
Total crack length [mm]	11.15	11.49	12.43	12.60	12.16	**12.13**

3PT24:

Reading	1	2	3	4	Mean
Thickness, B [mm]	11.16	11.20	11.19	11.19	**11.19**
Width, W [mm]	24.22	24.28	24.22	24.22	**24.24**
Knife edges to back face, W [mm]	3.04	3.04	3.08	2.98	**3.04**

	min	max	0.25%B	0.5%B	0.75%B	Mean
Total crack length [mm]	10.98	11.39	12.12	12.60	12.27	**12.04**

3PT25: - Scrapped

Reading	1	2	3	4	Mean
Thickness, B [mm]	11.20	11.24	11.38	11.16	**11.25**
Width, W [mm]	24.22	24.22	24.22	24.18	**24.21**
Knife edges to back face, W [mm]	3.10	3.08	3.01	3.03	**3.06**

	min	max	0.25%B	0.5%B	0.75%B	Mean
Total crack length [mm]	10.75	11.15	11.85	12.02	11.96	**11.70**

3PT26:

Reading	1	2	3	4	Mean
Thickness, B [mm]	11.18	11.18	11.16	11.10	**11.16**
Width, W [mm]	24.22	24.23	24.24	24.22	**24.23**
Knife edges to back face, W [mm]	3.14	3.12	3.14	3.17	**3.14**

	min	max	0.25%B	0.5%B	0.75%B	Mean
Total crack length [mm]	11.82	11.38	12.60	12.80	12.33	**12.34**

3PT27: - Scrapped

Reading	1	2	3	4	Mean
Thickness, B [mm]	11.28	11.28	11.28	11.26	**11.28**
Width, W [mm]	24.22	24.22	24.22	24.22	**24.22**
Knife edges to back face, W [mm]	3.08	3.12	3.18	3.10	**3.12**

	min	max	0.25%B	0.5%B	0.75%B	Mean
Total crack length [mm]	11.92	11.96	12.99	12.99	12.63	**12.64**

3PT28: - Scrapped

Reading	1	2	3	4	Mean
Thickness, B [mm]	11.18	11.20	11.26	11.09	**11.18**
Width, W [mm]	24.22	24.22	24.22	24.22	**24.22**
Knife edges to back face, W [mm]	3.20	3.14	3.16	3.20	**3.18**

	min	max	0.25%B	0.5%B	0.75%B	Mean
Total crack length [mm]	11.85	11.65	13.07	13.17	12.50	**12.62**

3PT29:

Reading	1	2	3	4	Mean
Thickness, B [mm]	11.14	11.17	11.22	11.13	**11.17**
Width, W [mm]	24.26	24.22	24.22	24.20	**24.23**
Knife edges to back face, W [mm]	3.05	3.08	3.02	3.04	**3.05**

	min	max	0.25%B	0.5%B	0.75%B	Mean
Total crack length [mm]	11.19	11.82	12.32	12.45	12.20	**12.12**

3PT30:

Reading	1	2	3	4	Mean
Thickness, B [mm]	11.21	11.24	11.24	11.24	**11.23**
Width, W [mm]	24.22	24.23	24.23	24.23	**24.23**
Knife edges to back face, W [mm]	3.00	3.00	2.96	2.99	**2.99**

	min	max	0.25%B	0.5%B	0.75%B	Mean
Total crack length [mm]	10.99	11.53	12.09	12.36	12.29	**12.00**

3PT31:

Reading	1	2	3	4	Mean
Thickness, B [mm]	11.23	11.27	11.27	11.20	**11.24**
Width, W [mm]	24.20	24.22	24.22	24.22	**24.22**
Knife edges to back face, W [mm]	3.01	3.03	3.07	3.06	**3.04**

	min	max	0.25%B	0.5%B	0.75%B	Mean
Total crack length [mm]	11.04	11.22	11.82	12.40	11.92	**11.82**

NEW C-SHAPE:

3CUR1: - Scrapped

Reading	1	2	3	4	Mean
Thickness, B [mm]	15.00	15.00	15.00	14.98	**15.00**
Width, W [mm]	13.90	13.76	13.48	12.96	**13.53**
Knife edges to back face, W [mm]	2.86	2.92	3.08	2.72	**2.90**

	min	max	0.25%B	0.5%B	0.75%B	Mean
Total crack length [mm]	7.86	6.74	8.88	9.12	9.12	**8.61**

3CUR2:

Reading	1	2	3	4	Mean
Thickness, B [mm]	15.80	15.94	15.94	15.86	**15.89**
Width, W [mm]	14.78	14.76	14.44	14.08	**14.52**
Knife edges to back face, W [mm]	2.63	2.88	2.88	2.89	**2.82**

	min	max	0.25%B	0.5%B	0.75%B	Mean
Total crack length [mm]	6.94	6.90	8.46	8.84	8.76	**8.25**

3CUR3: - Scrapped

Reading	1	2	3	4	Mean
Thickness, B [mm]	14.98	15.02	15.04	14.96	**15.00**
Width, W [mm]	13.33	13.10	12.74	12.77	**12.99**
Knife edges to back face, W [mm]	2.61	2.12	3.44	3.52	**2.92**

	min	max	0.25%B	0.5%B	0.75%B	Mean
Total crack length [mm]	6.38	6.24	8.70	9.16	9.02	**8.30**

3CUR4:

Reading	1	2	3	4	Mean
Thickness, B [mm]	15.76	15.86	15.86	15.76	**15.81**
Width, W [mm]	13.86	13.76	13.58	13.64	**13.71**
Knife edges to back face, W [mm]	3.19	3.20	2.77	2.32	**2.87**

	min	max	0.25%B	0.5%B	0.75%B	Mean
Total crack length [mm]	6.16	6.04	7.64	7.94	7.64	**7.33**

3CUR5:

Reading	1	2	3	4	Mean
Thickness, B [mm]	15.88	15.92	15.92	15.86	**15.90**
Width, W [mm]	12.86	12.67	12.74	13.27	**12.89**
Knife edges to back face, W [mm]	2.88	2.94	2.70	2.88	**2.85**

	min	max	0.25%B	0.5%B	0.75%B	Mean
Total crack length [mm]	5.42	5.68	7.34	7.74	7.68	**7.08**

3CUR6:

Reading	1	2	3	4	Mean
Thickness, B [mm]	15.64	15.72	15.87	15.78	**15.75**
Width, W [mm]	13.77	13.78	13.52	13.26	**13.58**
Knife edges to back face, W [mm]	2.83	2.81	2.92	2.98	**2.89**

	min	max	0.25%B	0.5%B	0.75%B	Mean
Total crack length [mm]	6.58	6.16	8.10	8.46	8.30	**7.81**

3CUR7:

Reading	1	2	3	4	Mean
Thickness, B [mm]	15.78	15.84	15.83	15.75	**15.80**
Width, W [mm]	13.60	13.55	13.82	13.68	**13.66**
Knife edges to back face, W [mm]	2.76	3.00	3.02	2.47	**2.81**

	min	max	0.25%B	0.5%B	0.75%B	Mean
Total crack length [mm]	5.94	6.20	7.60	7.86	8.12	**7.41**

3CUR8:

Reading	1	2	3	4	Mean
Thickness, B [mm]	15.77	15.86	15.82	15.76	**15.80**
Width, W [mm]	13.45	13.73	13.76	13.84	**13.70**
Knife edges to back face, W [mm]	3.20	2.86	2.35	2.48	**2.72**

	min	max	0.25%B	0.5%B	0.75%B	Mean
Total crack length [mm]	7.12	6.16	8.80	8.68	8.38	**8.13**

3CUR9:

Reading	1	2	3	4	Mean
Thickness, B [mm]	15.79	15.85	15.84	15.76	**15.81**
Width, W [mm]	12.66	12.93	13.06	13.13	**12.95**
Knife edges to back face, W [mm]	2.49	2.91	2.76	3.12	**2.82**

	min	max	0.25%B	0.5%B	0.75%B	Mean
Total crack length [mm]	5.86	5.08	8.06	8.32	8.02	**7.47**

3CUR10:

Reading	1	2	3	4	Mean
Thickness, B [mm]	15.89	15.88	15.88	15.83	**15.87**
Width, W [mm]	14.29	14.14	13.80	13.68	**13.98**
Knife edges to back face, W [mm]	2.06	2.38	3.29	2.82	**2.64**

	min	max	0.25%B	0.5%B	0.75%B	Mean
Total crack length [mm]	6.48	6.28	8.24	8.38	8.20	**7.80**

3CUR11:

Reading	1	2	3	4	Mean
Thickness, B [mm]	15.76	15.86	15.86	15.78	**15.82**
Width, W [mm]	13.36	13.58	13.82	13.80	**13.64**
Knife edges to back face, W [mm]	2.93	2.94	3.01	3.01	**2.97**

	min	max	0.25%B	0.5%B	0.75%B	Mean
Total crack length [mm]	6.34	4.64	8.72	9.34	8.94	**8.12**

3CUR12:

Reading	1	2	3	4	Mean
Thickness, B [mm]	14.86	14.87	14.87	14.82	**14.86**
Width, W [mm]	13.89	13.60	13.37	13.16	**13.51**
Knife edges to back face, W [mm]	2.86	2.74	2.95	2.78	**2.83**

	min	max	0.25%B	0.5%B	0.75%B	Mean
Total crack length [mm]	6.54	5.68	8.12	8.76	8.38	**7.84**

OLD C-SHAPE:

3CUR20:

Reading	1	2	3	4	Mean
Thickness, B [mm]	14.93	14.93	15.01	15.03	**14.98**
Width, W [mm]	13.36	13.10	12.97	13.02	**13.11**
Knife edges to back face, W [mm]	2.78	2.88	2.39	2.53	**2.65**

	min	max	0.25%B	0.5%B	0.75%B	Mean
Total crack length [mm]	6.34	5.70	6.80	6.70	6.58	**6.53**

3CUR21:

Reading	1	2	3	4	Mean
Thickness, B [mm]	15.27	15.24	15.09	14.99	**15.15**
Width, W [mm]	13.68	13.69	13.50	13.50	**13.59**
Knife edges to back face, W [mm]	2.60	2.42	2.80	2.92	**2.69**

	min	max	0.25%B	0.5%B	0.75%B	Mean
Total crack length [mm]	6.30	6.44	7.46	7.74	7.48	**7.26**

3CUR22:

Reading	1	2	3	4	Mean
Thickness, B [mm]	14.94	14.98	15.04	15.03	**15.00**
Width, W [mm]	13.63	13.59	13.50	13.46	**13.55**
Knife edges to back face, W [mm]	2.95	2.31	2.79	2.31	**2.59**

	min	max	0.25%B	0.5%B	0.75%B	Mean
Total crack length [mm]	6.28	6.58	7.10	7.28	7.24	**7.01**

3CUR23:

Reading	1	2	3	4	Mean
Thickness, B [mm]	14.91	14.94	14.92	14.87	**14.91**
Width, W [mm]	13.18	13.06	12.92	12.91	**13.02**
Knife edges to back face, W [mm]	2.76	2.91	3.46	3.30	**3.11**

	min	max	0.25%B	0.5%B	0.75%B	Mean
Total crack length [mm]	5.72	6.22	6.66	6.98	7.06	**6.67**

3CUR24:

Reading	1	2	3	4	Mean
Thickness, B [mm]	14.91	14.89	14.84	14.82	**14.87**
Width, W [mm]	12.96	13.04	12.88	12.94	**12.96**
Knife edges to back face, W [mm]	3.21	3.00	2.96	2.89	**3.02**

	min	max	0.25%B	0.5%B	0.75%B	Mean
Total crack length [mm]	6.58	6.12	7.06	7.34	6.98	**6.93**

3CUR25:

Reading	1	2	3	4	Mean
Thickness, B [mm]	14.79	14.79	14.81	14.85	**14.81**
Width, W [mm]	13.40	13.46	13.58	13.46	**13.48**
Knife edges to back face, W [mm]	2.51	2.37	2.55	2.69	**2.53**

	min	max	0.25%B	0.5%B	0.75%B	Mean
Total crack length [mm]	6.88	6.94	7.58	7.98	7.80	**7.57**

3CUR26:

Reading	1	2	3	4	Mean
Thickness, B [mm]	15.07	15.16	15.19	15.05	**15.12**
Width, W [mm]	13.06	13.18	13.32	13.61	**13.29**
Knife edges to back face, W [mm]	2.54	2.20	2.33	2.23	**2.33**

	min	max	0.25%B	0.5%B	0.75%B	Mean
Total crack length [mm]	7.16	7.34	8.02	8.34	8.10	**7.93**

3CUR27:

Reading	1	2	3	4	Mean
Thickness, B [mm]	14.88	14.83	14.86	14.93	**14.88**
Width, W [mm]	12.90	12.86	13.07	13.17	**13.00**
Knife edges to back face, W [mm]	2.99	3.20	3.02	2.92	**3.03**

	min	max	0.25%B	0.5%B	0.75%B	Mean
Total crack length [mm]	5.70	6.28	6.44	6.88	6.92	**6.56**

3CUR28:

Reading	1	2	3	4	Mean
Thickness, B [mm]	14.85	14.83	14.85	14.93	**14.87**
Width, W [mm]	12.74	12.79	12.82	12.90	**12.81**
Knife edges to back face, W [mm]	2.91	3.03	2.86	3.04	**2.96**

	min	max	0.25%B	0.5%B	0.75%B	Mean
Total crack length [mm]	5.94	6.64	7.06	7.40	7.34	**7.02**

3CUR29:

Reading	1	2	3	4	Mean
Thickness, B [mm]	14.89	14.86	14.85	14.87	**14.87**
Width, W [mm]	12.76	12.84	12.96	13.11	**12.92**
Knife edges to back face, W [mm]	2.88	2.42	2.99	2.36	**2.66**

	min	max	0.25%B	0.5%B	0.75%B	Mean
Total crack length [mm]	6.12	6.70	7.18	7.62	7.52	**7.18**

3CUR30:

Reading	1	2	3	4	Mean
Thickness, B [mm]	14.78	14.81	14.77	14.69	**14.76**
Width, W [mm]	13.59	13.53	13.65	13.67	**13.61**
Knife edges to back face, W [mm]	2.81	2.81	3.07	3.24	**2.98**

	min	max	0.25%B	0.5%B	0.75%B	Mean
Total crack length [mm]	6.36	6.38	7.10	7.24	7.24	**6.99**

3CUR31:

Reading	1	2	3	4	Mean
Thickness, B [mm]	14.95	14.92	14.92	14.91	**14.93**
Width, W [mm]	12.96	13.10	13.28	13.48	**13.21**
Knife edges to back face, W [mm]	2.75	2.64	2.84	2.66	**2.72**

	min	max	0.25%B	0.5%B	0.75%B	Mean
Total crack length [mm]	6.04	5.70	6.64	6.76	6.66	**6.48**